# NONLINEAR MODELING AND VIBRATION ANALYSIS OF HORIZONTAL DRUM TYPE WASHING MACHINES

A THESIS SUBMITTED TO
THE GRADUATE SCHOOL OF NATURAL AND APPLIED SCIENCES
OF
MIDDLE EAST TECHNICAL UNIVERSITY

BY

CEM BAYKAL

IN PARTIAL FULFILLMENT OF THE REQUIREMENTS
FOR
THE DEGREE OF MASTER OF SCIENCE
IN
MECHANICAL ENGINEERING

SEPTEMBER 2019

Approval of the thesis:

**NONLINEAR MODELING AND VIBRATION ANALYSIS OF HORIZONTAL DRUM TYPE WASHING MACHINES**

submitted by **CEM BAYKAL** in partial fulfillment of the requirements for the degree of **Master of Science in Mechanical Engineering Department, Middle East Technical University** by,

Prof. Dr. Halil Kalıpçılar
Dean, Graduate School of **Natural and Applied Sciences** ________________

Prof. Dr. Mehmet Ali Sahir Arıkan
Head of Department, **Mechanical Engineering** ________________

Assoc. Prof. Dr. Yiğit Yazıcıoğlu
Supervisor, **Mechanical Engineering, METU** ________________

Prof. Dr. Ender Ciğeroğlu
Co-Supervisor, **Mechanical Engineering, METU** ________________

**Examining Committee Members:**

Assoc. Prof. Dr. Mehmet Bülent Özer
Mechanical Engineering, METU ________________

Assoc. Prof. Dr. Yiğit Yazıcıoğlu
Mechanical Engineering, METU ________________

Prof. Dr. Ender Ciğeroğlu
Mechanical Engineering, METU ________________

Assist. Prof. Dr. Gökhan Özgen
Mechanical Engineering, METU ________________

Assoc. Prof. Dr. Sinan Kılıçaslan
Mechanical Engineering, Gazi University ________________

Date: 04.09.2019

**I hereby declare that all information in this document has been obtained and presented in accordance with academic rules and ethical conduct. I also declare that, as required by these rules and conduct, I have fully cited and referenced all material and results that are not original to this work.**

Name, Surname: Cem Baykal

Signature:

## ABSTRACT

### NONLINEAR MODELING AND VIBRATION ANALYSIS OF HORIZONTAL DRUM TYPE WASHING MACHINES



Baykal, Cem
Master of Science, Mechanical Engineering
Supervisor: Assoc. Prof. Dr. Yiğit Yazıcıoğlu
Co-Supervisor: Prof. Dr. Ender Ciğeroğlu



September 2019, 84 pages



Nonlinear two and three-dimensional dynamical models for horizontal drum type washing machines are developed considering rotating unbalance type excitation. Nonlinear differential equations of motion are converted into a set of nonlinear algebraic equations by using the Harmonic Balance Method (HBM). The resulting nonlinear algebraic equations are solved by using Newton's method with arc-length continuation. Several case studies are performed in order to observe the effects of orientation angles of springs and dampers between the drum and the cabinet. In order to reduce the steady-state vibration amplitude of the drum, suitable orientation angles of the springs and dampers and their implementation locations are identified. Furthermore, to further reduce the vibration amplitude of the drum at high frequencies, instead of viscous dampers, dry friction dampers are installed in the system. Effects of orientation angles and parameters of the dry friction damper and springs on the force transmitted to the cabinet are studied.



Keywords: 2D Washing Machine Model, 3D Washing Machine Model, Nonlinear Vibrations, Dry Friction Damper, Harmonic Balance Method.

# ÖZ

## YATAY TAMBURLU ÇAMAŞIR MAKİNELERİNİN DOĞRUSAL OLMAYAN MODELLENMESİ VE TİTREŞİM ANALİZİ

Baykal, Cem
Yüksek Lisans, Makina Mühendisliği
Tez Danışmanı: Doç. Dr. Yiğit Yazıcıoğlu
Ortak Tez Danışmanı: Prof. Dr. Ender Ciğeroğlu

Eylül 2019, 84 sayfa

Döner dengesizlik etkisindeki yatay tamburlu çamaşır makinelerinin iki ve üç boyutlu ve doğrusal olmayan matematiksel modeli çıkarılacaktır. Lineer olmayan diferansiyel denklemler, lineer olmayan cebirsel denklemler setine Harmonik Denge Metoduyla döndürülerek Newton metodunun yay boyu devam yoluyla birleşimi ile çözülecektir. Çeşitli örnek çalışmalarla yay ve damperlerin bağlantı açılarının tamburun titremesine olan etkisi incelenecektir. Kararlı haldeki titreşimi azaltmak için, uygun bağlantı açıları ve bağlantı noktaları belirlenecektir. Daha sonra, yüksek frekanslardaki ve rezonans frekansı yakınlarındaki titreşimi daha da azaltmak için, akışkan olmayan damperler yerine kuru sürtünme damperleri sisteme tanıtılacaktır. Çamaşır makinesinin kabinine aktarılan kuvvetler üzerinde kuru sürtünme damperlerinin oryantasyon açılarının ve parametrelerinin etkisi incelenecektir.



Anahtar Kelimeler: İki Boyutlu Çamaşır Makinesi Model, Üç Boyutlu Çamaşır Makinesi Modeli, Lineer Olmayan Titreşimler, Kuru Sürtünme Damperi, Harmonik Denge Methodu.

To My Grandfather

**ACKNOWLEDGEMENTS**

First of all, I would like to express my thanks to my advisors Assoc. Prof. Dr. Yiğit Yazıcıoğlu and Prof. Dr. Ender Ciğeroğlu for supporting me throughout my graduate education and for their guidance throughout my thesis.

I never forget the motivations and support of my valuable friend Elif Soycan and without the motivation she imposed, this study would be definitely harder.

I also would like to thank my family for their never-ending support. I really appreciate that they gave me the determination I need to finish this study.

I also want to thank my assistant friends and my classmates because they made me love my university, my job, and my studies.

Last but not least, I really want to thank my *daimonion* for letting me through all the difficulties. I will keep on trusting You in my future.

## TABLE OF CONTENTS

## LIST OF TABLES

TABLES

## LIST OF FIGURES

FIGURES

## LIST OF SYMBOLS

SYMBOLS

| | |
|---|---|
| $m_1$ | Mass of the Washing Machine |
| $m_2$ | Mass of the Laundry |
| $J_1$ | Inertia of the Drum in the Roll Axis in the Drum Frame |
| $J_2$ | Inertia of the Drum in the other two Axis in the Drum Frame |
| $R$ | Radius of the Drum |
| $\theta_k$ | Initial Orientation Angles of Springs |
| $\theta_k$ | Initial Orientation Angles of Dampers |
| $e_d$ | Eccentricity of the Laundry in the Drum Plane |
| $e_1$ | Eccentricity of the Laundry in the Roll Axis |
| $k$ | Spring Constant |
| $c$ | Viscous Damper Constant |
| $k_f$ | Free Length of Springs |
| $c_f$ | Free Length of Dampers |
| $k_d$ | Spring Constant of the Dry Friction Damper |
| $\mu N$ | Slip Load of the Dry Friction Damper |
| $L_r$ | Position of the resilient elements in $\vec{u}_1^{(0)}$ |
| $L_i$ | Half-length of the machine in $\vec{u}_i^{(0)}$ |

# CHAPTER 1

# INTRODUCTION & LITERATURE SURVEY

As the standards of living and customer expectations are going up, there has been a demand for reduced noise and minimized vibration of operating machines. To satisfy the expectations of customers, design criteria of any machine tend towards minimized vibration and noise. As one of the most common machines in today's world, horizontal drum type washing machines are also affected by this trend. Therefore, there have been many studies to reduce and minimize vibration and noise amplitudes of washing machines during the operation. In the literature, to better analyze the reason for these problems, different types of two-dimensional or three-dimensional washing machine dynamical models are used. Moreover, there are numerous studies related to Finite Element Methods (FEM) and a multitude of experimental studies measuring both vibration and noise amplitudes in this topic.

## 1.1. Two-dimensional dynamical models in the literature

There are many studies concentrated on two-dimensional dynamical models of horizontal drum type washing machines in the literature. Conrad and Soedel [1] worked on the oscillatory walking behavior of washing machines. They concentrated on the dry friction between the washing machine and the ground by using the Coulomb friction model. They also compared vertical drum type and horizontal drum type washing machines in terms of the tendency of walking while operating. Finally, they found a relation between unbalanced mass, which is laundry for washing machines, and oscillatory walk behavior of washing machines with a fundamental model. Aldrin et al. [2] created a one-directional two degrees of freedom primary suspension system. By using passive and adaptive passive absorbers, they tried to minimize transmitted force to the ground. They validated their model by using the classical Runge-Kutta routine and studied on the effective frequency range of passive dynamic absorbers.

Kuo & Wang [3] concentrated on centrifugal force analysis caused by the laundry. Frequency interval of which washing machine works is separated into five different segments and they are analyzed separately. They implemented a control system to servomotor of the washing machine and compared experiment results with their basic dynamic model.

Lyu et al. [4] worked with another one-directional two degrees of freedom system with Coulomb friction damping. They also introduced a stick and multi stick transition velocity friction model to improve the accuracy of their dynamical model. They compared their analytical results with experiments and proved that the modified stick transition velocity friction model is more accurate.

Bascetta et al. [5] used another two-dimensional three degrees of freedom model by concentrating on the driving motor of the washing machine. They also used an encoder to measure the angular orientation and deflection of the washing machine drum and introduced a closed-loop control system. They illustrated a methodology to analyze the effects of mechanical and control subsystems of a washing machine on the performance of velocity control, and ease the tuning of the velocity regulator to minimize vibration magnitude.

Boyraz & Gündüz [6] used the most common two-dimensional three degrees of freedom model by analyzing the system in the drum plane. Nonlinear equation of motion is solved with time integration, and they tried to find the instantaneous rotating speed of the drum at any time. With experiments, they validated their dynamical model and numerical solutions. They optimized parameters and initial orientation geometry of resilient elements by using the Genetic Algorithm for different scenarios such as minimizing the wobbling movement, reducing steady-state or transient vibration span.

Nguyen et al. [7] created a two-dimensional geometrically linearized model with magnetorheological (MR) dampers with different amount of coils. They also created a finite element model (FEM) and performed experiments to validate their model. They concentrated on the optimal design of MR dampers and with an appropriate controller, attenuating the excessive amount of vibration.

Clerc et al. [8] used a general geometrically linearized two-dimensional model with balancer rings added around the washing machine drum. Their novelty is using shaped trolleys, allowing the ring cross-section optimization and the control of the mobile masses' behavior in the balancer rings at a low rotational speed. They validated that correcting masses are extremely helpful in attenuating the displacement amplitude of the drum at different operating rates.

Yalçın & Erol [9] again used a geometrically linearized two-dimensional model and concentrated on four contact points of horizontal drum-type washing machines with the ground. To prevent walking behavior of washing machines, semi-active suspension elements introduced to the system, and with experiments, they proved that vibration amplitudes are attenuated and operating sound power levels (dBA) are significantly reduced with their suspension system.

### 1.2. Three-dimensional dynamical models in the literature

Türkay et al. [10] created a three-dimensional dynamical model by neglecting gyroscopic terms and assuming the inertia matrix is time-independent. The obtained equation of motion is solved with classical Runge Kutta routine. Both transient and steady-state response of the system is compared with preliminary experiment results, and dynamical model is validated. In another study [11], with the same dynamical model, they optimized the suspension system of the washing machine. After mentioning the walking behavior of the washing machines, they used different cost functions, such as the sum of vertical and horizontal displacement amplitudes, maximum orbit amplitude or maximum vertical or horizontal amplitudes, optimized the parameters of shock absorbers, dampers, and springs.

Papadopoulos & Papadimitriou [12] created a simplified three-dimensional model and included the forces between ground and washing machines into the equation of motion. By obtaining linear and simplified equations, they could calculate critical frequencies for the system that decides the walking behavior. They added two balancing masses around the drum with an active control system to prevent any walking.

Argentini et al. [13-14] created another mathematical three dimensional model with rheological dampers by using Lagrange's equation in the basket frame with linearized gyroscopic effects. They also used Finite Element Modeling and all results are compared with experiments. In another study [15], they designed a two degrees of freedom (DOF) tuned mass damper (TMD) and proved that it is beneficial in attenuating vibration amplitudes of the drum. They again used linearized matrices in the equation of motion and compared their results with experiments.

Lim et al. [16] created three dimensional 12 degrees of freedom (DOF) model by using the washing machine drum with bearings between the motor and the drum. By including gyroscopic effects as well, they created the equation of motion and solved it with classical Runge Kutta integration. They also analyzed the Campell diagram and the directional spectrum to figure out backward or forward circular motion. They validated their mathematical model by comparing their findings with experimental results.

Roizman et al. [17] created the equation of motion by using Lagrange of the second type and tried to obtain the solution linearly. They created an original test setup, which does not include the cabinet of the washing machine, and compared their calculations with experimental results.

Nygårds & Berbyuk [18] used their model with Coulomb dry frictions and cubic stiffness elements. They worked out their three-dimensional equation of motion with time integration and compared their results with both experiments and the FEM model. They also investigated Campell diagram to better analyze the whirling movement of the washing machine drum. To minimize the undesired vibration, they introduced counterbalancing masses to the system. In another study [19], they analyzed the stability problem of the dynamical model. Including counterweights to attenuate the vibration amplitudes, they focused on inertia distribution problem and using Pareto optimization and with transmitted vertical force as cost function; they optimized parameters of stiffness, dampers, and counterweights.

Buśkiewicz et al. [20-21] created their model by assuming the tube does not spin around its roll axis and does not translate along the drum axis. Using Lagrange's equation and time integration, results are obtained in the time domain, and they are compared with their experiments. They focused on trajectories of motion in different frequencies and introduced on-off viscous dampers to the system to attenuate transmitted force to the cabinet at high frequencies. Minorowicz et al. [22] designed a share mode magnetorheological damper and inserted it into a horizontal type washing machine. With experiments, they proved their dampers are very useful attenuating vibration amplitudes of the drum.

Chen et al. [23] created their dynamical model and obtained a three-dimensional equation of motion by using Lagrangian. They solved the system with both time integration and made stability analysis in the frequency domain by labeling different types of bifurcation. After placing a ball balancer to the system, changes in the drum's vibration angle due to variations of the mass centers of the unbalance and the tub were studied. Later [24], magnetorheological dampers are introduced to the system with the automatic balancer with multiple balls. Forces on the MR dampers are modeled with nonlinear regressions after experimental data is obtained. By defining cost function as minimum motion space of the tub at the transient stage, control current of the MR dampers are optimized by using Genetic Algorithm and Sequential Quadratic Programming together. Results proved that ball balancer is very useful for reducing vibration in the steady-state; however, they increase transient state vibration. It is also suggested to make control current of MR damper zero at the steady-state to improve vibration isolation performance.

### 1.3. Other related models in the literature

Since it is a general issue, there are many other types of studies related to the vibration problem of washing machines. These are concentrated on various topics; such as, lifetime prediction of washing machines [25], actively controlling magnetorheological or different type dampers to attenuating vibration amplitudes [26-29], quickly obtaining reliability information of a washing machine [30], estimation of amount and distribution of unbalanced load [31-32], analyzing the effects of the leg stiffness to the natural frequencies of the system [33], controlling the driving motor of the washing machine to mitigate the vibration [34-35], using various methods to directly decrease operating dBA level of the machines [36-37], or directly identifying the overall sound intensity of washing machines [38-40].

In this introduction, several studies related to horizontal drum type washing machines are presented. Vertical type washing machines, or top-loading washing machines, are popular as much as horizontal, or front-loading, ones and there are many types of studies related to top-loading washing machines but they will not be mentioned in this thesis. In general, the main motivation behind these studies is mitigating the vibration amplitude of the drum or minimizing the transmitted force to the cabinet or both of them at the same time. To reach this objective, different dynamical models are used with many types of dampers in it. In the literature, finite, numerical or linearized analytical analyses are performed, mostly in the time domain to analyze transient response of the drum.

However, analyzing the dynamics of horizontal drum type washing machines in the frequency domain is very helpful to observe the response in a wide frequency range. Moreover, Frequency Response Function can be used in the optimization process and it will save the computational effort compared to the time domain solutions. In this thesis, two-dimensional and three-dimensional dynamical models are introduced for horizontal drum type washing machines. Nonlinear equations of motion are solved with the Harmonic Balance Method in the frequency domain and steady-state response of the drum is analyzed as a response of rotating laundry unbalance. In order to mitigate vibration amplitude of drum and transmitted force to the washing machine cabinet, orientation angles and parameters of resilient elements are studied.

# CHAPTER 2

# METHODOLOGY

Steady-state solution of a stable system converges in a limit cycle and the main structure behind the limit cycles is Fourier Transform Theory. Fourier Transform breaks down a periodic function into the sum of sinusoidal functions and when the steady-state response is considered, the solution is automatically periodic. Following integrals will give the coefficients of sinusoidal terms, and a basis term.

$$\begin{aligned} x_0 &= \frac{1}{T}\int_0^T f(t)\cdot dt \\ x_{k_s} &= \frac{2}{T}\int_0^T f(t)\cdot \sin(k\cdot\omega\cdot t)\cdot dt \\ x_{k_c} &= \frac{2}{T}\int_0^T f(t)\cdot \cos(k\cdot\omega\cdot t)\cdot dt \end{aligned} \tag{2.1}$$

After this transformation periodic function which has a period of $T$, can be represented as follows:

$$f(t) = x_0 + \sum_{k=1}^{n}(x_{k_s}\cdot\sin(k\cdot\omega\cdot t) + x_{k_c}\cdot\cos(k\cdot\omega\cdot t)) \tag{2.2}$$

In this chapter, achieving steady-state solution of nonlinear equations of motion and basics of three-dimensional dynamics are studied.

## 2.1. Harmonic Balance Method

Fourier series, a combination of sinusoids, can represent a regular periodic solution of an ordinary or differential-algebraic equation system. In many cases, a reasonably accurate approximation is already achieved when only a small number of sinusoids is considered. Thus, a natural approach seems to seek an approximate solution in the form of a truncated Fourier series [41]. Harmonic Balance Method (HBM) is based on a very simple idea where an assumed form of a periodic solution, which is expressed in the truncated Fourier series, is inserted into the nonlinear equation of motion and the coefficients of similar terms are balanced to determine the unknown one.

### 2.1.1. Integrable Nonlinearities – Case Study: Cubic Stiffness

As a difference from a linear oscillatory system, a cubic stiffness element is attached between the mass and ground with the coefficient of $k_c$ and with the forcing of $F(t) = F_0 \cdot \cos(\omega \cdot t)$. The nonlinear equation of motion can be written as follows:

$$
\begin{aligned}
m \cdot \ddot{x} + c \cdot \dot{x} + k \cdot x + f_{nl}\left(x, t\right) &= F_0 \cdot \cos(\omega \cdot t) \\
m \cdot \ddot{x} + c \cdot \dot{x} + k \cdot x + k_c \cdot x^3 &= F_0 \cdot \cos(\omega \cdot t)
\end{aligned}
\tag{2.3}
$$

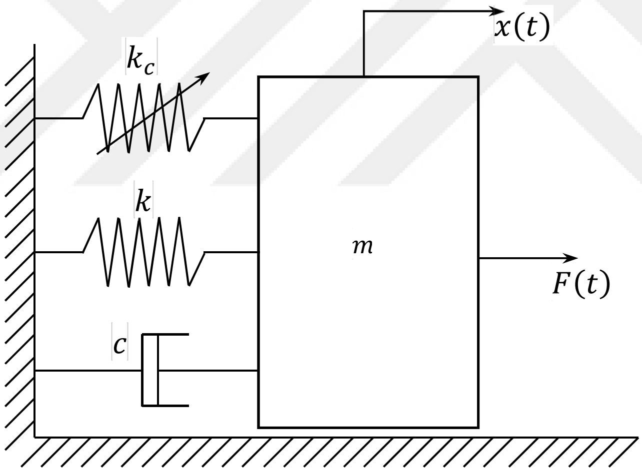


Figure 2.1. A nonlinear one degree of freedom system.

As a first step, one can define the solution by using only a single harmonic. The assumed solution and its derivatives are as follows:

$$x(t) = x_{1s} \cdot \sin(\omega \cdot t) + x_{1c} \cdot \cos(\omega \cdot t),\ Period : T = \frac{2 \cdot \pi}{\omega}$$
$$\dot{x}(t) = \omega \cdot x_{1s} \cdot \cos(\omega \cdot t) - \omega \cdot x_{1c} \cdot \sin(\omega \cdot t) \tag{2.4}$$
$$\ddot{x}(t) = -\omega^2 \cdot x_{1s} \cdot \sin(\omega \cdot t) - \omega^2 \cdot x_{1c} \cdot \cos(\omega \cdot t)$$

It is also useful to expand the nonlinear term $x^3$:

$$\begin{aligned} x(t)^3 &= x_{1c}{}^3 \cdot \cos^3(\omega \cdot t) + 3 \cdot x_{1c}{}^2 \cdot x_{1s} \cos^2(\omega \cdot t) \cdot \sin(\omega \cdot t) \\ &+3 \cdot x_{1c} \cdot x_{1s}{}^2 \cos(\omega \cdot t) \cdot \sin^2(\omega \cdot t) + x_{1s}{}^3 \cdot \sin^3(\omega \cdot t) \end{aligned} \tag{2.5}$$

By using the following trigonometric identities, Equation (2.5) can be written in a more nested form:

$$\begin{aligned} x(t)^3 &= \frac{3}{4} \cdot (x_{1c}{}^3 + x_{1c} \cdot x_{1s}{}^2) \cdot \cos(\omega \cdot t) + \frac{3}{4} \cdot (x_{1s}{}^3 + x_{1c}{}^2 \cdot x_{1s}) \cdot \sin(\omega \cdot t) \\ &+(\ldots) \cdot \cos(3 \cdot \omega \cdot t) + (\ldots) \cdot \sin(3 \cdot \omega \cdot t) \end{aligned} \tag{2.6}$$

$$\begin{aligned} \cos^3(a) &= \frac{3}{4} \cdot \cos(a) + \frac{1}{4} \cdot \cos(3 \cdot a) \\ \cos^2(a) \cdot \sin(a) &= \frac{1}{4} \cdot \sin(a) + \frac{1}{4} \cdot \sin(3 \cdot a) \\ \cos(a) \cdot \sin^2(a) &= \frac{1}{4} \cdot \cos(a) - \frac{1}{4} \cdot \cos(3 \cdot a) \\ \sin^3(a) &= \frac{3}{4} \cdot \sin(a) - \frac{1}{4} \cdot \sin(3 \cdot a) \end{aligned} \tag{2.7}$$

Substituting the assumed solution into the equation of motion of the system will lead to:

$$\begin{aligned} &-m \cdot \omega^2 \cdot (x_{1s} \cdot \sin(\omega \cdot t) + x_{1c} \cdot \cos(\omega \cdot t)) + k \cdot (x_{1s} \cdot \sin(\omega \cdot t) + x_{1c} \cdot \cos(\omega \cdot t)) \\ &+c \cdot \omega \cdot (x_{1s} \cdot \cos(\omega \cdot t) - \omega \cdot x_{1c} \cdot \sin(\omega \cdot t)) + k_c \cdot x^3 = F_0 \cdot \cos(\omega \cdot t) \end{aligned} \tag{2.8}$$

Inserting Equation (2.6) into Equation (2.8) and collecting the coefficients of harmonics yields:

$$\sin(\omega\cdot t)\cdot(-m\cdot\omega^2\cdot x_{1s}+c\cdot\omega\cdot x_{1c}+k\cdot x_{1s}+\frac{3}{4}\cdot({x_{1s}}^3+{x_{1c}}^2\cdot x_{1s}))$$
$$+\cos(\omega\cdot t)\cdot(-m\cdot\omega^2\cdot x_{1c}+c\cdot\omega\cdot x_{1s}+k\cdot x_{1c}+\frac{3}{4}\cdot({x_{1c}}^3+x_{1c}\cdot{x_{1s}}^2)-F_0) \quad (2.9)$$
$$+(\ldots)\cdot\cos(3\cdot\omega\cdot t)+(\ldots)\cdot\sin(3\cdot\omega\cdot t)=0$$

At this point considering only the harmonic(s) contained in the assumed solution, i.e. neglecting the terms with the frequency of $3\omega$ will be convenient. The considered terms are balanced individually, by setting the associated Fourier coefficients to zero. This step leads to the following set of algebraic equations:

$$\begin{aligned}
-m\cdot\omega^2\cdot x_{1s}+c\cdot\omega\cdot x_{1c}+k\cdot x_{1s}+\frac{3}{4}\cdot({x_{1s}}^3+{x_{1c}}^2\cdot x_{1s})=0\\
-m\cdot\omega^2\cdot x_{1c}+c\cdot\omega\cdot x_{1s}+k\cdot x_{1c}+\frac{3}{4}\cdot({x_{1c}}^3+x_{1c}\cdot{x_{1s}}^2)-F_0=0
\end{aligned} \quad (2.10)$$

Equation (2.10) is a set of nonlinear algebraic equations that can be solved by using Newton's method. The unknowns are coefficients of harmonics, $x_{1s}$ and $x_{1c}$. The rest consists of system parameters, forcing and the frequency of interest.

At this point, it is convenient to normalize the time and frequency multiplication as $\theta=\omega\cdot t$ to fix all functions' periods to $2\pi$. In this case, Equation (2.1) turns into the following shape:

$$\begin{aligned}
x_0&=\frac{1}{2\cdot\pi}\int_0^{2\cdot\pi} f(\theta)\cdot d\theta\\
x_{k_s}&=\frac{1}{\pi}\int_0^{2\cdot\pi} f(\theta)\cdot\sin(k\cdot\theta)\cdot d\theta\\
x_{k_c}&=\frac{1}{\pi}\int_0^{2\cdot\pi} f(\theta)\cdot\cos(k\cdot\theta)\cdot d\theta
\end{aligned} \quad (2.11)$$

And Equation (2.2) becomes:

$$f(\theta) = x_0 + \sum_{k=1}^{n} (x_{k_s} \cdot \sin(k \cdot \theta) + x_{k_c} \cdot \cos(k \cdot \theta)) \tag{2.12}$$

Equations (2.11&2.12) becomes an excellent pair for calculating Fourier transforms of continuous and periodic functions. However, different types of nonlinearities require different types of solution techniques.

### 2.1.2. Not Integrable Nonlinearities – Gauss-Quadrature Integration

In this case, it is necessary to take the integrals in Equation (2.11) numerically. Using Gauss-Quadrature as the numerical integration method is sensible since it is the most accurate one. The main idea behind numerical integration is a strategy of replacing a complicated function with an approximating function that can be easily integrated.

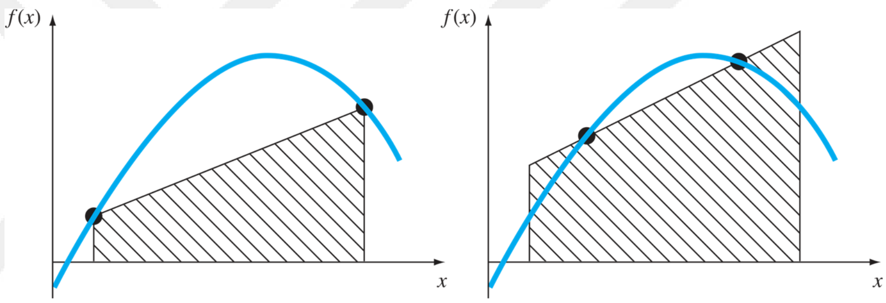


Figure 2.2. Graphical depiction of the importance of the selection of base points [42].

As depicted in Figure (2.2a), the numerical integration idea is based on taking the area under the straight line connecting the two values at the ends of the integration interval. The formula to compute the integral is as follows:

$$I \cong (b-a) \cdot \frac{f(a) + f(b)}{2} \tag{2.13}$$

Where $a$ and $b$ are the limits of the integration. As in the case of Figure (2.2a), this approach may lead to higher errors than expected. By selecting the base points wisely, as in the case of Figure (2.2b), one can define a new line segment that would balance the positive and negative errors and arrive at an improved estimate of integral. This technique is named as Gauss quadrature and the result of integral estimation can be calculated as follows:

$$I \cong c_0 \cdot f(x_0) + c_1 \cdot f(x_1) \tag{2.14}$$

Where $c$ values are constants, also called as weights, $x_0$ and $x_1$ are function arguments to be determined. Demanding that the integral estimation fits the integral of higher-order parabolic functions, the following four equations can be used to determine the unknown coefficients.

$$\begin{aligned}
&f(x) = 1; c_0 \cdot 1 + c_1 \cdot 1 = \int_{-1}^{1} 1dx = 2 \\
&f(x) = x; c_0 \cdot x_0 + c_1 \cdot x_1 = \int_{-1}^{1} xdx = 0 \\
&f(x) = x^2; c_0 \cdot x_0{}^2 + c_1 \cdot x_1{}^2 = \int_{-1}^{1} x^2dx = \frac{2}{3} \\
&f(x) = x^3; c_0 \cdot x_0{}^3 + c_1 \cdot x_1{}^3 = \int_{-1}^{1} x^3dx = 0
\end{aligned} \tag{2.15}$$

This set of equations can be solved using Newton’s method and unknown parameters can be calculated as follows:

$$c_0 = 1,\ \ c_1 = 1,\ \ x_0 = -\frac{1}{\sqrt{3}},\ \ x_1 = -\frac{1}{\sqrt{3}} \tag{2.16}$$

As the last step, integration can be evaluated as follows:

$$I \cong f(-\frac{1}{\sqrt{3}}) + f(\frac{1}{\sqrt{3}}) \tag{2.17}$$

Equation (2.17) will find exact values for integrating polynomials up to third order polynomials since they are used to create two points Gauss-Legendre formula. With the same idea, Equation (2.14) can be modified by including more function arguments and weights. Moreover, an increasing number of arguments and weights will provide obtaining exact results for higher-order polynomials. Since this is a very general solution as a numerical integration technique, all these weights and function arguments are tabulated in the literature and added in the appendix.

Notice that the integration limits in Equation (2.15) are from $-1$ to 1. This is done to simplify the mathematics and obtain a more general form in calculating weights and function arguments. All integral limits are transformed into a pre-specified range; therefore, calculated weights and function arguments are the same for all functions. However, to transform integral limits, it is necessary to make a change of variables. This is accomplished by assuming that a new variable $x_d$ is related to the original variable $x$ in a linear fashion:

$$x = a_0 + a_1 \cdot x_d \tag{2.18}$$

Lower and upper limits are needed to be considered. If the lower limit $x = a$ corresponds to $x_d = -1$ and upper limit $x = b$ corresponds to $x_d = 1$, then:

$$\begin{aligned} a &= a_0 + a_1 \cdot (-1) \\ b &= a_0 + a_1 \cdot 1 \end{aligned} \tag{2.19}$$

These equations can be solved to calculate the transformation constants and can be substituted into Equation (2.18)

$$\left.\begin{aligned} a_0 &= \frac{b+a}{2}, a_1 = \frac{b-a}{2} \\ x &= \frac{(b+a)+(b-a)\cdot x_d}{2} \end{aligned}\right\} \tag{2.20}$$

To insert $x_d$ into the integral, it is necessary to define the derivative of it:

$$dx = \frac{(b-a)\cdot dx_d}{2} \tag{2.21}$$

At last, one can substitute these expressions into the general integral:

$$\int_a^b f(x)dx = \int_{-1}^{1} f(\frac{(b+a)+(b-a)\cdot x_d}{2})\cdot\frac{(b-a)}{2}dx_d \qquad (2.22)$$

In the case of the Harmonic Balance Method, all integrals are from $0$ to $2\pi$. Inserting the Gauss quadrature method to integrals in equation (82) will lead:

$$x_0 = \frac{1}{2\cdot\pi}\cdot\int_{-1}^{1} f(\pi+\pi\cdot x_d)\cdot\pi\cdot dx_d = \frac{1}{2}\cdot\int_{-1}^{1} f(\pi+\pi\cdot x_d)\cdot dx_d \qquad (2.23)$$

$$\begin{aligned} x_{k_s} &= \frac{1}{\pi}\cdot\int_{-1}^{1} f(\pi+\pi\cdot x_d)\cdot\sin(k\cdot(\pi+\pi\cdot x_d))\cdot\pi\cdot dx_d \\ x_{k_s} &= \int_{-1}^{1} f(\pi+\pi\cdot x_d)\cdot\sin(k\cdot(\pi+\pi\cdot x_d))\cdot dx_d \end{aligned} \qquad (2.24)$$

$$\begin{aligned} x_{k_c} &= \frac{1}{\pi}\cdot\int_{-1}^{1} f(\pi+\pi\cdot x_d)\cdot\cos(k\cdot(\pi+\pi\cdot x_d))\cdot\pi\cdot dx_d \\ x_{k_c} &= \int_{-1}^{1} f(\pi+\pi\cdot x_d)\cdot\cos(k\cdot(\pi+\pi\cdot x_d))\cdot dx_d \end{aligned} \qquad (2.25)$$

And all the integrals in the equations (2.23-2.25) can be calculated by using two points, as in Equation (2.17), or more points with Gauss quadrature integration, according to the desired accuracy.

### 2.1.3. Piecewise Nonlinearities – Case Study: Dry Friction

If the reason of the nonlinearity is a piecewise function, then it is necessary to divide the integral into many segments and deal with each of them, separately. As an example case, dry friction damper model can be analyzed. In dry friction, there is an upper limit for the force exerted to the mass by the surrounding rigid bodies that are in contact with the mass. The force applied to the mass by the ground can be represented by the following piecewise function.

$$f_g(t)=\begin{cases} slip\ case: -\mu \cdot N\ if\ F(t) \geq \mu N \\ stick\ case: -F(t)\ if\ \mu \cdot N \geq F(t) \geq -\mu N \\ slip\ case: \mu \cdot N\ if\ F(t) \leq -\mu N \end{cases} \tag{2.26}$$

This dry friction damper can be modeled with a spring and two generalized coordinates as follows:

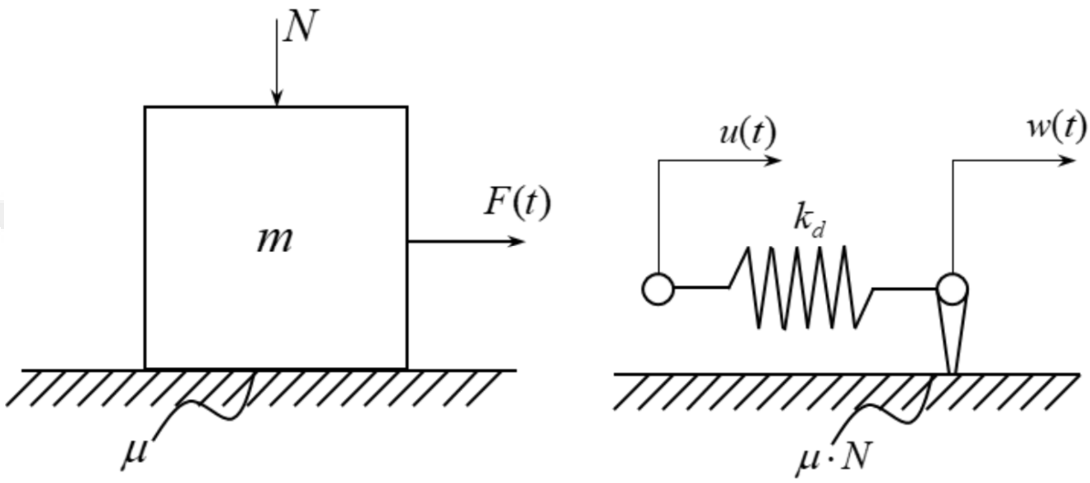


Figure 2.3. Dry friction and its mathematical model.

By using Figure (2.3) a mathematical model can be derived as follows:

$$\begin{aligned} f_g(t) &= k_d \cdot (u(t) - w(t)) \\ \dot{f}_g(t) &= k_d \cdot (\dot{u}(t) - \dot{w}(t)) \end{aligned} \tag{2.27}$$

Where $u(t)$ is the displacement input coming to the dry friction damper and $w(t)$ is the intermediate generalized coordinate of the resilient element. Normalizing the time and frequency multiplication will replace the independent variable $t$ to $\theta$ and fix the boundaries of the integral to $[0, 2\pi]$, leading to:

$$\begin{aligned} f_g(\theta) &= k_d \cdot (u(\theta) - w(\theta)) \\ \dot{f}_g(\theta) &= k_d \cdot (\dot{u}(\theta) - \dot{w}(\theta)) \end{aligned} \tag{2.28}$$

In total there will be three types of motion; slip in a positive direction, slip in a negative direction and stick. It is essential to catch transition points between these three cases to divide the whole integral range into small portions. During slip:

$$\left.\begin{aligned} f_g(\theta) &= k_d \cdot (u(\theta) - w(\theta)) = \pm\mu \cdot N \\ \dot{f}_g(\theta) &= k_d \cdot (\dot{u}(\theta) - \dot{w}(\theta)) = 0 \\ \dot{u}(\theta) &= \dot{w}(\theta) \end{aligned}\right\} \tag{2.29}$$

During stick, $\dot{w}(\theta)$ will be zero, i.e. there will be no motion in the dry friction damper. At slip-to-stick transition, equation (2.29) turns into $\dot{u}(\theta) = 0$ where $u(\theta)$ is a truncated Fourier series and there are many solutions. By using the Newton Raphson method and making an incremental search between $[0, 2\pi]$, all $\theta_s$ values can be calculated where $\theta_s$ refers slip-to-stick transition angles.

Whenever the friction force reaches its limiting value $\mu N$, the stick-to-slip transition occurs. In slip state $u(\theta) - w(\theta)$ becomes constant and the friction interface will move with $u(\theta)$. The force relation can be written as follows:

$$f_g(\theta) = k_d \cdot (u(\theta) - u_0) + f_0 = \pm\mu N \tag{2.30}$$

Where $u_0$ and $f_0$ are the displacement and friction force at the beginning of the stuck state. Again equation (2.30) can be solved for $\theta$ and identify stick-to-slip transition angles. The $\pm$ sign in the equation (2.30) determines if the slip is in the positive or the negative direction. However, without solving both equations, it is impossible to determine the direction. In Figure (2.4), an example study is shown with the given parameters:

$$\left.\begin{aligned} u(\theta) &= 0.1 \cdot \sin(\theta) + 0.2 \cdot \cos(\theta) + 0.3 \cdot \sin(2 \cdot \theta) + 0.4 \cdot \cos(2 \cdot \theta)\ m \\ k &= 500 \frac{N}{m}, \mu N = 100 N \end{aligned}\right\} \tag{2.31}$$

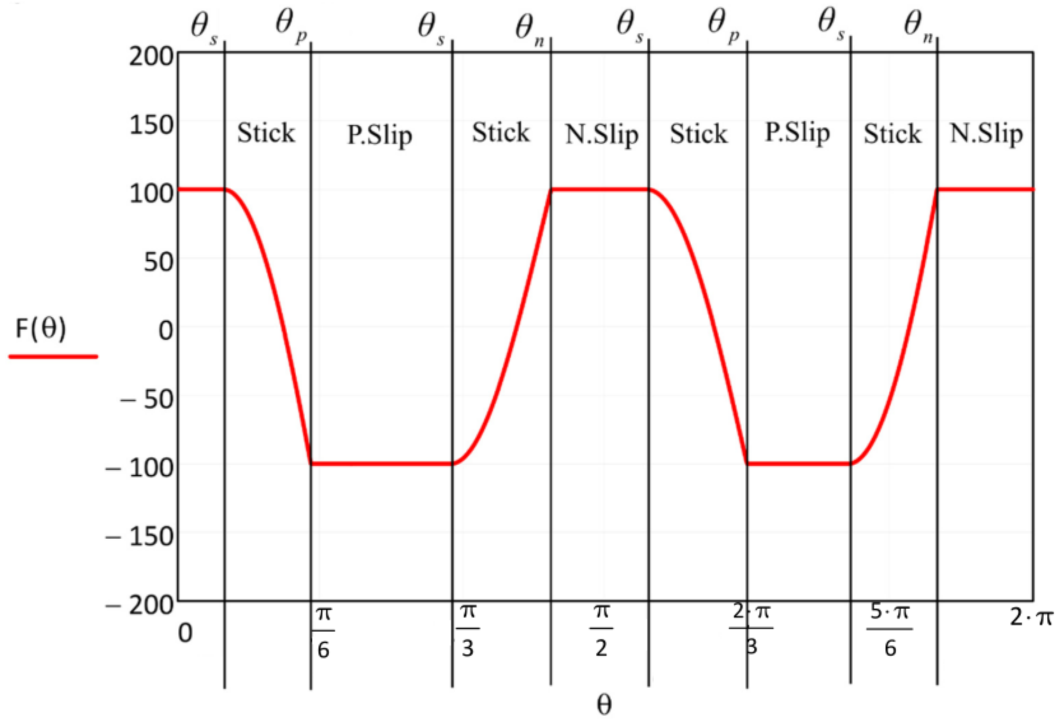


Figure 2.4. A case study for dry friction dampers.

Transition angles are determining the limits of the integral segments. After transition angles are tabulated, the only thing remains is calculating the integrals. From Equations (2.29 & 2.30) integrals of the dry friction damper for each segment can be written by referring Equation (2.11) as follows:

$$\text{During P.Slip:} \begin{cases} x_0 = \int_{\theta_p}^{\theta_s} -\mu N \cdot d\theta \\ x_{k_s} = \int_{\theta_p}^{\theta_s} -\mu N \cdot \sin(k \cdot \theta) \cdot d\theta \\ x_{k_c} = \int_{\theta_p}^{\theta_s} -\mu N \cdot \cos(k \cdot \theta) \cdot d\theta \end{cases} \tag{2.32}$$

$$\text{During N.Slip:}\begin{cases} x_0 = \int_{\theta_n}^{\theta_s} \mu N \cdot d\theta \\ x_{k_s} = \int_{\theta_n}^{\theta_s} \mu N \cdot \sin(k\cdot\theta)\cdot d\theta \\ x_{k_c} = \int_{\theta_n}^{\theta_s} \mu N \cdot \cos(k\cdot\theta)\cdot d\theta \end{cases} \tag{2.33}$$

$$\text{During stick:}\begin{cases} x_0 = \int_{\theta_s}^{\theta_n \text{ or } \theta_p} k_d\cdot(u(\theta)-u_0)+f_0\cdot d\theta \\ x_{k_s} = \int_{\theta_s}^{\theta_n \text{ or } \theta_p} (k_d\cdot(u(\theta)-u_0)+f_0)\cdot\sin(k\cdot\theta)\cdot d\theta \\ x_{k_c} = \int_{\theta_s}^{\theta_n \text{ or } \theta_p} (k_d\cdot(u(\theta)-u_0)+f_0)\cdot\cos(k\cdot\theta)\cdot d\theta \end{cases} \tag{2.34}$$

Since $u(\theta)$ is a truncated Fourier series, all above equations can be calculated analytically. After the integrals for all segments are calculated, the result can be placed into equation (2.11).

## 2.2. Frequency Response Functions of Nonlinear Systems with Newton's Method with Arc-length Continuation

Frequency response functions of a linear system can be expressed analytically; however, for non-linear systems, frequency response functions can only be obtained numerically. The Equation (2.8) in the cubic stiffness example can be solved for all frequencies, however, frequency response functions of nonlinear systems may have a memory as depicted in Figure (2.5). Firstly, for some frequency values, the system has three different solutions. Secondly, when the solution path changes direction, the determinant of the Jacobian matrix becomes zero. To overcome these problems, a new parameter, the arc-length, is added to the set of nonlinear algebraic equations which makes the Jacobian matrix non-singular at the turning points. Moreover, instead of the frequency, the path following parameter will be arc-length. Hence, Newton's method becomes available at tracing the solution even the path is turning back. The arc-length parameter is denoted with $s$ , which is the radius of a hypothetical sphere in which the next solution point is searched.

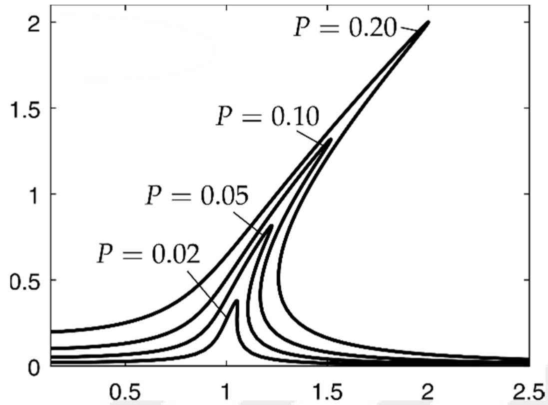


Figure 2.5. Frequency Response Function of a nonlinear system for different levels of excitation [41].

For the modified system, the frequency will also be unknown as well as the coefficients of the truncated Fourier series. With the addition of the arc-length parameter, the vector of unknowns for the new system of a nonlinear set of equations becomes:

$$\mathbf{q} = \begin{Bmatrix} \mathbf{x} \\ s \end{Bmatrix} \tag{2.35}$$

Here $q$ is the new vector of unknowns. Since the frequency is also an unknown, a new equation is necessary which is the equation of the hypothetical sphere with a radius of $s$ and centered at the previous solution point.

$$(\mathbf{x}_k - \mathbf{x}_{k-1})^T \cdot (\mathbf{x}_k - \mathbf{x}_{k-1}) + (\omega_k - \omega_{k-1})^2 = s^2 \tag{2.36}$$

The new equation set can be represented as follows:

$$h(\mathbf{x}, \omega) = (\mathbf{x}_k - \mathbf{x}_{k-1})^T \cdot (\mathbf{x}_k - \mathbf{x}_{k-1}) + (\omega_k - \omega_{k-1})^2 - s^2 = 0 \tag{2.37}$$

As the last step, the Jacobian matrix in Newton's Method can be modified as follows:

$$\mathbf{q}_{k+1} = \mathbf{q}_k - \begin{bmatrix} \dfrac{\partial R(\mathbf{x},\omega)}{\partial \mathbf{x}} & \dfrac{\partial R(\mathbf{x},\omega)}{\partial \omega} \\ \dfrac{\partial h(\mathbf{x},\omega)}{\partial \mathbf{x}} & \dfrac{\partial h(\mathbf{x},\omega)}{\partial \omega} \end{bmatrix}^{-1} \cdot \begin{Bmatrix} R(\mathbf{x},\omega) \\ h(\mathbf{x},\omega) \end{Bmatrix} \tag{2.38}$$

### 2.3. Fundamentals of Three-Dimensional Dynamics

#### 2.3.1. Particle Dynamics

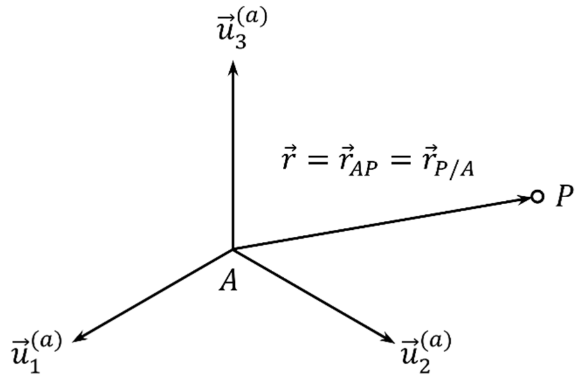


Figure 2.6. Position of a particle with respect to a selected frame [43].

In three dimensional space, the position of $P$ with respect to a suitable frame $F_a$ is shown in Figure (2.6). Origin of the frame $F_a$ is shown with $A$ and basis vectors of $F_a$ can be represented as $u_a = \{\vec{u}_1^{(a)}, \vec{u}_2^{(a)}, \vec{u}_3^{(a)}\}$. Conventionally, orthogonal and right-handed reference frames are preferable. To consider a reference frame as orthogonal, its basis vectors should be perpendicular to each other. To check this property, following scalar multiplication (dot product) is necessary.

$$\vec{u}_i^{(a)} \cdot \vec{u}_j^{(a)} = \delta_{ij} = \begin{cases} 1, \text{ if } i = j \\ 0, \text{ if } i \neq j \end{cases} \tag{2.39}$$

To consider a reference frame as right-handed, following cross products should hold:

$$\left.\begin{aligned}\vec{u}_1^{(a)} \times \vec{u}_2^{(a)} &= \vec{u}_3^{(a)} \\ \vec{u}_2^{(a)} \times \vec{u}_3^{(a)} &= \vec{u}_1^{(a)} \\ \vec{u}_3^{(a)} \times \vec{u}_1^{(a)} &= \vec{u}_2^{(a)}\end{aligned}\right\} \tag{2.40}$$

And the position of $P$ with respect to $F_a$ can be represented as follows:

$$\vec{r} = \vec{r}_{AP} = \vec{u}_1^{(a)} \cdot r_1^{(a)} + \vec{u}_2^{(a)} \cdot r_2^{(a)} + \vec{u}_3^{(a)} \cdot r_3^{(a)} \tag{2.41}$$

$r_i^{(a)}$ represents the $i^{th}$ component of the vector $\vec{r}$ in the reference frame $F_a$. When the basis vectors of the orthogonal and right-handed reference frame are resolved in their own reference frame, the following results are obtained:

$$\left[\vec{u}_1^{(a)}\right]^{(a)} = \overline{u}_1^{(a/a)} = \overline{u}_1 = \begin{bmatrix}1\\0\\0\end{bmatrix},\ \overline{u}_2 = \begin{bmatrix}0\\1\\0\end{bmatrix},\ \overline{u}_3 = \begin{bmatrix}0\\0\\1\end{bmatrix} \tag{2.42}$$

### 2.3.2. Matrix Representations of Vectors

With the aid of computational calculations, instead of using vectors in the calculations, it is more convenient to prefer matrices since they are much easier to implement in the computational environment**.**

#### 2.3.2.1. Column Matrix Representations of Vectors

After expressing a vector with basis vectors of only one frame, the following column matrix can be created.

$$\overline{r}^{(a)} = \left[\vec{r}\right]^{(a)} = \begin{bmatrix} r_1^{(a)} \\ r_2^{(a)} \\ r_3^{(a)} \end{bmatrix} \tag{2.43}$$

This column matrix is a column matrix of vector $\vec{r}$, in the reference frame $F_a$. It is achieved by resolving the vector $\vec{r}$, in the reference frame $F_a$.

#### 2.3.2.2. Relations Between the Vector Operations and Matrices

The dot product of two vectors $\vec{p}$ and $\vec{q}$ can be represented with their elements in the reference frame $F_a$ as follows:

$$s = \vec{p} \cdot \vec{q} = p_1{}^{(a)} \cdot q_1{}^{(a)} + p_2{}^{(a)} \cdot q_2{}^{(a)} + p_3{}^{(a)} \cdot q_3{}^{(a)} \tag{2.44}$$

The same result can be achieved with the following matrix multiplication in the reference frame $F_a$.

$$\left.\begin{aligned} s = \overline{p}^{(a)^t} \cdot \overline{q}^{(a)} = \begin{bmatrix} p_1{}^{(a)} & p_2{}^{(a)} & p_3{}^{(a)} \end{bmatrix} \cdot \begin{bmatrix} q_1{}^{(a)} \\ q_2{}^{(a)} \\ q_3{}^{(a)} \end{bmatrix} \\ s = \overline{q}^{(a)^t} \cdot \overline{p}^{(a)} = \begin{bmatrix} q_1{}^{(a)} & q_2{}^{(a)} & q_3{}^{(a)} \end{bmatrix} \cdot \begin{bmatrix} p_1{}^{(a)} \\ p_2{}^{(a)} \\ p_3{}^{(a)} \end{bmatrix} \end{aligned}\right\} \tag{2.45}$$

The cross product of two vectors $\vec{p}$ and $\vec{q}$ can be represented with their elements in the reference frame $F_a$ as follows:

$$\vec{r} = \vec{p} \times \vec{q};\ \overline{r}^{(a)} = \begin{bmatrix} p_2{}^{(a)} \cdot q_3{}^{(a)} - p_3{}^{(a)} \cdot q_2{}^{(a)} \\ p_3{}^{(a)} \cdot q_1{}^{(a)} - p_1{}^{(a)} \cdot q_3{}^{(a)} \\ p_1{}^{(a)} \cdot q_2{}^{(a)} - p_2{}^{(a)} \cdot q_1{}^{(a)} \end{bmatrix} \tag{2.46}$$

The same result can be achieved with the following matrix multiplication in the reference frame $F_a$.

$$\overline{r}^{(a)} = \tilde{p}^{(a)} \cdot \overline{q}^{(a)} = \begin{bmatrix} 0 & -p_3{}^{(a)} & p_2{}^{(a)} \\ p_3{}^{(a)} & 0 & -p_1{}^{(a)} \\ -p_2{}^{(a)} & p_1{}^{(a)} & 0 \end{bmatrix} \cdot \begin{bmatrix} q_1{}^{(a)} \\ q_3{}^{(a)} \\ q_3{}^{(a)} \end{bmatrix} \tag{2.47}$$

The $\tilde{p}^{(a)}$ matrix is called the cross-product matrix and it is skew-symmetric.

### 2.3.3. Rodrigues Formula and Rotation Matrix

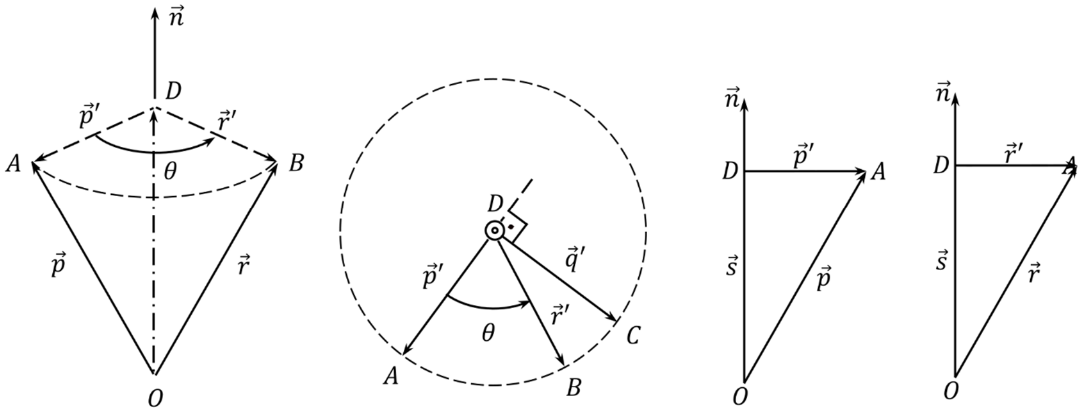


Figure 2.7. Rotation of a vector around an arbitrary axis[43].

In the figure above, the vector $\vec{p}$ turns into a vector $\vec{r}$ with the rotation angle of $\theta$ around a unit vector $\vec{n}$. During the rotation, vector $\vec{p}$ follows a conical path and a top view is depicted on the right side. From this figure, the following equations can be written:

$$\left.\begin{aligned} &\vec{p}^{'} = \vec{p} - \vec{s},\ \vec{r}^{'} = \vec{r} - \vec{s} \\ &\vec{s} = (\vec{p}\cdot\vec{n})\vec{n} = \vec{n}(\vec{n}\cdot\vec{p}) \\ &\vec{q}^{'} = \vec{n}\times\vec{p}^{'} = \vec{n}\times\left(\vec{p} - (\vec{p}\cdot\vec{n})\cdot\vec{n}\right) \end{aligned}\right\} \tag{2.48}$$

And the vector $\vec{r}^{'}$ can be obtained through planar equations:

$$\vec{r}^{'} = \vec{p}^{'}\cdot\cos(\theta) + \vec{q}^{'}\cdot\sin(\theta) \tag{2.49}$$

Inserting Equation (2.47) into the Equation (2.48) will result as follows:

$$\left.\begin{aligned} &\vec{r} - \vec{s} = (\vec{p} - \vec{s})\cdot\cos(\theta) + (\vec{n}\times\vec{p})\cdot\sin(\theta) \\ &\vec{r} = \vec{p}\cdot\cos(\theta) + (\vec{n}\times\vec{p})\cdot\sin(\theta) + \vec{s}\cdot(1-\cos(\theta)) \\ &\vec{r} = \vec{p}\cdot\cos(\theta) + (\vec{n}\times\vec{p})\cdot\sin(\theta) + \vec{n}(\vec{n}\cdot\vec{p})\cdot(1-\cos(\theta)) \end{aligned}\right\} \tag{2.50}$$

The last row of the Equation (2.49) is known as Rodrigues Formula. In matrix form, in an orthogonal and right-handed reference frame $F_a$, this formula can be expressed as follows:

$$\overline{r}^{(a)} = \overline{p}^{(a)} \cdot \cos(\theta) + \left(\tilde{n}^{(a)} \overline{p}^{(a)}\right) \cdot \sin(\theta) + \overline{n}^{(a)} \cdot \left(\overline{n}^{(a)^t} \cdot \overline{p}^{(a)}\right) \cdot \left(1 - \cos(\theta)\right) \quad (2.51)$$

One can collect the column matrix $\overline{p}^{(a)}$ out of the equation. Since the multiplication $\overline{n}^{(a)} \cdot \overline{n}^{(a)^t}$ and the cross product matrix have the size of $3 \times 3$, an identity matrix with the size of $3 \times 3$ should be replaced after $\overline{p}^{(a)}$ is collected:

$$\begin{aligned} \overline{r}^{(a)} &= \left(\hat{I} \cdot \cos(\theta) + \tilde{n}^{(a)} \cdot \sin(\theta) + \overline{n}^{(a)} \cdot \overline{n}^{(a)^t} \cdot \left(1 - \cos(\theta)\right)\right) \cdot \overline{p}^{(a)} \\ \overline{r}^{(a)} &= \hat{R}^{(a)} \cdot \overline{p}^{(a)} \end{aligned} \quad (2.52)$$

$\hat{R}^{(a)}$ is called the rotation matrix and it is expressed in the reference frame $F_a$. When the rotation is around the basis vectors of the reference frame $F_a$, the following rotation matrices are obtained:

$$\begin{aligned} &\vec{n} = \vec{u}_1^{(a)};\ \overline{n}^{(a)} = \overline{u}_1^{(a/a)} = \begin{bmatrix} 1 & 0 & 0 \end{bmatrix}^t \\ &\hat{R}_1^{(a)} = \left(\hat{I} \cdot \cos(\theta) + \tilde{u}_1 \cdot \sin(\theta) + \overline{u}_1 \cdot \overline{u}_1^{\,t} \cdot \left(1 - \cos(\theta)\right)\right) \\ &\hat{R}_1^{(a)} = \begin{bmatrix} 1 & 0 & 0 \\ 0 & \cos(\theta) & -\sin(\theta) \\ 0 & \sin(\theta) & \cos(\theta) \end{bmatrix} \end{aligned} \quad (2.53)$$

With the same idea transformation matrix of other basis vectors can be calculated:

$$\vec{n} = \vec{u}_2^{(a)};\ \bar{n}^{(a)} = \bar{u}_2^{(a/a)} = \begin{bmatrix} 0 & 1 & 0 \end{bmatrix}^t$$
$$\hat{R}_2^{(a)} = \left(\hat{I} \cdot \cos(\theta) + \tilde{u}_2 \cdot \sin(\theta) + \bar{u}_2 \cdot \bar{u}_2^{\,t} \cdot \left(1 - \cos(\theta)\right)\right)$$
$$\hat{R}_2^{(a)} = \begin{bmatrix} \cos(\theta) & 0 & \sin(\theta) \\ 0 & 1 & 0 \\ -\sin(\theta) & 0 & \cos(\theta) \end{bmatrix} \tag{2.54}$$

Rotation matrix of the rotation around the last basis vector of $F_a$ in the $F_a$ is:

$$\vec{n} = \vec{u}_3^{(a)};\ \bar{n}^{(a)} = \bar{u}_3^{(a/a)} = \begin{bmatrix} 0 & 0 & 1 \end{bmatrix}^t$$
$$\hat{R}_3^{(a)} = \left(\hat{I} \cdot \cos(\theta) + \tilde{u}_3 \cdot \sin(\theta) + \bar{u}_3 \cdot \bar{u}_3^{\,t} \cdot \left(1 - \cos(\theta)\right)\right)$$
$$\hat{R}_3^{(a)} = \begin{bmatrix} \cos(\theta) & -\sin(\theta) & 0 \\ \sin(\theta) & \cos(\theta) & 0 \\ 0 & 0 & 1 \end{bmatrix} \tag{2.55}$$

If these rotation matrices define the rotation between two frames $F_a$ and $F_b$ they are written as $\hat{C}^{(a,b)}$.

## CHAPTER 3

# TWO-DIMENSIONAL MATHEMATICAL MODELING OF HORIZONTAL DRUM TYPE WASHING MACHINES

### 3.1. Mathematical Model

A two-dimensional dynamic model for washing machine drum is developed considering resilient elements as shown in Figure (3.1a). Points $1-4$ and $f_1 - f_4$ indicates the connection points of springs and dampers. To better analyze the motion, the sketch of the exaggerated view of motion is shown in Figure (3.1b). In the equation of motion, $x, y$ and $\theta$ are used as generalized coordinates, which are displacements with respect to the origin and the rotation of the drum, respectively. Throughout the study, the cabinet is assumed as fixed.

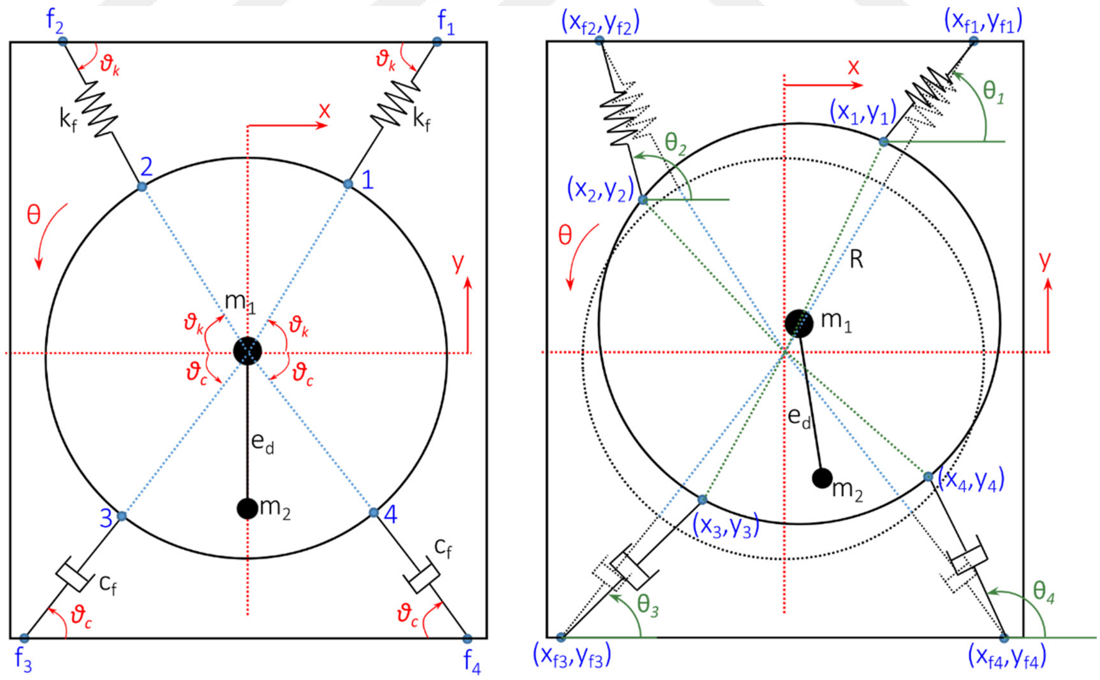


Figure 3.1. Two-dimensional dynamical model and exaggerated view of the motion.

To write down the equation of motion, position and velocities at the connection points of the resilient elements should be defined. Related position and angle variables are as follows:

$$\left.\begin{aligned} x_1 = r\cdot\cos(\theta_k+\theta)+x,\ y_1 = r\cdot\sin(\theta_k+\theta)+y \\ x_2 = r\cdot\cos(\pi-\theta_k+\theta)+x,\ y_2 = r\cdot\sin(\pi-\theta_k+\theta)+y \\ x_3 = r\cdot\cos(\pi+\theta_c+\theta)+x,\ y_3 = r\cdot\sin(\pi+\theta_c+\theta)+y \\ x_4 = r\cdot\cos(-\theta_c+\theta)+x,\ y_4 = r\cdot\sin(-\theta_c+\theta)+y \end{aligned}\right\} \tag{3.1}$$

$$\left.\begin{aligned} x_{f1} = (r+k_f)\cdot\cos(\theta_k),\ y_{f1} = (r+k_f)\cdot\sin(\theta_k) \\ x_{f2} = (r+k_f)\cdot\cos(\pi-\theta_k),\ y_{f2} = (r+k_f)\cdot\sin(\pi-\theta_k) \\ x_{f3} = (r+c_f)\cdot\cos(\pi+\theta_c),\ y_{f3} = (r+c_f)\cdot\sin(\pi+\theta_c) \\ x_{f4} = (r+c_f)\cdot\cos(-\theta_c),\ y_{f4} = (r+c_f)\cdot\sin(-\theta_c) \end{aligned}\right\} \tag{3.2}$$

$$\left.\begin{aligned} \theta_1 = atan_2(y_{f1}-y_1, x_{f1}-x_1) \\ \theta_2 = atan_2(y_{f2}-y_2, x_{f2}-x_2) \\ \theta_3 = atan_2(y_3-y_{f3}, x_3-x_{f3}) \\ \theta_4 = atan_2(y_4-y_{f4}, x_4-x_{f4}) \end{aligned}\right\} \tag{3.3}$$

With this information, one can write forces on the springs;

$$\left.\begin{aligned} F_{k1} = k\cdot\left(\sqrt{(x_{f1}-x_1)^2+(y_{f1}-y_1)^2}-k_f\right) \\ F_{k2} = k\cdot\left(\sqrt{(x_{f2}-x_2)^2+(y_{f2}-y_2)^2}-k_f\right) \end{aligned}\right\} \tag{3.4}$$

To describe forces on the dampers, velocities of the endpoints of the resilient elements are necessary. Since the cabinet side is assumed as fixed, describing the drum side is sufficient.

$$\left.\begin{aligned} \dot{x}_3 = -r\cdot\sin(\pi+\theta_c+\theta)\cdot\dot{\theta}+\dot{x},\ \dot{y}_3 = r\cdot\cos(\pi+\theta_c+\theta)\cdot\dot{\theta}+\dot{y} \\ \dot{x}_4 = -r\cdot\sin(-\theta_c+\theta)\cdot\dot{\theta}+\dot{x},\ \dot{y}_4 = r\cdot\cos(-\theta_c+\theta)\cdot\dot{\theta}+\dot{y} \end{aligned}\right\} \tag{3.5}$$

Projections of the velocities along the instantaneous direction of dampers are as follows:

$$\left.\begin{aligned} v_3 &= \dot{x}_3 \cdot \cos(\theta_3) + \dot{y}_3 \cdot \sin(\theta_3) \\ v_4 &= \dot{x}_4 \cdot \cos(\theta_4) + \dot{y}_4 \cdot \sin(\theta_4) \end{aligned}\right\} \tag{3.6}$$

Forces on the dampers are:

$$\left.\begin{aligned} F_{c3} &= -c \cdot v_3 \\ F_{c4} &= -c \cdot v_4 \end{aligned}\right\} \tag{3.7}$$

The equation of motion is to be written in generalized coordinates. Therefore, $x$ and $y$ components of forces and moments of these forces are also necessary.

$$\begin{aligned} &\left.\begin{aligned} F_{k1x} &= F_{k1} \cdot \cos(\theta_1),\ F_{k1y} = F_{k1} \cdot \sin(\theta_1) \\ F_{k2x} &= F_{k2} \cdot \cos(\theta_2),\ F_{k2y} = F_{k2} \cdot \sin(\theta_2) \\ F_{c3x} &= F_{c3} \cdot \cos(\theta_3),\ F_{c3y} = F_{c3} \cdot \sin(\theta_3) \\ F_{c4x} &= F_{c4} \cdot \cos(\theta_4),\ F_{c4y} = F_{c4} \cdot \sin(\theta_4) \end{aligned}\right\} \\ &\left.\begin{aligned} M_1 &= (x_1 - x) \cdot F_{k1y} - (y_1 - y) \cdot F_{k1x} \\ M_2 &= (x_2 - x) \cdot F_{k2y} - (y_2 - y) \cdot F_{k2x} \\ M_3 &= (x_3 - x) \cdot F_{c3y} - (y_3 - y) \cdot F_{c3x} \\ M_4 &= (x_4 - x) \cdot F_{c4y} - (y_4 - y) \cdot F_{c4x} \end{aligned}\right\} \end{aligned} \tag{3.8}$$

At this point equation of motion for three degrees of freedom system can be written:

$$\begin{aligned} \sum F_x &= (m_1 + m_2) \cdot \ddot{x} = F_{k1x} + F_{k2x} + F_{c3x} + F_{c4x} + m_2 e\omega^2 \cdot \sin(\omega \cdot t) \\ \sum F_y &= (m_1 + m_2) \cdot \ddot{y} = F_{k1y} + F_{k2y} + F_{c3y} + F_{c4y} + m_2 e\omega^2 \cdot \cos(\omega \cdot t) \\ \sum M &= (J_1 + m_2 \cdot e) \cdot \ddot{\theta} = M_1 + M_2 + M_3 + M_4 \end{aligned} \tag{3.9}$$

If the small-angle assumption was made the equation of motion would be as follows:

$$\begin{aligned} (m_1 + m_2) \cdot \ddot{x} + 2c \cdot \cos(\theta_c) \cdot \dot{x} + 2k \cdot \cos(\theta_k) \cdot x &= m_2 e\omega^2 \cdot \sin(\omega \cdot t) \\ (m_1 + m_2) \cdot \ddot{y} + 2c \cdot \sin(\theta_c) \cdot \dot{y} + 2k \cdot \sin(\theta_k) \cdot y &= m_2 e\omega^2 \cdot \cos(\omega \cdot t) \end{aligned} \tag{3.10}$$

Of course, the system can only be modeled with two degrees of freedom with the small-angle assumption, i.e. neglecting $\theta$ and decoupling $x$ and $y$ coordinates. The linear and nonlinear equation of motion for the system are solved with the methods described in the methodology section.

### 3.2. Results and Discussion

In the solution, all forces are represented by utilizing eight harmonics and sample results obtained are given in Fig. (3.2-3.5). Parameters used in this chapter are given in Table 2 unless otherwise specified.

Table 3.1. Numerical values for 2D system.

| | | | |
|---|---|---|---|
| $m_1$ | $40\ kg$ | $R$ | $300\ mm$ |
| $m_2$ | $6\ kg$ | $k$ | $4000\ N/m$ |
| $J_1$ | $1.25\ Nm^2 + m_2 \cdot e_d^{\ 2}$ | $c$ | $200\ Ns/m$ |
| $e_d$ | $100\ mm$ | $k_d$ | $4000\ N/m$ |
| $\theta_k$ | $45^o$ | $\mu N$ | $100\ N$ |
| $\theta_c$ | $45^o$ | $L_i$ | $500\ mm$ |

It is clearly observed in Figure (3.3) that, there is a 25% difference between the results of linear and nonlinear systems. Secondly, solving with just one harmonic gives almost the same result with the solution with eight harmonics. Thirdly, vertical forces at high frequencies overcome the weight of the machine and friction force between washing machine and ground becomes not large enough to hold the washing machine stationary. As a result, since the horizontal forces on the cabinet are much higher than the friction force between the cabinet and the floor; it leads to walking motion. To prevent excessive forces at high frequencies, dry friction dampers are introduced instead of viscous dampers. As a first step, a case study is done to dedicate how many harmonics are enough and necessary to express the total solution. The result is depicted in Figures (3.6 & 3.7) and again, only one harmonic is enough, moreover, the dry friction damper model has an analytical solution for the single harmonic representation and it will drastically improve the computational effort.

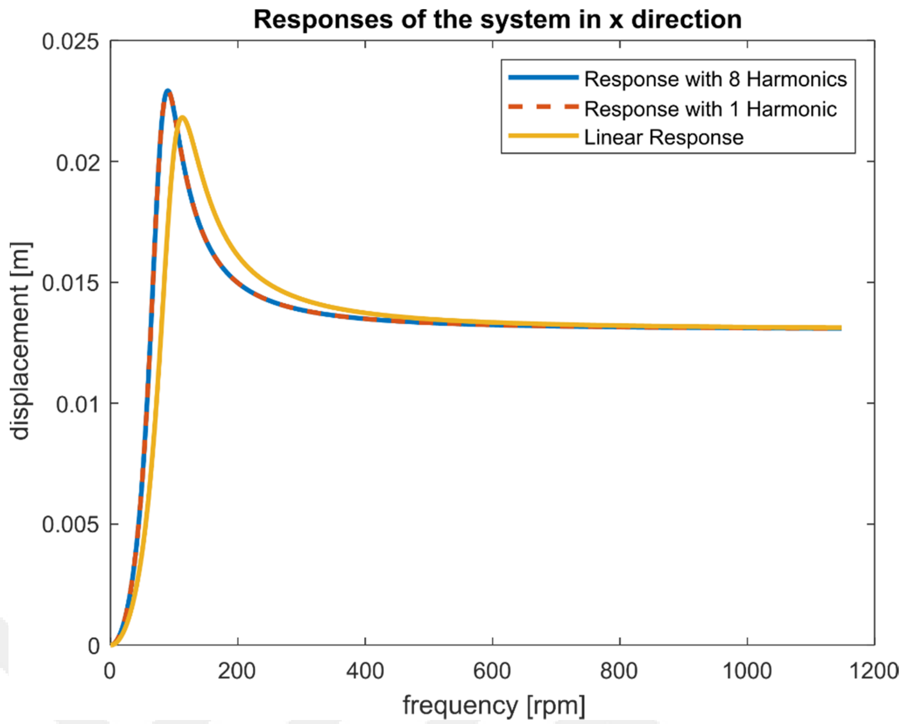


Figure 3.2 A case study with viscous dampers, $\theta_k \neq \theta_c \neq 45^o$ . Response in x direction.

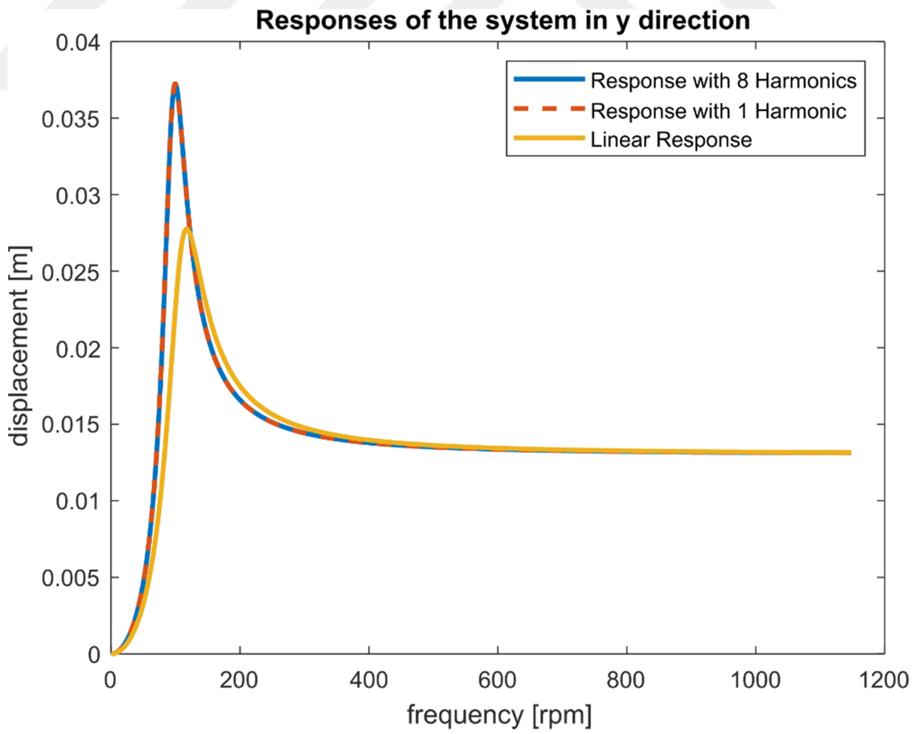


Figure 3.3. A case study with viscous dampers, $\theta_k \neq \theta_c \neq 45^o$ . Response in y direction.

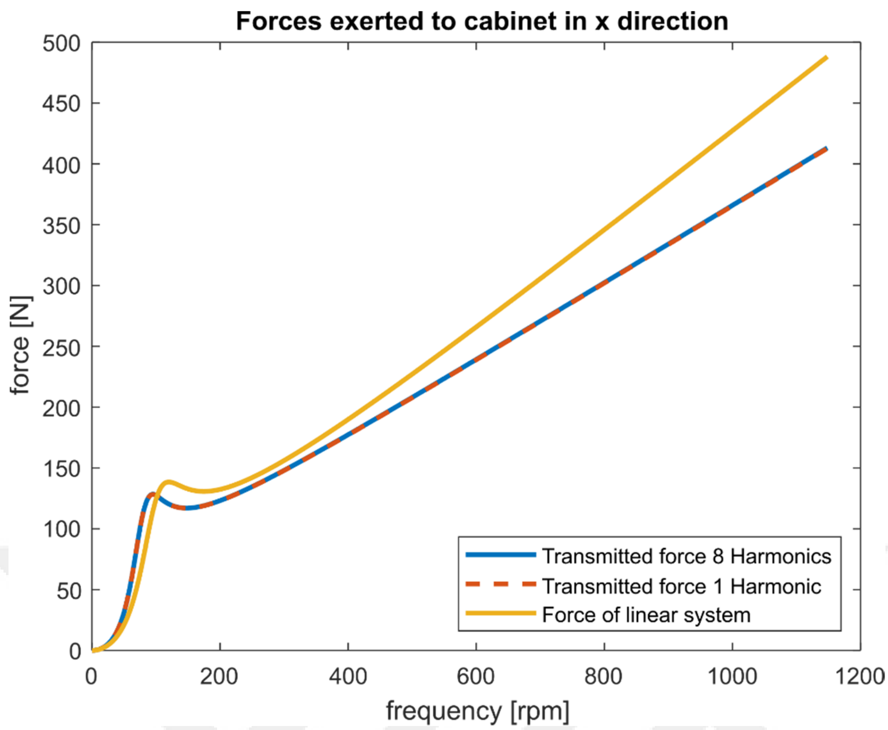


Figure 3.4 A case study with viscous dampers, $\theta_k \neq \theta_c \neq 45^o$ . Transmitted force in x direction.

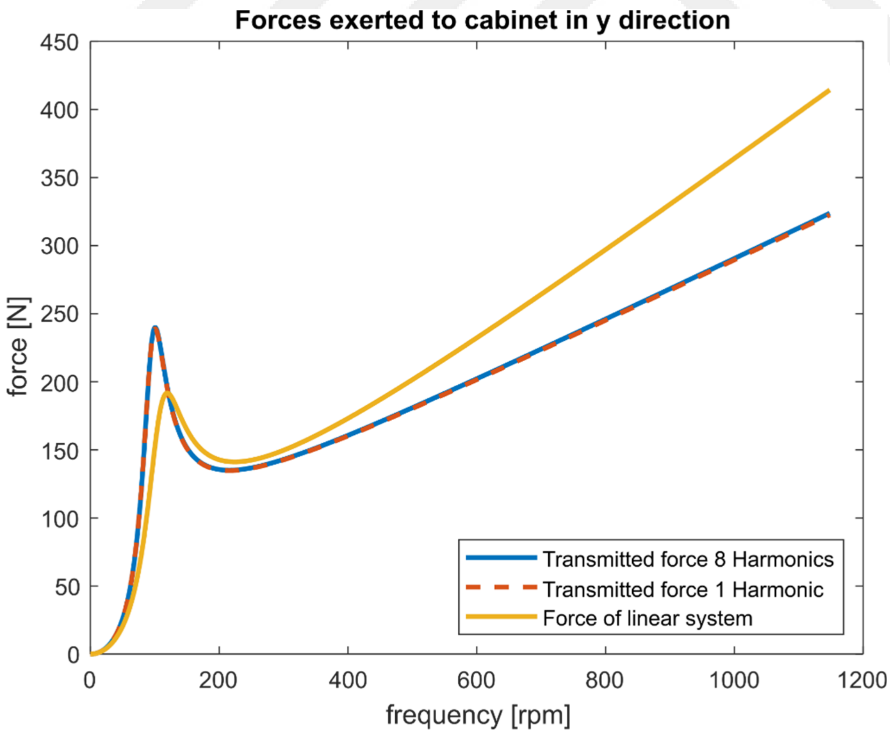


Figure 3.5. A case study with viscous dampers, $\theta_k \neq \theta_c \neq 45^o$ . Transmitted force in y direction.

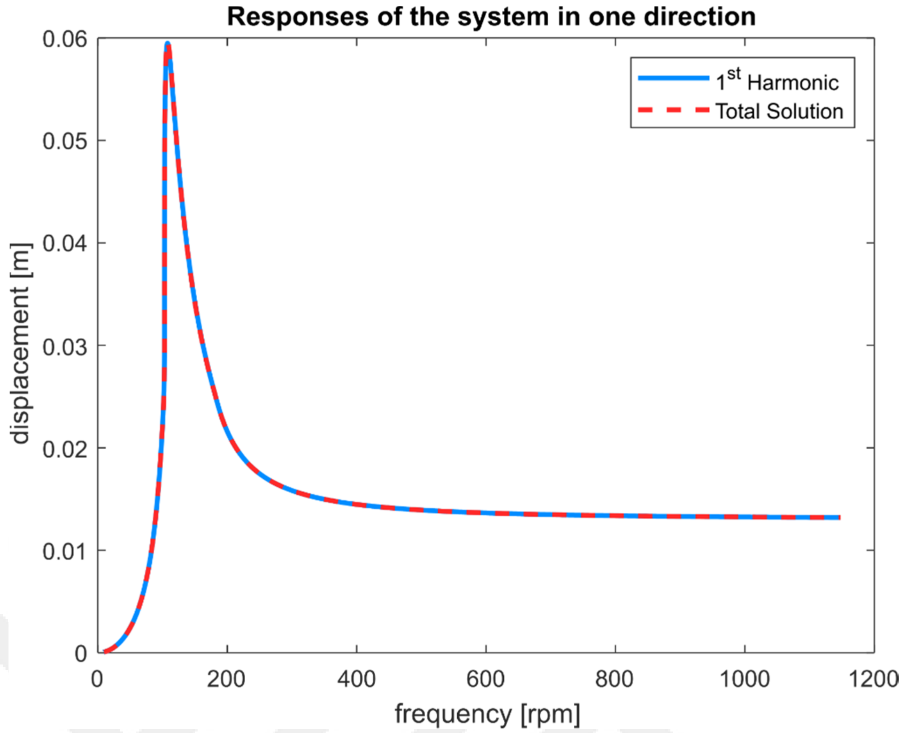


Figure 3.6 Effect of the first harmonic, dry friction case.

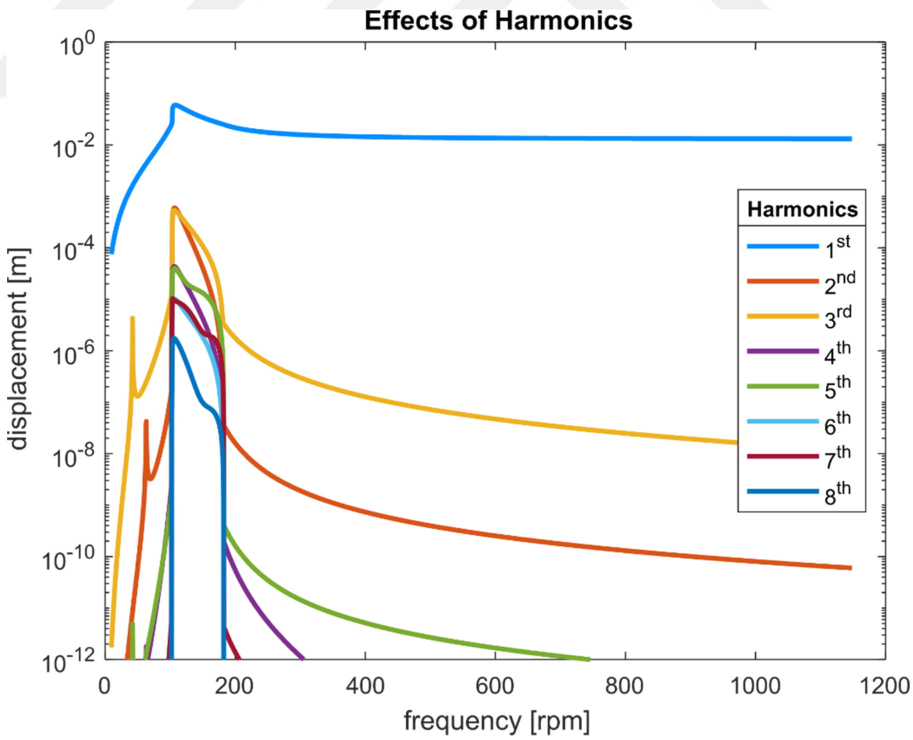


Figure 3.7. Effect of eight harmonics, dry friction case.

Results for both systems with viscous or dry friction dampers obey the expectations of the rotating unbalance excitation. FRF graph starts from zero and converges to $me/M$ as the frequency goes to infinity. When the frequency is low or high, forces acting on the dry friction dampers are too small to move them; therefore, they are acting like springs and at all frequencies but resonant frequencies, the system acts like it has only four springs. Around the natural frequency of the drum, dry friction dampers start working and drastically decrease the amplitude of vibrations, as expected. It is clearly seen that from Figure (3.4), for higher frequencies the vertical and horizontal forces settles to a low value compared to viscous dampers in which case they increase as frequency increases.

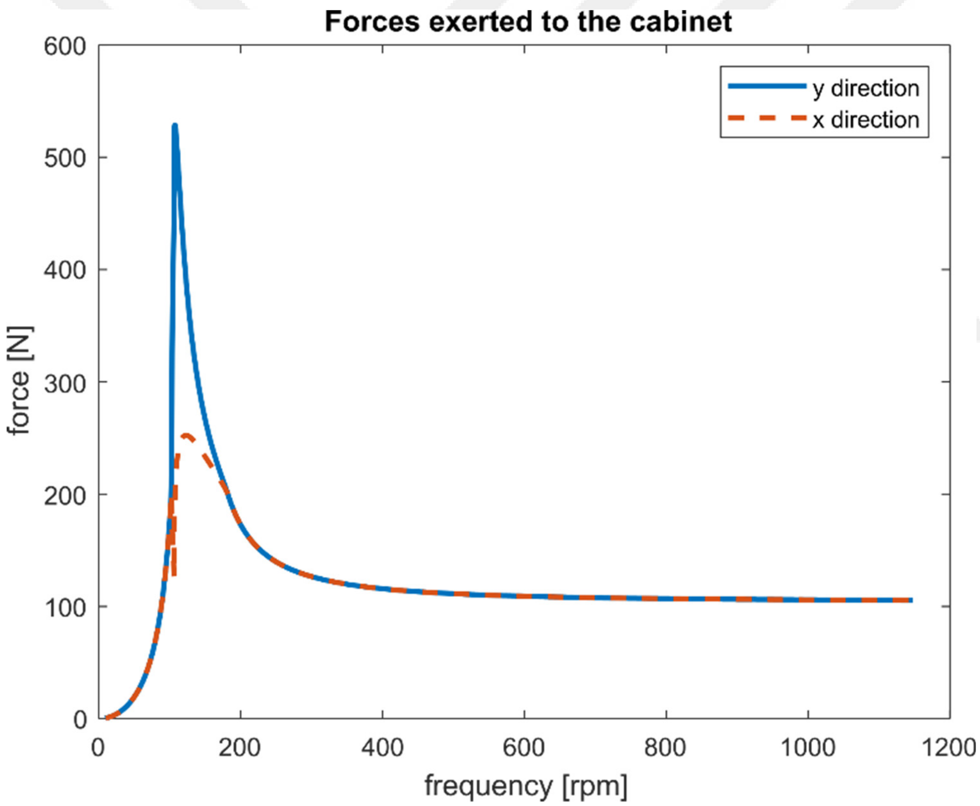


Figure 3.8. A case study with orientation angles different from 45 degrees with dry friction dampers.

Selecting a dry friction damper with a low slip load, $\mu N$, significantly decreases the transmitted force to the cabinet at the spinning cycle; however, it increases the displacement of the drum and the transmitted force to the cabinet at the frequencies close to the natural frequency, compared to viscous dampers. This engineering trade-off is clearly seen by comparing Figures (3.4 & 3.5) and (3.8). At this point, observing effects of the spring constant of dry friction and slip load are vital, however; they will be taken into consideration after analyzing the effects of orientation angles of springs and dampers.

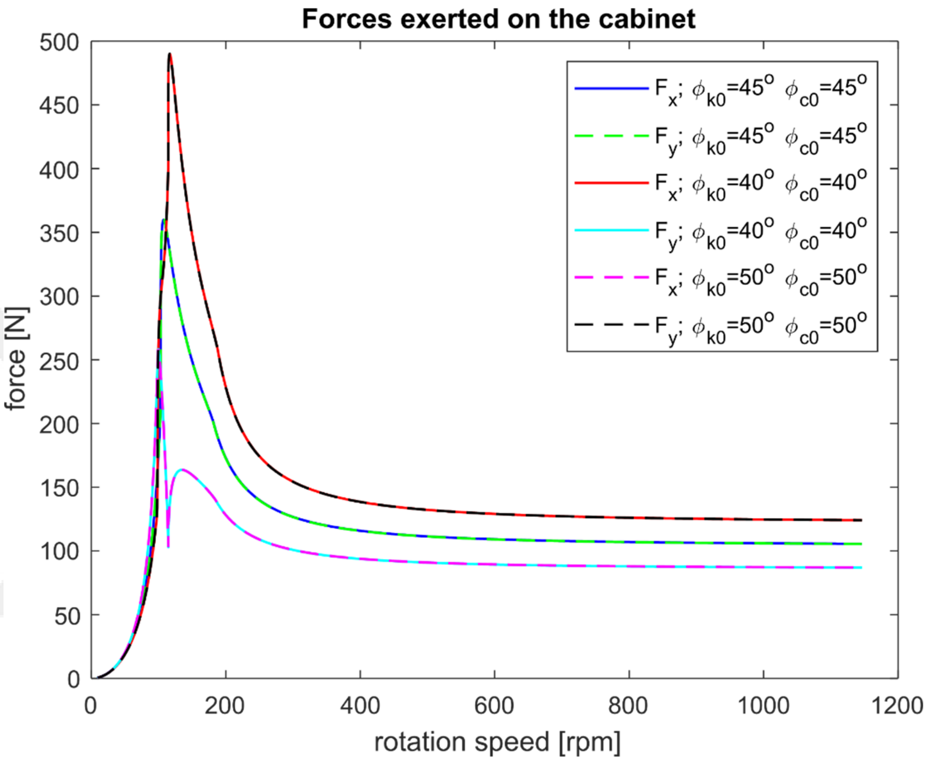


Figure 3.9. Effect of orientation angles in the transmitted force, first case study.

It is expected to have a correlation between orientation angles and transmitted forces to the cabinet. As depicted in Figures (3.9-3.12), orientation angles have a direct effect on the transmitted force in $x$ and $y$ directions when the amplitude of the oscillations is high; however, they do not affect the spinning cycle process as observed from Figures (3.9-3.12). When $\theta_k$ and $\theta_c$ are selected as $45^o$, complete symmetry is produced throughout both $x$ and $y$ directions and total transmitted force in $x$ and $y$ direction becomes the same, as expected. Changing the orientation angles of springs and dry friction dampers inversely, lead to considerable differences in terms of transmitted force to the cabinet in $x$ and $y$ directions. However, the total transmitted force is almost the same in the whole frequency range as seen from Fig. (3.12).

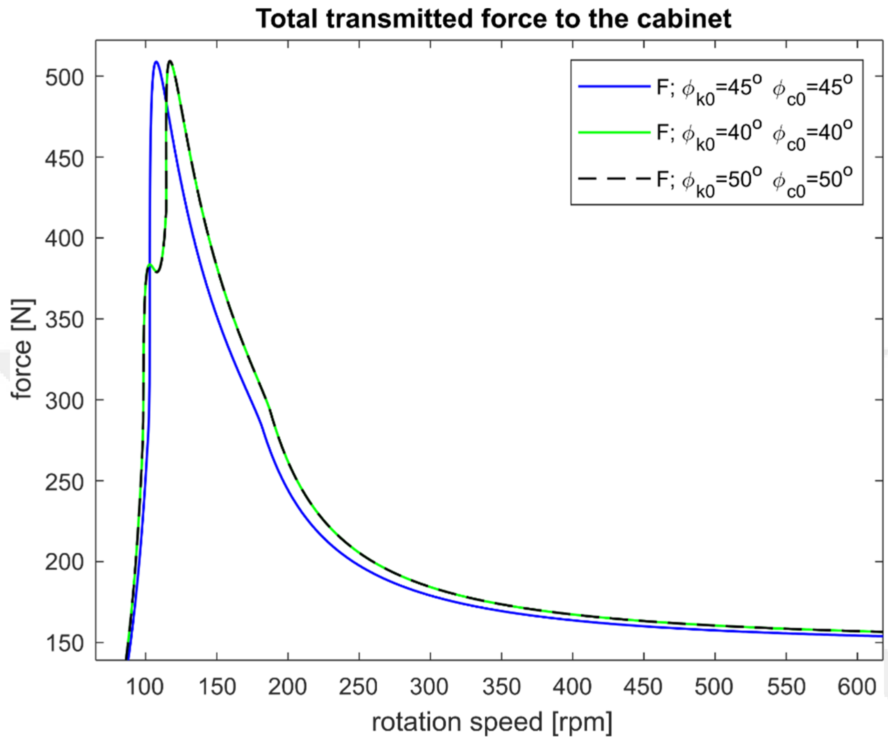


Figure 3.10. Effect of orientation angles in the total transmitted force, first case study.

Changing the orientation angles of the springs and dry friction dampers in the same direction increase the total nonlinearity of the system. At limiting cases, it is equal to attaching components only in $x$ or $y$ directions, which is not feasible. In Figures (3.9 & 3.10), similar results with inversely changing orientation angles are given. In this case, there is a significant difference between transmitted forces in x and y directions. However, the resultant force exerted to the cabinet is almost the same for all operating frequency range. When studying Figure (3.10), it is clearly seen that, even if the total transmitted forces are the same for three cases, their directions are not the same.

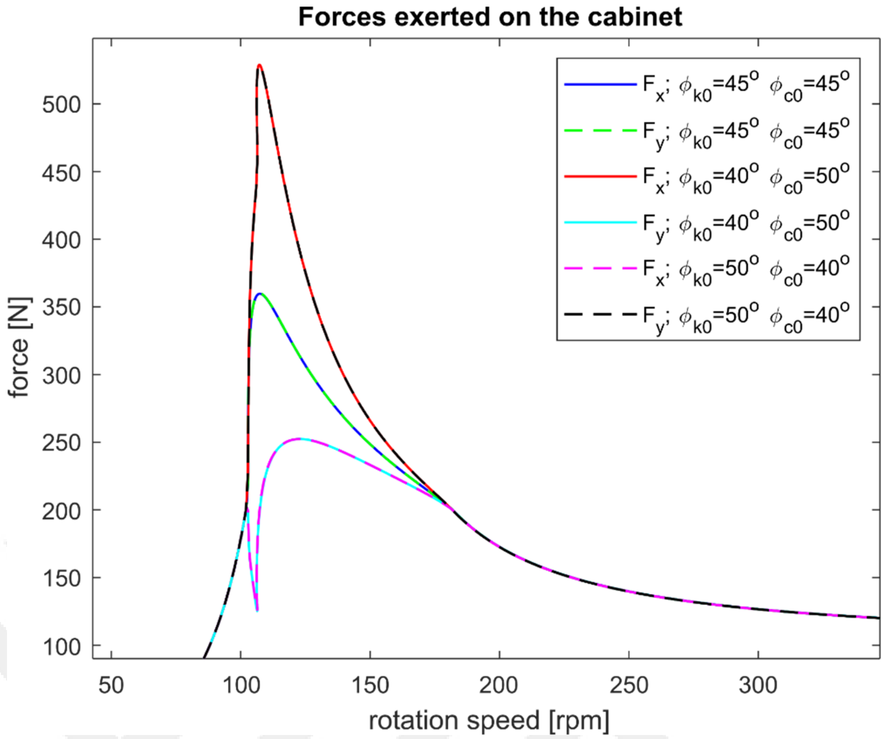


Figure 3.11 Effect of orientation angles in the transmitted force, second case study.

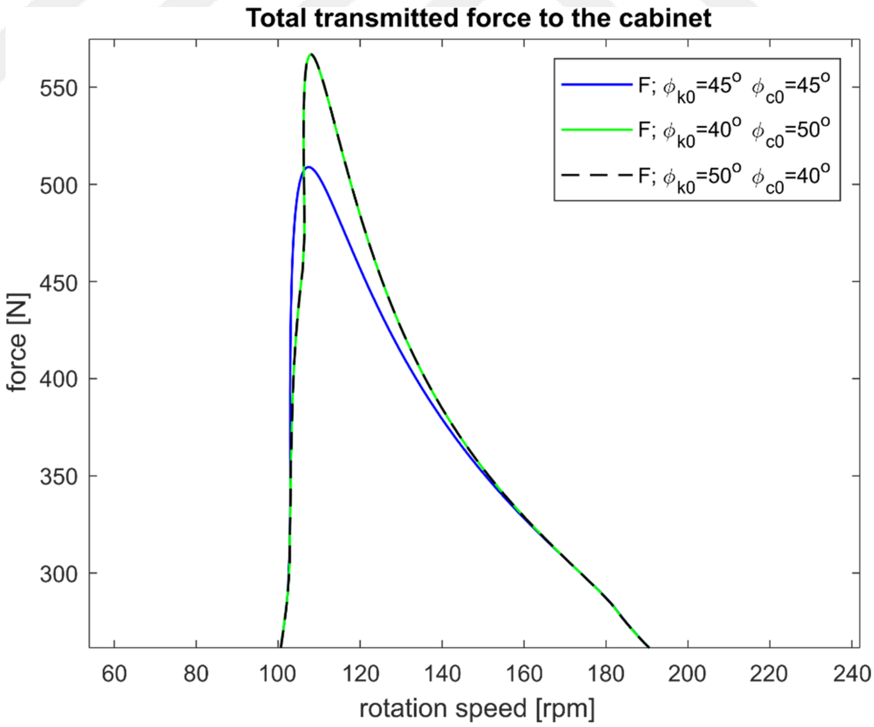


Figure 3.12. Effect of orientation angles in the total transmitted force, second case study.

Choosing both of the implementation angles as $45^o$ have many advantages. It provides the minimum resultant force exerted to the cabinet; moreover, it results in the distribution of the resultant force evenly, which definitely prolongs the cabinet's life. It prevents nonlinearities in transmitted forces and in displacements as observed from Fig. (3.9-3.12). For some special cases, manufacturers may want to have different magnitudes of forces in $x$ and $y$ direction; however, in this thesis minimizing total resultant force is considered and $45^o$ is selected as the best orientation for the springs and dampers.

At this point, final parameters to be considered are the spring stand slip load of the dry friction dampers to minimize force acting on the cabinet. Dry friction damper starts to apply a constant force to the drum whenever the displacement gets larger. The value of the slip load becomes an important parameter for the low frequencies. However; in the spinning cycle, the total displacement of the drum is not enough to cause a slip in the dry friction damper. Therefore, slip load loses its effect on the transmitted force to the cabinet and contact stiffness $k$ becomes the important parameter for high frequencies. Selecting both of them as small as possible leads to minimum transmitted force to the cabinet as observed from Figures (3.13 & 3.14), but it will create large displacements that are not feasible. The amplitude of the displacement becomes a physical constraint in this problem and throughout an optimization process, it has to be taken into consideration.

In Figures (3.15 & 3.16), it is clearly seen that lower slip loads decrease the transmitted force to the cabinet around the resonance frequency and increase the total displacement of the drum. However, making the dry friction force very small causes the drum to vibrate in an asymmetrical way with different vibration amplitudes in $x$ and $y$ directions. It is also observed that lower spring constant values decrease the transmitted force to the cabinet in the spinning cycle. However, this leads to higher vibration amplitudes during the washing process, i.e. <400 rpm.

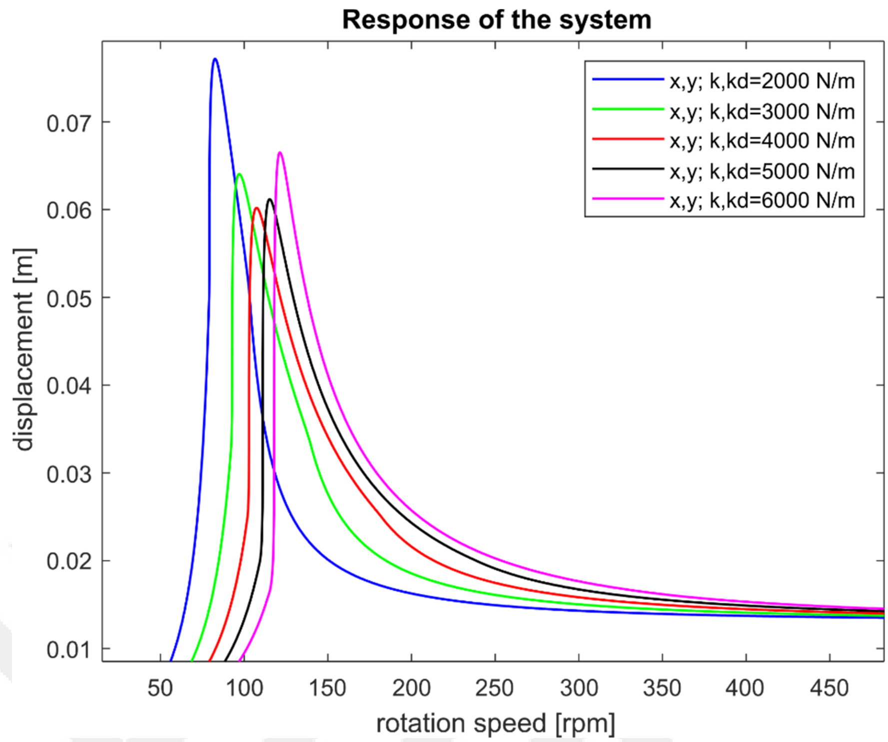


Figure 3.13 Effect of spring constants in the displacement.

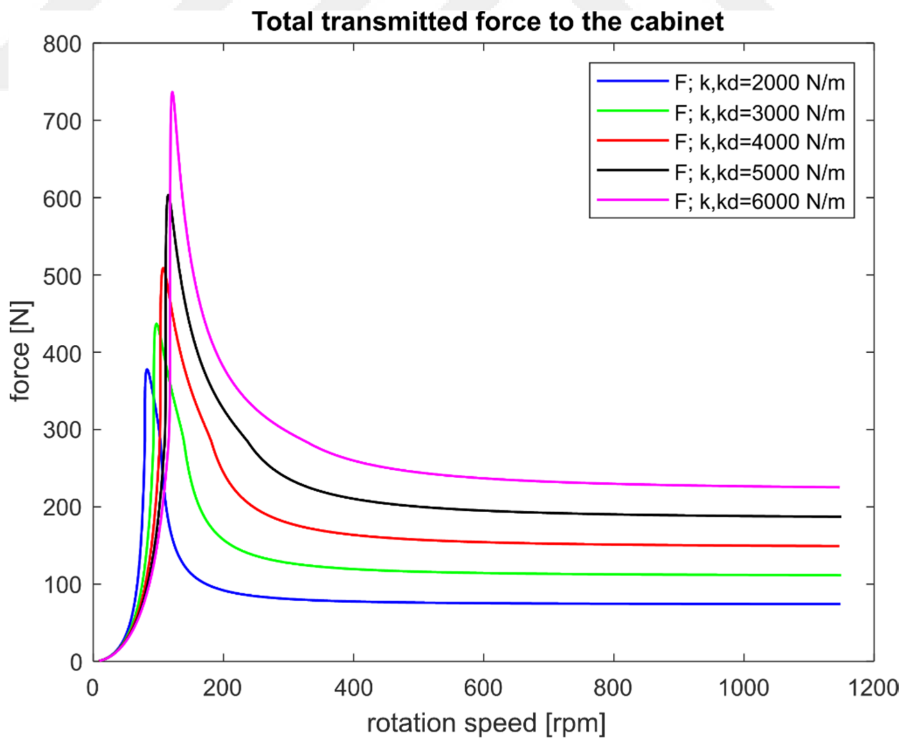


Figure 3.14. Effect of spring constants in the total transmitted force.

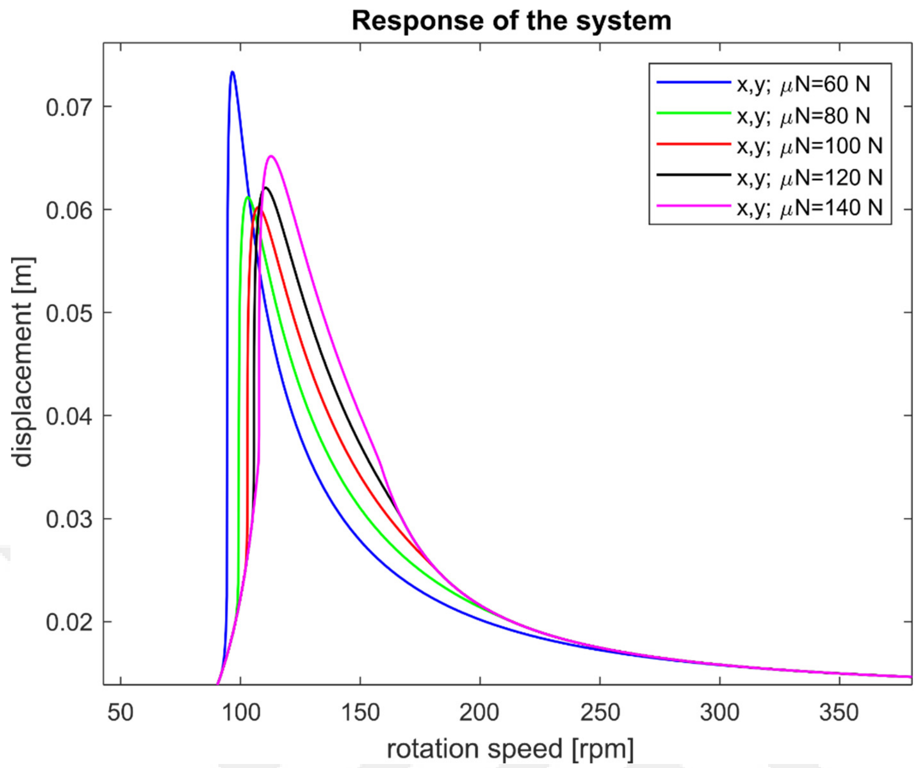


Figure 3.15 Effect of the slip load in the response.

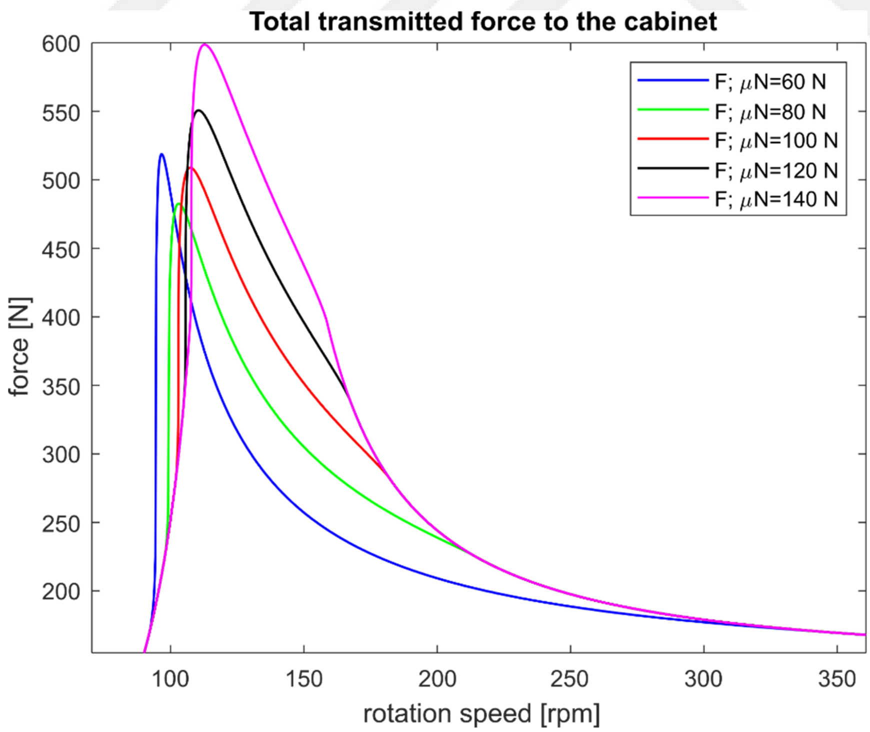


Figure 3.16. Effect of the slip load in the total transmitted force.

In Figure (3.17) the effect of slip load on the maximum of the total transmitted force is analyzed while all other parameters remain constant.

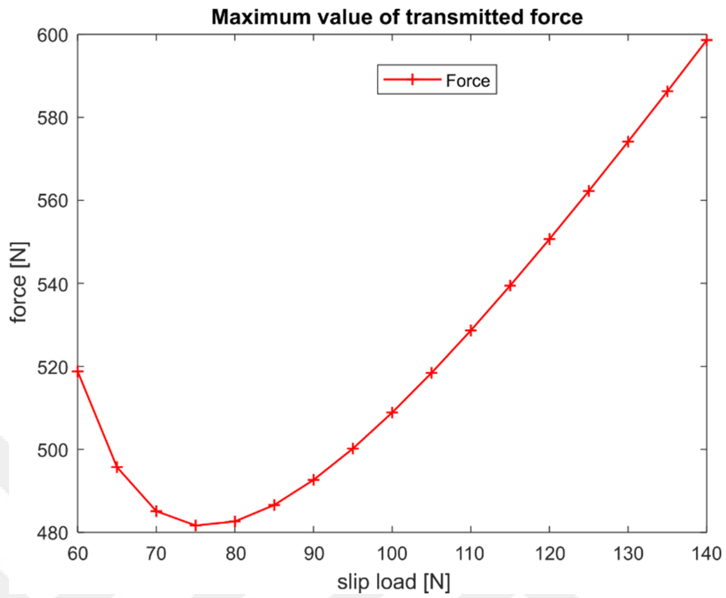


Figure 3.17. Effect of the slip load in the total transmitted force, grid study.

In Figure (3.18), mainly stick response, mainly stuck response and an average response is analyzed for dry friction dampers.

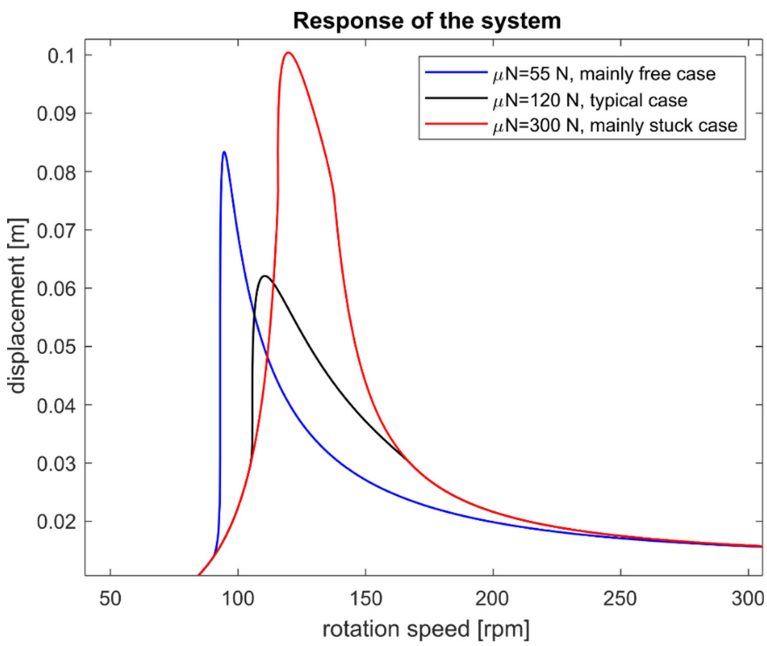


Figure 3.18. Dry friction damper free response, stuck response, and a typical case.

CHAPTER 4

# THREE-DIMENSIONAL MATHEMATICAL MODELING OF HORIZONTAL DRUM TYPE WASHING MACHINES

## 4.1. Mathematical Model

Three-dimensional six degrees of freedom mathematical model is developed for the drum of the horizontal type washing machines in this chapter. The only assumption made is that the cabinet remains fixed, and this assumption causes an increase in the forces on the resilient elements that are also transmitted to the cabinet. The most common dynamical model of the horizontal drum type washing machines is depicted in Figure (4.1). An inertial reference frame $F_0$ is placed at the geometrical center of the washing machine, and a non-inertial reference frame $F_d$ is placed on the center of the drum. When there is no motion, two reference frames are coincident as shown in Figure (4.1).

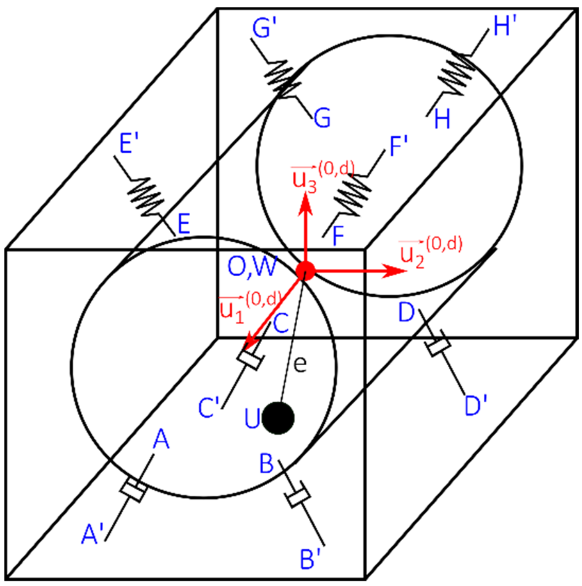


Figure 4.1. Isometric view of the dynamical model of a horizontal drum type washing machine.

Initial-Frame-Based (IFB) 1-2-3 sequence is used to describe the transformation between the inertial and the non-inertial frames. The transformation matrix $\hat{C}^{(0,d)}$ is created by using the Rodrigues' rotation formula as follows:

$$\hat{C}^{(0,d)} = \hat{R}_1^{(a/a)}(\theta_1)\cdot\hat{R}_2^{(a/a)}(\theta_2)\cdot\hat{R}_3^{(a/a)}(\theta_3) = \begin{bmatrix} c_{11} & c_{12} & c_{13} \\ c_{21} & c_{22} & c_{23} \\ c_{31} & c_{32} & c_{33} \end{bmatrix} \tag{4.1}$$

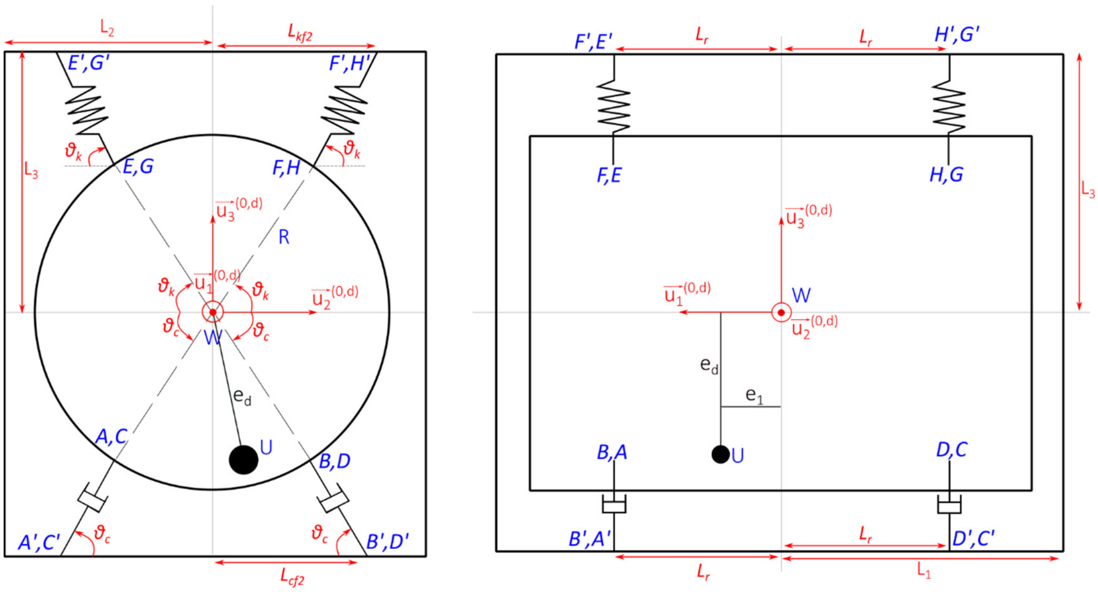


Figure 4.2. Front and side views of horizontal type washing machines.

To write down the equation of motion, front and side views of the washing machine is depicted in Figure (4.2), in the most general form. When the commercial washing machines are analyzed which resilient elements are placed in the same $\vec{u}_2^{(0)},\vec{u}_3^{(0)}$ plane. However, the eccentricity of the laundry mass in the roll axis makes the drum to move along the roll axis. To prevent this motion, generally, two sets of resilient elements are placed into the horizontal drum type washing machines. As observed from the front view, resilient elements are modeled as symmetric around the yaw axis and resilient elements can be modeled as they are oriented towards the geometrical center of the drum at the equilibrium state. In the equation of motion, $x$, $y$, $z$, $\theta_1$, $\theta_2$ and $\theta_3$ are used as generalized coordinates for the motion of the drum in the basis vectors of the base frame and since IFB rotation is used, the rotation angles are around the basis vectors of the inertial frame, respectively. To write down forces on the resilient elements, it is essential to determine the positions of ends of the resilient elements. The distance between the origins of the base and drum frame can be represented as follows by using vectors of inertial frame:

$$\vec{r}_{O,W} = x \cdot \vec{u}_1^{(0)} + y \cdot \vec{u}_2^{(0)} + z \cdot \vec{u}_3^{(0)} \tag{4.2}$$

Geometrical parameters $L_{cf2}, L_{cf3}, L_{kf2}, L_{kf3}$ are calculated by using dimensions of the washing machine and orientation angles of the resilient elements $\theta_c$ and $\theta_k$. Fixed side of the resilient elements can be represented as follows:

$$\left.\begin{aligned}
\vec{r}_{O,A'} &= L_r \cdot \vec{u}_1^{(0)} - L_{cf2} \cdot \vec{u}_2^{(0)} - L_{cf3} \cdot \vec{u}_3^{(0)} \\
\vec{r}_{O,B'} &= L_r \cdot \vec{u}_1^{(0)} + L_{cf2} \cdot \vec{u}_2^{(0)} - L_{cf3} \cdot \vec{u}_3^{(0)} \\
\vec{r}_{O,C'} &= -L_r \cdot \vec{u}_1^{(0)} - L_{cf2} \cdot \vec{u}_2^{(0)} - L_{cf3} \cdot \vec{u}_3^{(0)} \\
\vec{r}_{O,D'} &= -L_r \cdot \vec{u}_1^{(0)} + L_{cf2} \cdot \vec{u}_2^{(0)} - L_{cf3} \cdot \vec{u}_3^{(0)} \\
\vec{r}_{O,E'} &= L_r \cdot \vec{u}_1^{(0)} - L_{kf2} \cdot \vec{u}_2^{(0)} + L_{kf3} \cdot \vec{u}_3^{(0)} \\
\vec{r}_{O,F'} &= L_r \cdot \vec{u}_1^{(0)} + L_{kf2} \cdot \vec{u}_2^{(0)} + L_{kf3} \cdot \vec{u}_3^{(0)} \\
\vec{r}_{O,G'} &= -L_r \cdot \vec{u}_1^{(0)} - L_{kf2} \cdot \vec{u}_2^{(0)} + L_{kf3} \cdot \vec{u}_3^{(0)} \\
\vec{r}_{O,H'} &= -L_r \cdot \vec{u}_1^{(0)} + L_{kf2} \cdot \vec{u}_2^{(0)} + L_{kf3} \cdot \vec{u}_3^{(0)}
\end{aligned}\right\} \tag{4.3}$$

Drum side of the resilient elements can be represented as follows:

$$\left.\begin{aligned}
\vec{r}_{W,A} &= L_r \cdot \vec{u}_1^{(d)} + R\cdot\cos(\pi+\theta_c)\cdot\vec{u}_2^{(d)} + R\cdot\sin(\pi+\theta_c)\cdot\vec{u}_3^{(d)} \\
\vec{r}_{W,B} &= L_r \cdot \vec{u}_1^{(d)} + R\cdot\cos(-\theta_c)\cdot\vec{u}_2^{(d)} + R\cdot\sin(-\theta_c)\cdot\vec{u}_3^{(d)} \\
\vec{r}_{W,C} &= -L_r \cdot \vec{u}_1^{(d)} + R\cdot\cos(\pi+\theta_c)\cdot\vec{u}_2^{(d)} + R\cdot\sin(\pi+\theta_c)\cdot\vec{u}_3^{(d)} \\
\vec{r}_{W,D} &= -L_r \cdot \vec{u}_1^{(d)} + R\cdot\cos(-\theta_c)\cdot\vec{u}_2^{(d)} + R\cdot\sin(-\theta_c)\cdot\vec{u}_3^{(d)} \\
\vec{r}_{W,E} &= L_r \cdot \vec{u}_1^{(d)} + R\cdot\cos(\pi-\theta_k)\cdot\vec{u}_2^{(d)} + R\cdot\sin(\pi-\theta_k)\cdot\vec{u}_3^{(d)} \\
\vec{r}_{W,F} &= L_r \cdot \vec{u}_1^{(d)} + R\cdot\cos(\theta_k)\cdot\vec{u}_2^{(d)} + R\cdot\sin(\theta_k)\cdot\vec{u}_3^{(d)} \\
\vec{r}_{W,G} &= -L_r \cdot \vec{u}_1^{(d)} + R\cdot\cos(\pi-\theta_k)\cdot\vec{u}_2^{(d)} + R\cdot\sin(\pi-\theta_k)\cdot\vec{u}_3^{(d)} \\
\vec{r}_{W,H} &= -L_r \cdot \vec{u}_1^{(d)} + R\cdot\cos(\theta_k)\cdot\vec{u}_2^{(d)} + R\cdot\sin(\theta_k)\cdot\vec{u}_3^{(d)}
\end{aligned}\right\} \tag{4.4}$$

Vectors of resilient elements can be written as follows :

$$\vec{r}_{i',i} = \vec{r}_{O,W} + \vec{r}_{W,i} - \vec{r}_{O,i'}, \quad i = A,B,C,D,E,F,G,H \tag{4.5}$$

As observed from equations (3, 5 & 6) the only way of expressing the position vectors of resilient elements is using vectors of both drum and base frames. Before deciding the working frame for the system, checking the other external and inertial forces is essential and as another external force, unbalance force should be analyzed. It is much more convenient to describe the unbalance force in the drum plane as follows:

$$\vec{F}_{ub} = m_2 \cdot e_d \cdot \omega^2 \cdot \cos(-\pi/2+\theta)\cdot\vec{u}_2^{(d)} + m_2 \cdot e_d \cdot \omega^2 \cdot \sin(-\pi/2+\theta)\cdot\vec{u}_3^{(d)} \tag{4.6}$$

Where $\theta$ is the instantaneous angular orientation of the unbalanced mass with respect to the roll axis of $F_d$. The instantaneous position of the unbalanced mass with respect to the center of the drum is:

$$\vec{r}_{W,U} = e_1 \cdot \vec{u}_1^{(d)} + e_d \cdot \cos(-\pi/2+\theta)\cdot\vec{u}_2^{(d)} + e_d \cdot \sin(-\pi/2+\theta)\cdot\vec{u}_3^{(d)} \tag{4.7}$$

As observed above, vectors of the dynamical systems consist of basis vectors of both base and drum frame, however, to write down the equation of motion, all vectors should be represented in one frame. In general, Newton–Euler formulation can be written as follows:

$$\left.\begin{array}{l}\sum \vec{F} = m \cdot \vec{a} \\ \sum \vec{M} = \breve{J} \cdot \vec{\alpha} + \vec{\omega} \times \breve{J} \cdot \vec{\omega}\end{array}\right\} \tag{4.8}$$

Since basis vectors of drum frame much more used to describe the vectors of interest, it seems convenient to use the drum frame and resolve Newton–Euler equations in drum frame. However, it is much easier to resolve the angular velocity between the inertial and non-inertial frames, $\vec{\omega}_{d/0}$, and derivative of the angular velocity with respect to the base frame, $\vec{\alpha}_{d/0}$, in the base frame by avoiding using Coriolis Transport theorem. This is an engineering tradeoff and base frame is selected as the mainframe, in contrast to the tradition of advanced dynamics. Then, all position, force and moment vectors should be resolved in the inertial frame and inserted into the equation of motion:

$$\overline{r}_{i',i}^{\;(0)} = \overline{r}_{O,W}^{\;(0/0)} + \hat{C}^{(0,d)} \cdot \overline{r}_{W,i}^{\;(d/d)} - \overline{r}_{O,i'}^{\;(0/0)},\; i = A,B,C,D,E,F,G,H \tag{4.9}$$

After expressing the vectors of resilient elements, the forces on the resilient elements can be calculated. Forces on the springs are:

$$\overline{F}_i^{(0)} = k \cdot (k_f - norm(\overline{r}_{i',i}^{\;(0)})),\; i = E,F,G,H \tag{4.10}$$

Since the system is equilibrium in Figures (4.1 & 4.2), the free length of the spring is taken as the lengths at Figures (4.1 & 4.2). To write forces on the dampers, velocities of the connection points along the instantaneous orientation of dampers are necessary. To calculate velocities and express them in column matrices in the base frame, a differentiation of Equation (4.10) in the inertial frame is necessary:

$$\begin{aligned} D_0(\overline{r}_{i',i}^{\;(0)}) &= D_0(\overline{r}_{O,W}^{\;(0/0)}) + D_0(\hat{C}^{(0,d)} \cdot \overline{r}_{W,i}^{\;(d/d)}) - D_0(\overline{r}_{O,i'}^{\;(0/0)}) \\ \dot{\overline{r}}_{i',i}^{\;(0)} &= \dot{\overline{r}}_{O,W} + \hat{C}^{(0,d)} \cdot \dot{\overline{r}}_{W,i} + \dot{\hat{C}}^{(0,d)} \cdot \overline{r}_{W,i} - \dot{\overline{r}}_{O,i'} \\ \dot{\overline{r}}_{i',i}^{\;(0)} &= \begin{bmatrix} \dot{x} \\ \dot{y} \\ \dot{z} \end{bmatrix} + \begin{bmatrix} \dot{c}_{11} & \dot{c}_{12} & \dot{c}_{13} \\ \dot{c}_{21} & \dot{c}_{22} & \dot{c}_{23} \\ \dot{c}_{31} & \dot{c}_{32} & \dot{c}_{33} \end{bmatrix} \cdot \overline{r}_{W,i},\; i = A,B,C,D \end{aligned} \tag{4.11}$$

Then forces on the viscous dampers can be expressed as follows:

$$\overline{F}_i^{(0)} = -c \cdot norm(\dot{\overline{r}}_{i',i}{}^{(0)}),\ i = A,B,C,D \tag{4.12}$$

With the information of position vectors of elastic elements, components of the forces are easy to achieve in the base frame. Total moments caused by the forces on the resilient elements are simply cross products:

$$\vec{M}_i = \vec{r}_{W,i} \times \vec{F}_i,\ i = A,B,C,D,E,F,G,H \tag{4.13}$$

Resolving these moment vectors in the base frame will lead to:

$$\overline{r}_{W,i}{}^{(0)} = \hat{C}^{(0,d)} \cdot \overline{r}_{W,i}{}^{(d/d)},\ \overline{M}_i{}^{(0)} = \tilde{r}_{W,i}{}^{(0)} \cdot \overline{F}_i^{(0)},\ i = A,B,C,D,E,F,G,H \tag{4.14}$$

On the other hand, the rotating unbalance force and moment vector can be written as follows:

$$\overline{F}_{ub}{}^{(0)} = \hat{C}^{(0,d)} \cdot \overline{F}_{ub}{}^{(d/d)}, \overline{M}_{ub}{}^{(d)} = \tilde{r}_{W,U}{}^{(d)} \cdot \overline{F}_{ub}{}^{(d)}, \overline{M}_{ub}{}^{(0)} = \hat{C}^{(0,d)} \cdot \overline{M}_{ub}{}^{(d)} \tag{4.15}$$

Transformation matrix of IFB 1-2-3 & Rotating Frame-Based 3-2-1 rotation sequences are same. The relative angular velocity between the drum and the base frame is:

$$\vec{\omega}_{d/0} = \dot{\theta}_3 \cdot \vec{u}_3{}^{(0)} + \dot{\theta}_2 \cdot \vec{u}_2{}^{(1)} + \dot{\theta}_1 \cdot \vec{u}_1{}^{(2)} \tag{4.16}$$

Where $F_1(O)$ and $F_2(O)$ are intermediate fictitious reference frames. The transformation matrix between the base and fictitious frames can be identified as follows:

$$\hat{C}^{(0,1)} = \hat{R}_3(\theta_3), \hat{C}^{(0,2)} = \hat{R}_3(\theta_3) \cdot \hat{R}_2(\theta_2) \tag{4.17}$$

Then, the relative angular velocity vector $\vec{\omega}_{d/0}$, can be resolved in the base frame:

$$\bar{\omega}_{d/0}{}^{(0)} = \dot{\theta}_3 \cdot \bar{u}_3{}^{(0)} + \dot{\theta}_2 \cdot \hat{C}^{(0,1)} \cdot \bar{u}_2{}^{(1/1)} + \dot{\theta}_1 \cdot \hat{C}^{(0,2)} \cdot \bar{u}_1{}^{(2/2)}$$

$$\bar{\omega}_{d/0}{}^{(0)} = \begin{bmatrix} -\dot{\theta}_2 \cdot \sin(\theta_3) + \dot{\theta}_1 \cdot \cos(\theta_2) \cdot \cos(\theta_3) \\ \dot{\theta}_2 \cdot \cos(\theta_3) + \dot{\theta}_1 \cdot \cos(\theta_2) \cdot \sin(\theta_3) \\ \dot{\theta}_3 - \dot{\theta}_1 \cdot \sin(\theta_2) \end{bmatrix} \tag{4.18}$$

Since the base frame is selected as the mainframe, the expression of relative angular acceleration is simply derivative of the relative angular velocity:

$$\bar{\alpha}_{d/0}{}^{(0)} = D_0(\bar{\omega}_{d/0}{}^{(0)}) = \dot{\bar{\omega}}_{d/0}{}^{(0)} \tag{4.19}$$

The last term in the Newton–Euler formulation is the inertia of the drum. Since it can be modeled as a hollow cylinder, Its inertia about its center can be expressed as a diagonal tensor in its own frame:

$$\hat{J}^{(0)} = \hat{C}^{(0,d)} \cdot \hat{J}^{(d/d)} \cdot \hat{C}^{(d,0)}$$

$$\hat{J}^{(0)} = \begin{bmatrix} c_{11} & c_{12} & c_{13} \\ c_{21} & c_{22} & c_{23} \\ c_{31} & c_{32} & c_{33} \end{bmatrix} \cdot \begin{bmatrix} J_1 & 0 & 0 \\ 0 & J_2 & 0 \\ 0 & 0 & J_2 \end{bmatrix} \cdot \begin{bmatrix} c_{11} & c_{21} & c_{31} \\ c_{12} & c_{22} & c_{32} \\ c_{13} & c_{23} & c_{33} \end{bmatrix} \tag{4.20}$$

The Newton–Euler formulation is now can be written as follows:

$$\left. \begin{aligned} \sum \bar{F}^{(0)} &= \sum_{i=A}^{H} \bar{F}_i^{(0)} + \bar{F}_{ub}{}^{(0)} = \left(m_d + m_u\right) \cdot \bar{a}^{(0)} \\ \sum \bar{M}^{(0)} &= \sum_{i=A}^{H} \bar{M}_i{}^{(0)} + \bar{M}_{ub}{}^{(0)} = \hat{J}^{(0)} \cdot \bar{\alpha}^{(0)} + \tilde{\omega}^{(0)} \cdot \hat{J}^{(0)} \cdot \bar{\omega}^{(0)} \end{aligned} \right\} \tag{4.21}$$

These six nonlinear differential equations are converted into a set of algebraic equations by utilizing with Harmonic Balance Method (HBM). In HBM, periodic external forces and the response of the system is represented by truncated Fourier series. These representations are substituted into the differential equations of motion and coefficients of harmonics are balanced which results in a set of nonlinear algebraic equations. Since nonlinear frequency response functions may have memory, these algebraic equations are solved Newton's Method with arc-length continuation.

## 4.2. Results and Discussion

Numerical values used in this study are given in Table 4.1 unless otherwise is specified.

Table 4.1. *Numerical values for 3D system.*

| | | | |
|---|---|---|---|
| $m_1$ | $40\ kg$ | $R$ | $300\ mm$ |
| $m_2$ | $6\ kg$ | $k$ | $2000\ N/m$ |
| $J_1$ | $1.25\ N \cdot m^2 + m_2 \cdot e_d^{\ 2}$ | $c$ | $100\ Ns/m$ |
| $J_2$ | $14\ N \cdot m^2 + m_2 \cdot e_1^{\ 2}$ | $k_d$ | $2000\ N/m$ |
| $\theta_k$ | $45^o$ | $\mu N$ | $50\ N$ |
| $\theta_c$ | $45^o$ | $L_r$ | $300\ mm$ |
| $e_1$ | $100\ mm$ | $L_i$ | $500\ mm$ |
| $e_d$ | $100\ mm$ | | |

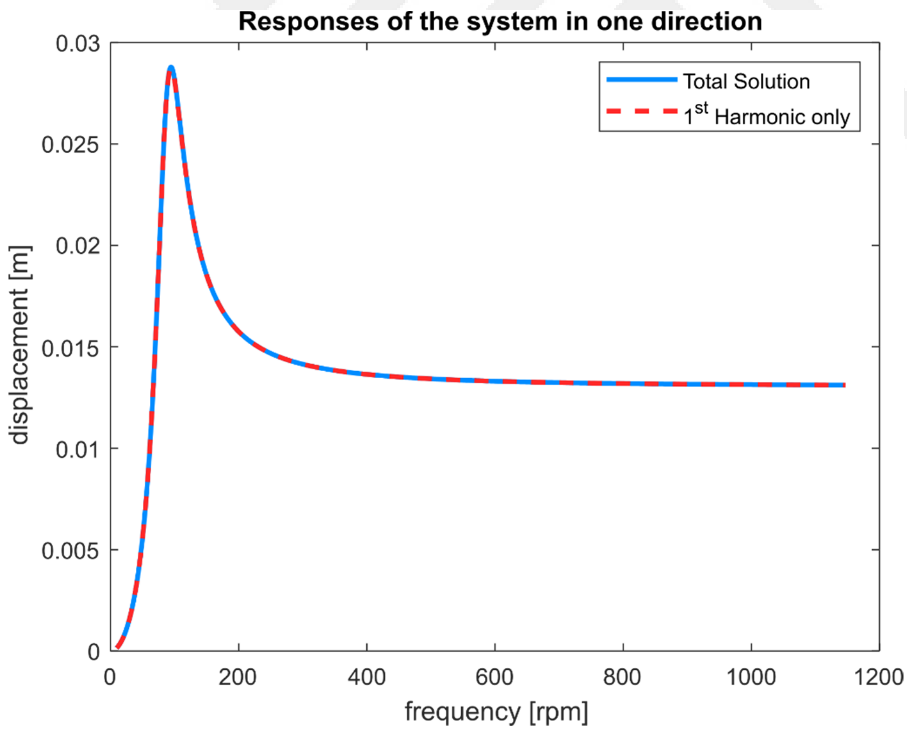


Figure 4.3. A case study with viscous dampers $\theta_k = \theta_c = 45^o$. Response in both directions.

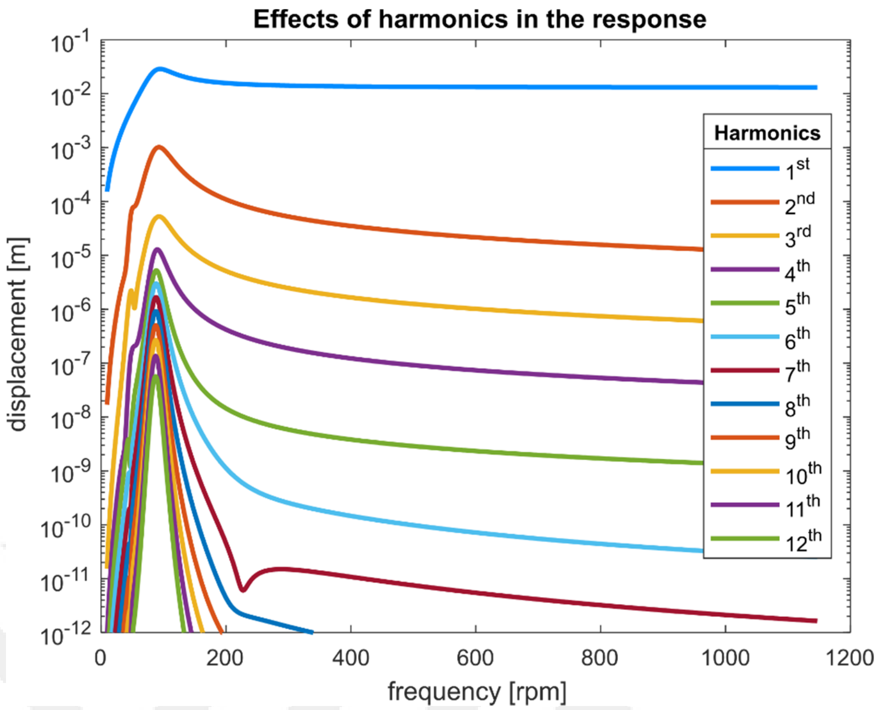


Figure 4.4 A case study with viscous dampers $\theta_k = \theta_c = 45^o$. Effect of harmonics in the response.

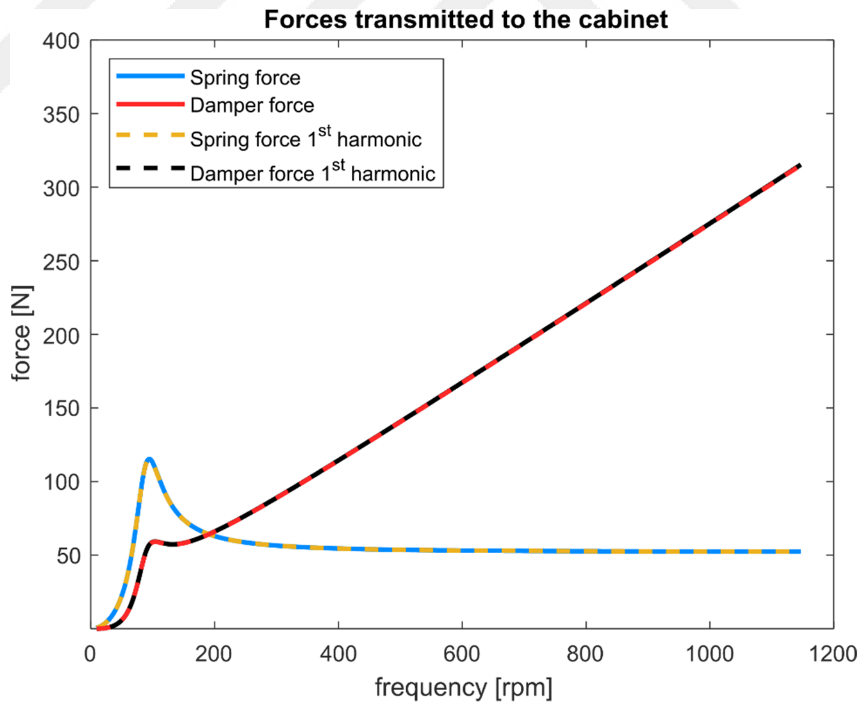


Figure 4.5. A case study with viscous dampers $\theta_k = \theta_c = 45^o$. Transmitted force in both directions.

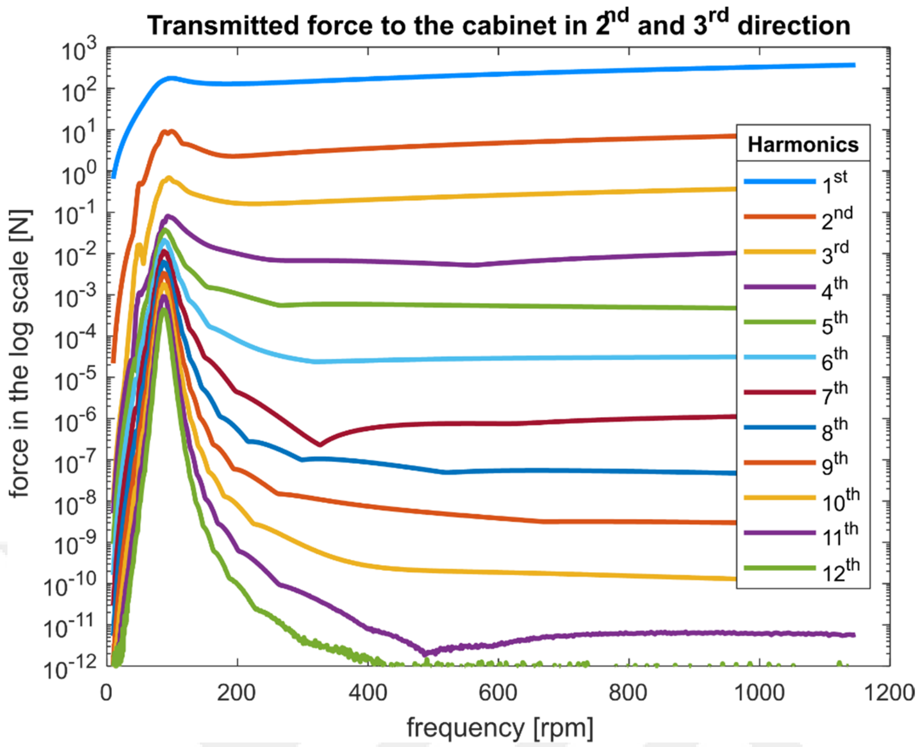


Figure 4.6 A case study with viscous dampers $\theta_k = \theta_c = 45^o$. Effect of harmonics in the transmitted force.

Again, representing the motion with only one harmonic is sufficient, moreover, the dry friction damper model has an analytical solution for single harmonic representation and it will drastically improve the computational effort.

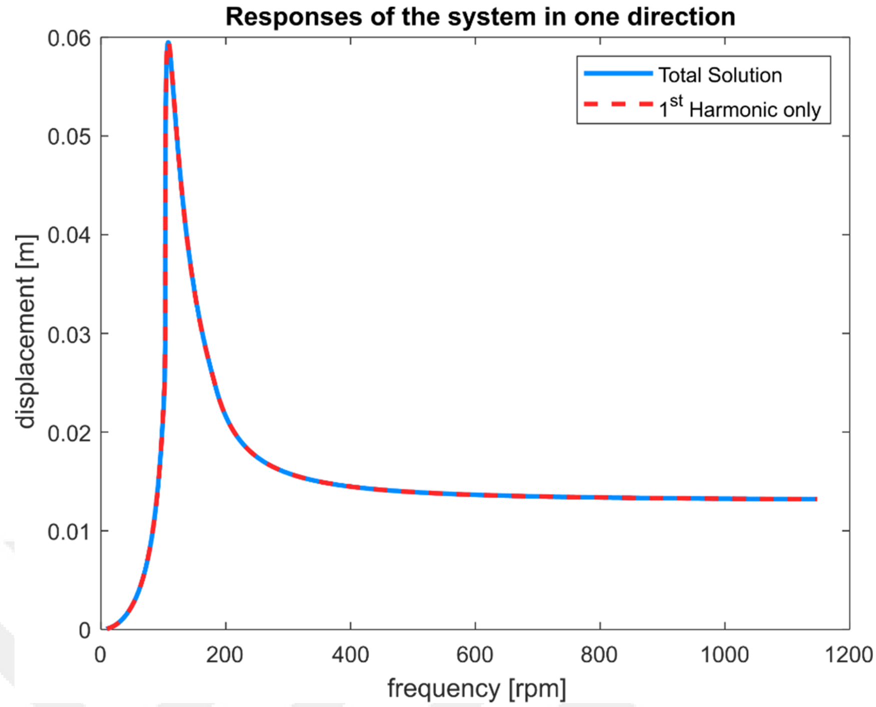


Figure 4.7 Effect of the first harmonic, dry friction case.

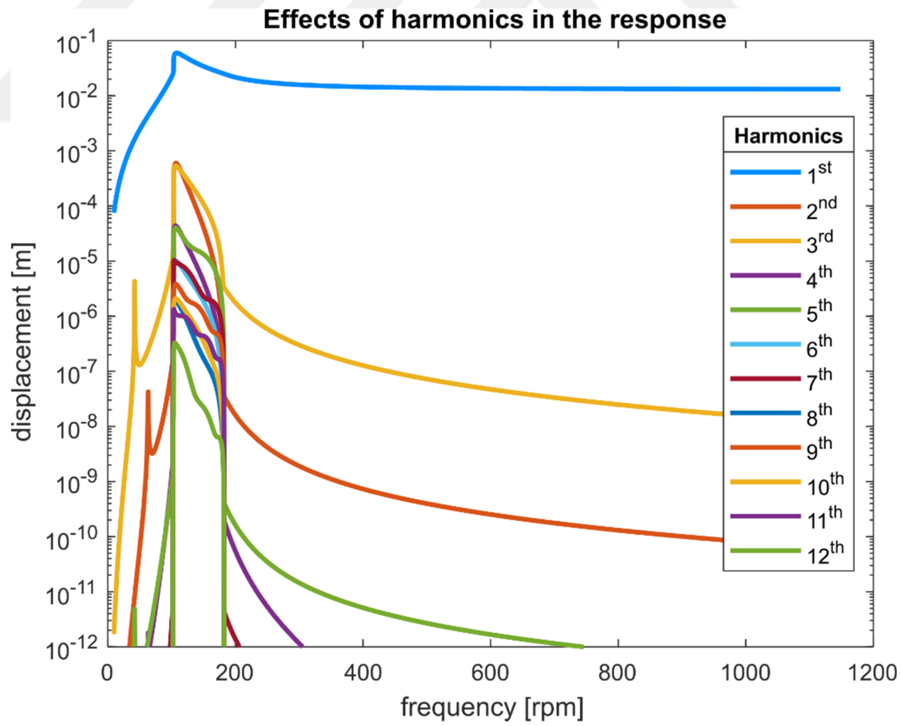


Figure 4.8. Effect of the 12 harmonics, dry friction case.

After a suitable damper is implemented into the system, it is also necessary to observe the effects of the parameters of resilient elements and their attachment locations. The effect of the orientation angles of the resilient elements is depicted in Figures (4.7 & 4.8). The coordination of resilient elements has a direct effect on the transmitted force to the cabinet and the response of the drum. Changing the orientation angles $\theta_c$ and $\theta_k$ of the resilient elements increases the total nonlinearity of the system as observed from the Frequency Response Functions. This deviation from $45^o$ in the orientation leads to considerable differences in terms of the difference between the directions of the response of the system and the directions of the transmitted force. However, total transmitted forces are almost same and $45^o$ orientation has a slight advantage to mitigate the maximum value of the exerted force to the cabinet. Selecting all the orientation angles as $45^o$ creates complete symmetry and it also provides minimum transmitted force to the cabinet in the resonant frequency range. On the other hand, it also leads to a minimum response in both directions at the same time, which also creates monotony in the directions of transmitted force and it definitely prolongs the life of the cabinets of the horizontal drum type washing machines. For some special designs, manufacturers may want to have a different distribution of transmitted force; however, in this paper minimizing total resultant force is taken into consideration and the best orientation angles are selected as $45^o$. At this point, parameters of resilient elements are taken into consideration and the effects of spring constant, spring constant of dry friction damper and slip load should be analyzed.

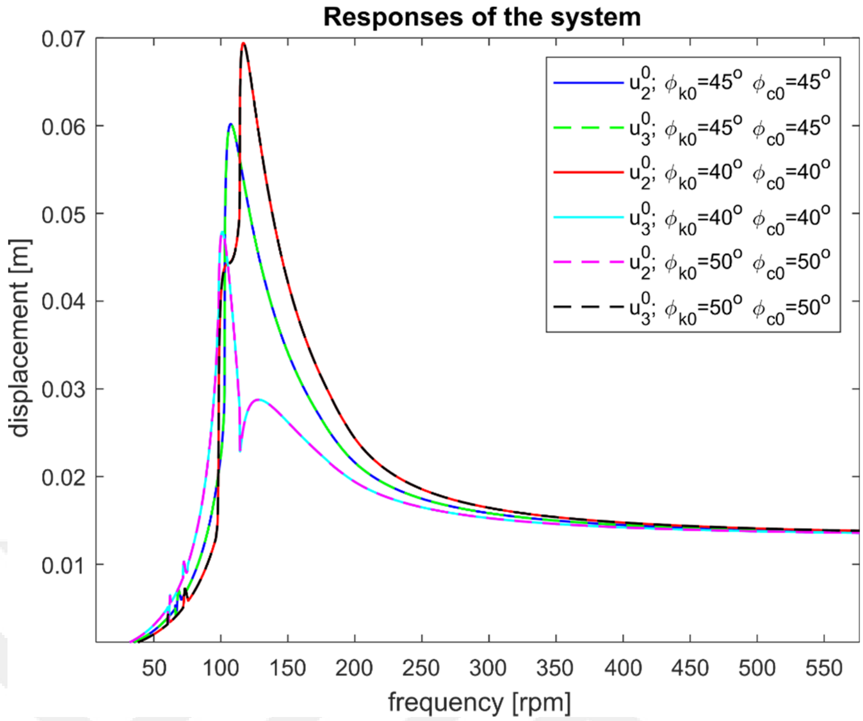


Figure 4.9 Effect of orientation angles in the response, first case study.

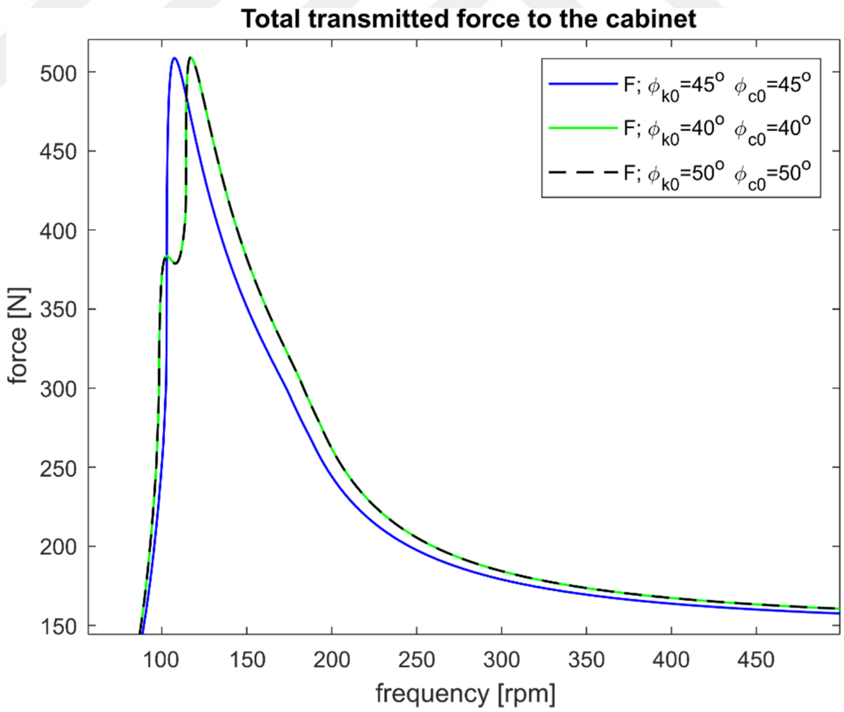


Figure 4.10. Effect of orientation angles in the total transmitted force, first case study

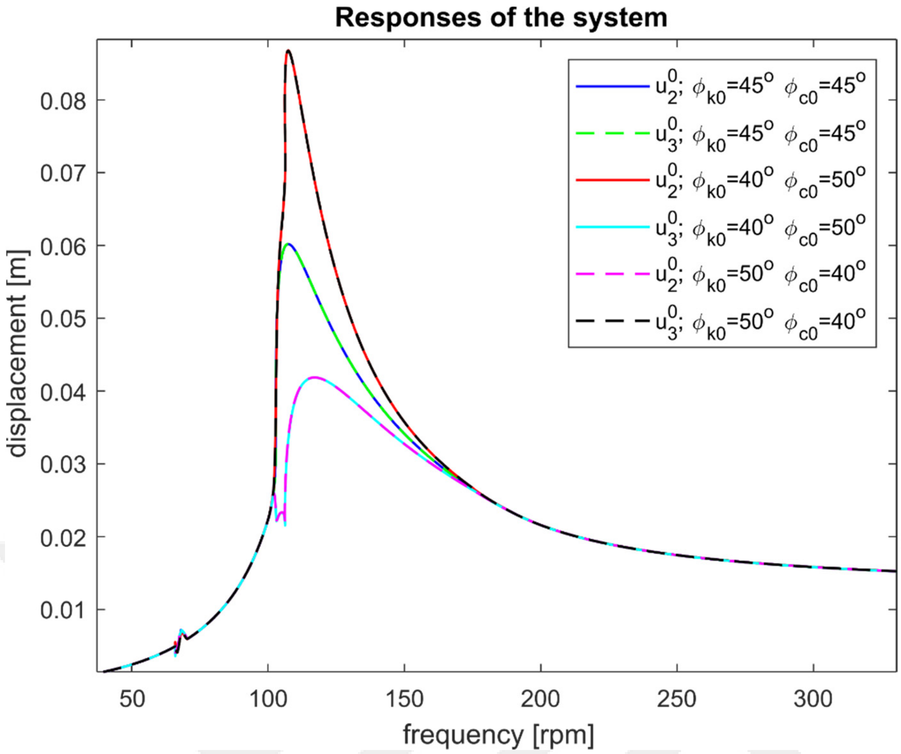


Figure 4.11 Effect of orientation angles in the response, second case study.

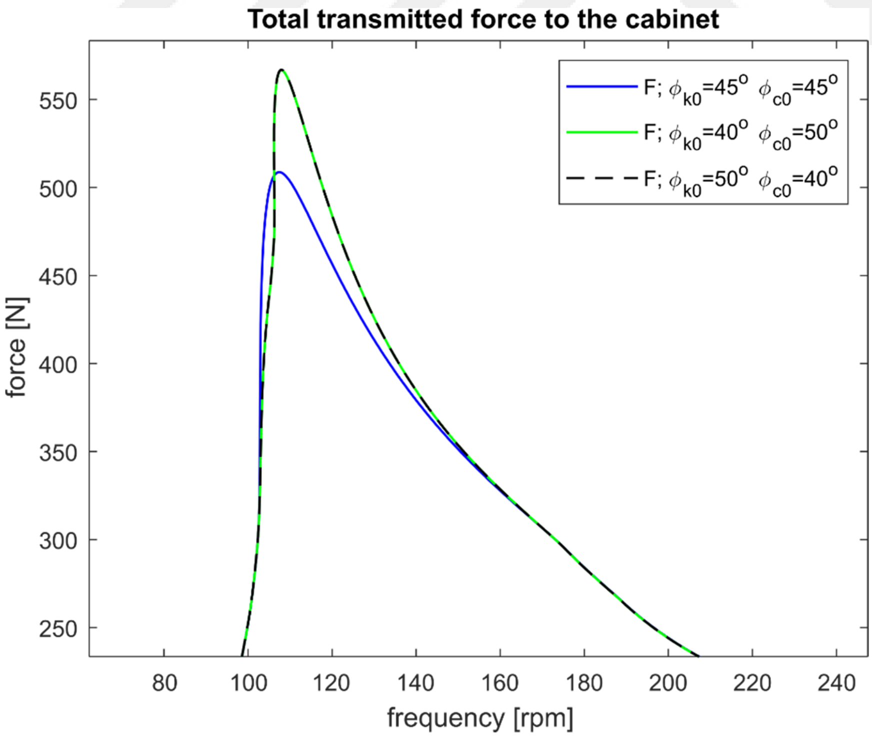


Figure 4.12. Effect of orientation angles in the total transmitted force, second case study

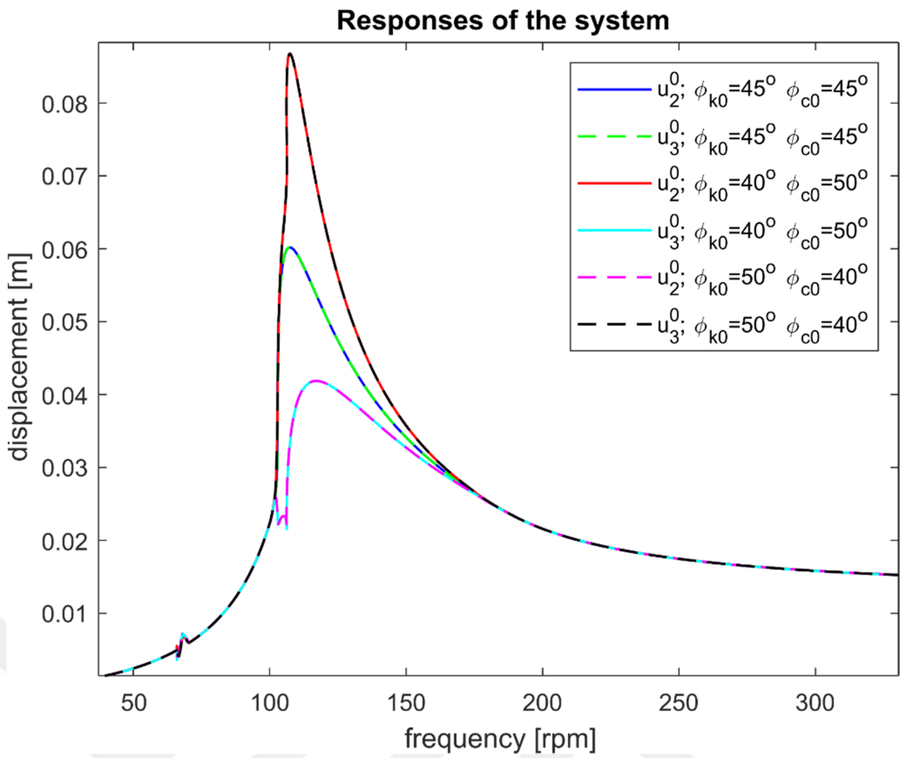


Figure 4.13 Effect of orientation angles in the response, second case study.

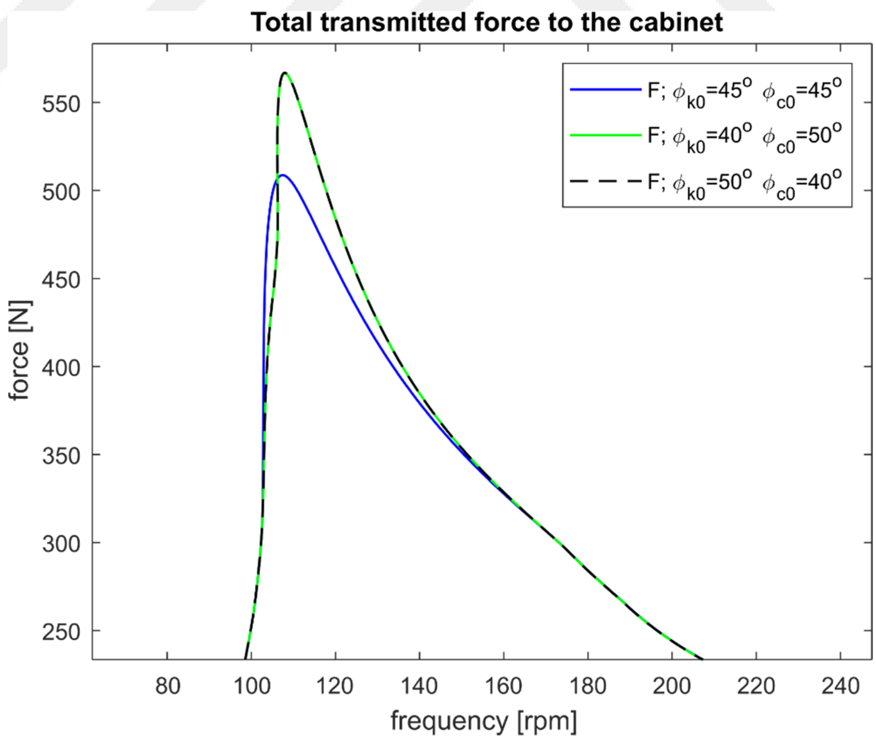


Figure 4.14. Effect of orientation angles in the total transmitted force, second case study

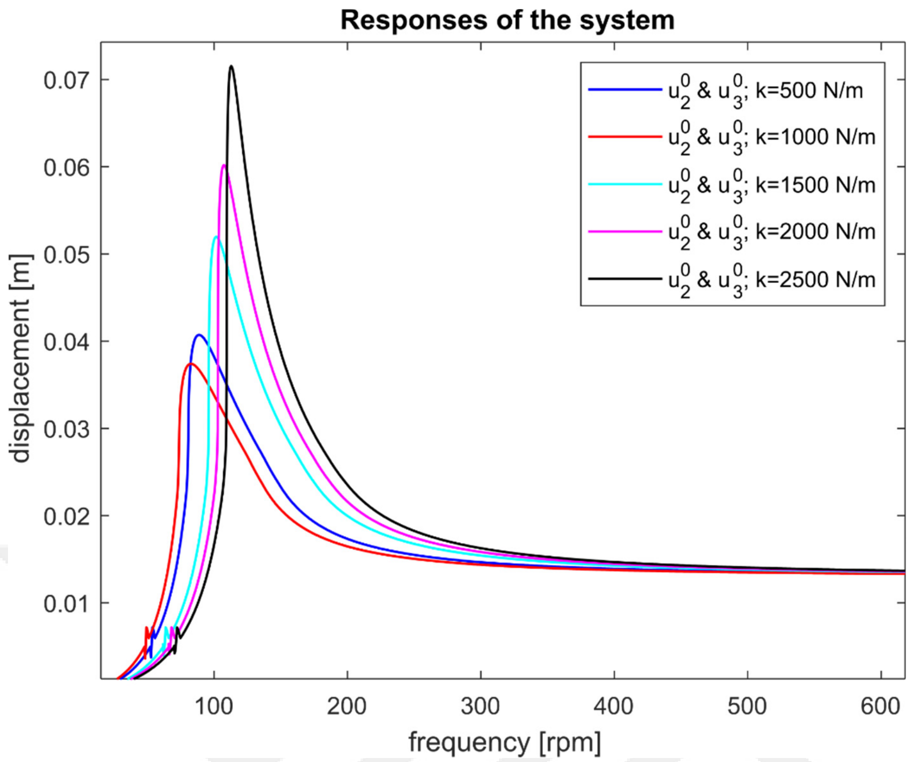


Figure 4.15. Effect of the spring constant in the displacement.

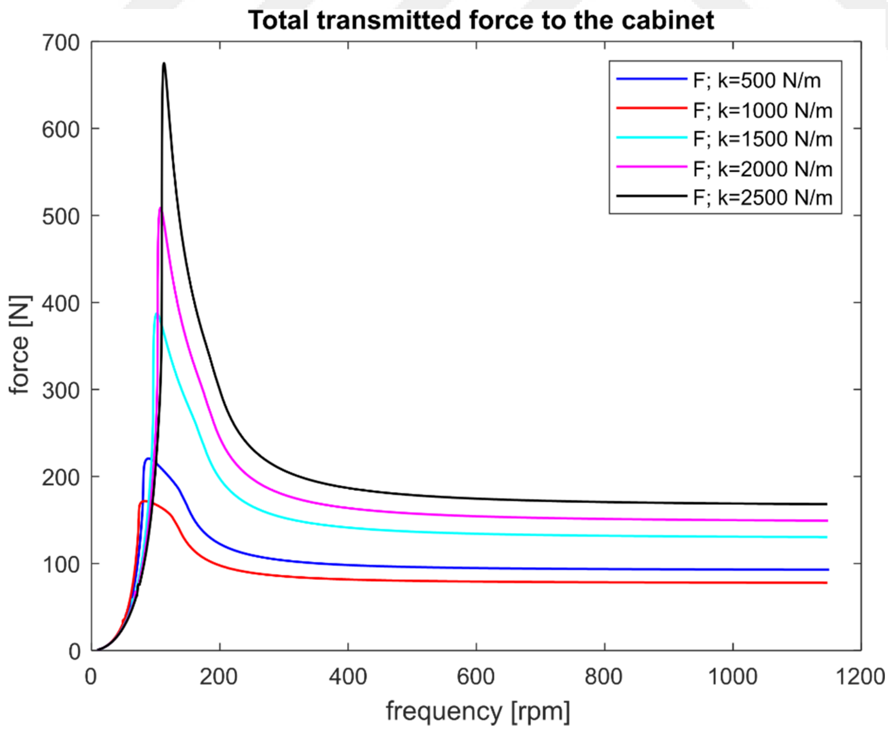


Figure 4.16. Effect of the spring constant in the total transmitted force.

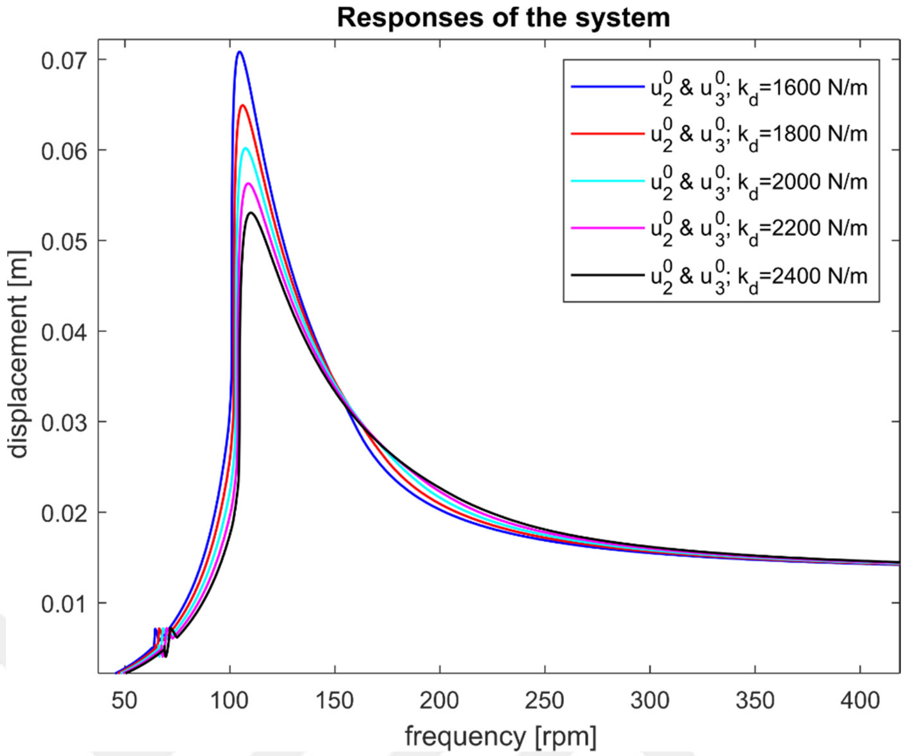


Figure 4.17. Effect of the dry friction damper spring constant in the response.

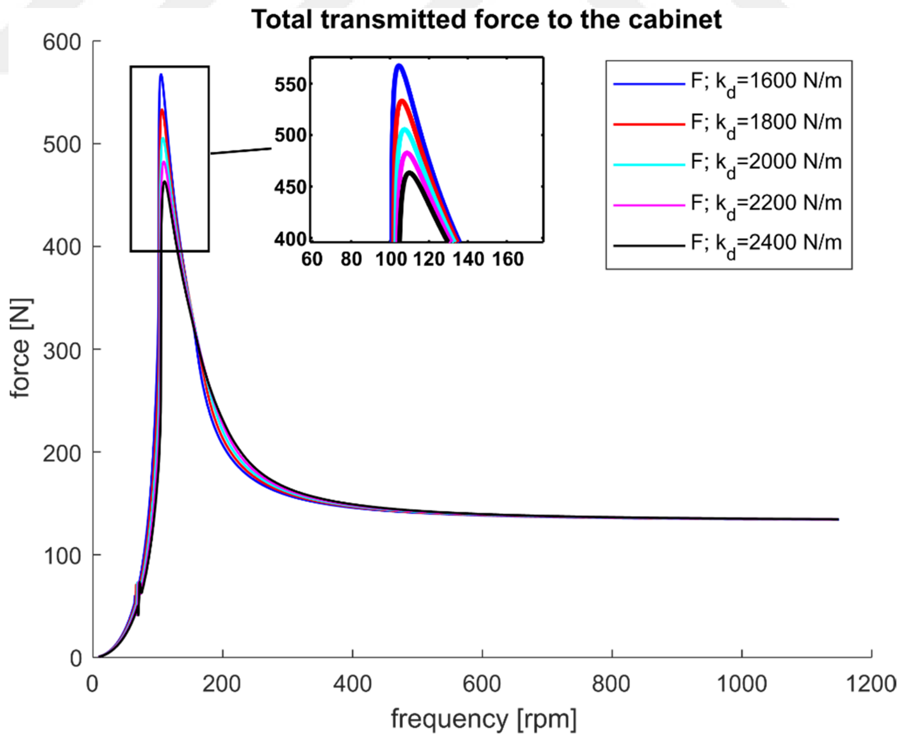


Figure 4.18. Effect of the dry friction damper in the total transmitted force.

In Figures (4.15 & 4.16), it is observed that there is no linear correlation between the spring constant and the total response and the transmitted force to the cabinet. Roughly speaking, lower spring constant values decrease the vibration and the transmitted force in both spinning and washing processes, i.e. all the frequency span. In Figures (4.17 & 4.18), the effects of spring constants of dry friction dampers are analyzed. Dry friction damper starts to apply a constant force to the drum whenever the displacement gets larger and acts like springs at the small displacements. Increasing the spring constant of the damper is simply increasing the total stiffness of the system whenever dampers are inactive. As observed from Figure (4.16), higher values lead to smaller maximum force values in the washing process, however, it will increase the total transmitted force in the spinning cycle. Again, creating a linear relationship between $k_d$ and the response is impossible.

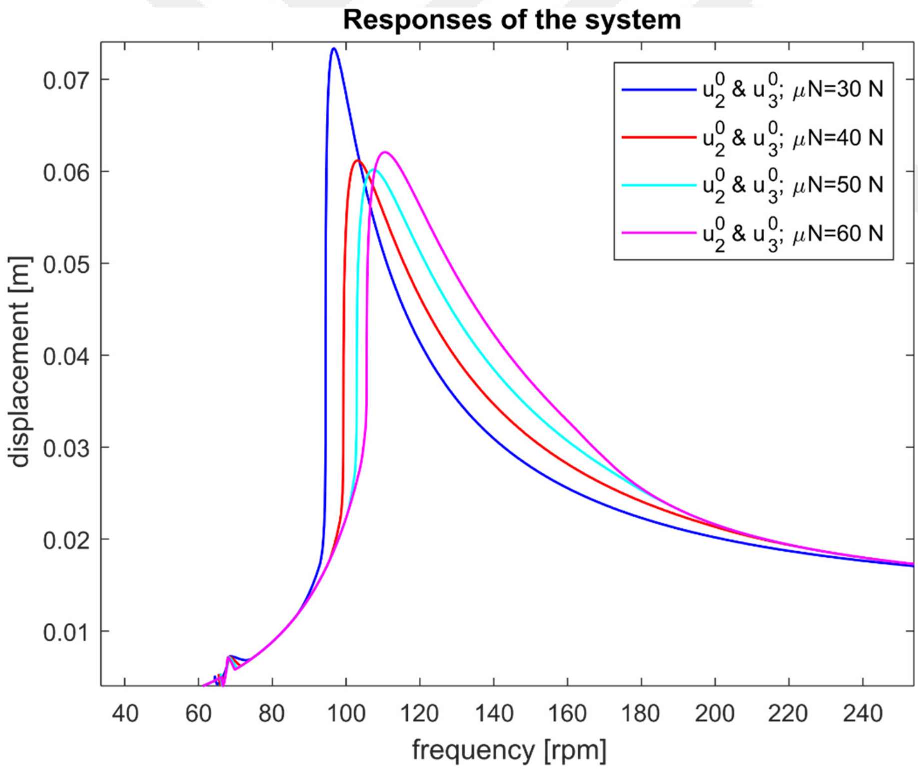


Figure 4.19. Effect of the slip load in the response.

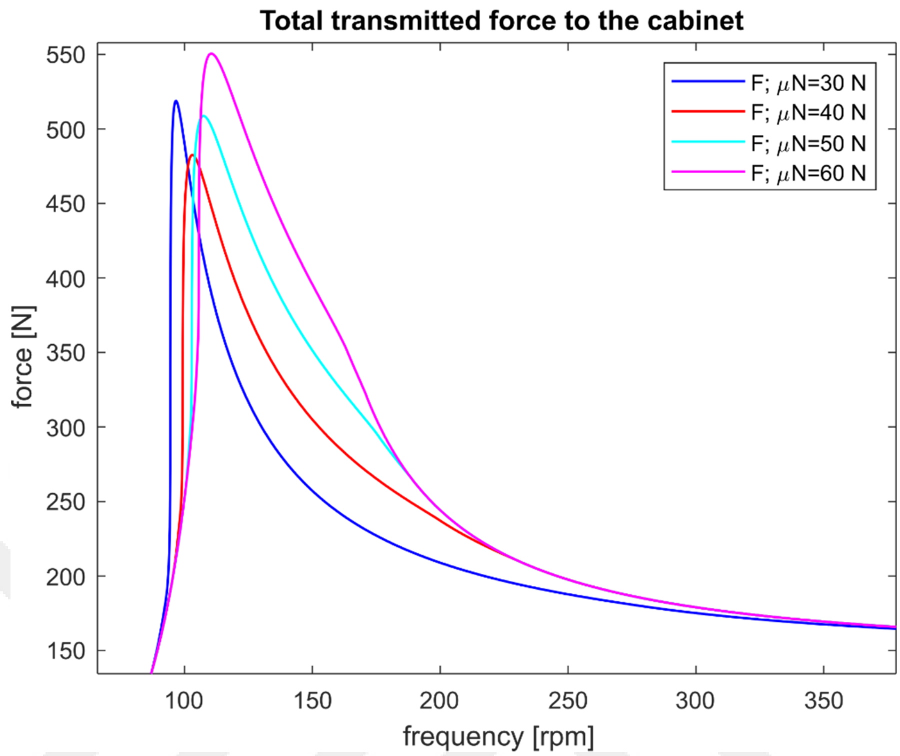


Figure 4.20. Effect of the slip load in the total transmitted force.

In Figures (4.19 & 4.20), the effects of slip load on the system are analyzed. The value of the slip load is an important parameter for lower frequencies, however, in the spinning cycle, total displacements are not enough to cause a slip in the dampers and slip load loses its effect on the system. Again, creating a linear correlation between the slip load and the transmitted force to the system is impossible but roughly it can be said that lower slip loads lead smaller exerted forces on the cabinet. In Figure (4.21) the effect of slip load on the maximum of the total transmitted force is analyzed while all other parameters remain constant.

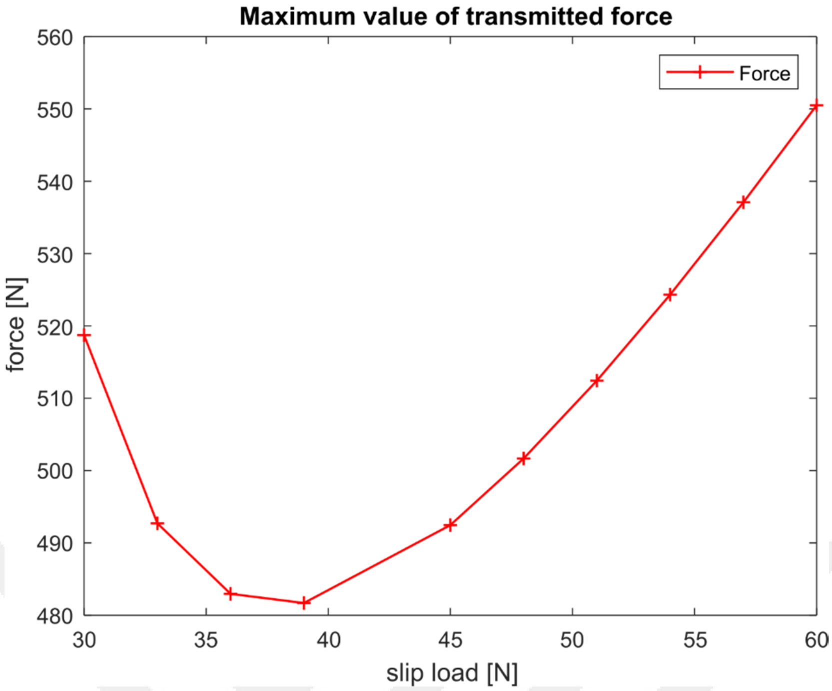


Figure 4.21. Effect of the slip load in the total transmitted force, grid study.

It is observed that there is almost no difference between the results of two-dimensional and three-dimensional studies. However, implementing the gasket between the drum and the front side of the cabinet into the equation of motion and observe the effects of it is easy by means of the three-dimensional modeling. Since all the equations are solved in the inertial frame, i.e. in the cabinet frame, and gasket is directly attached to the front side of the cabinet, the gasket can be directly put in into the equation of motion as follows:

$$\left.\begin{array}{l} F_{g_i}^{(0)} = k_{g_i} \cdot u_i^{(0)} \quad , \; i=1,2,3 \\ \bar{M}_g^{(0)} = \tilde{r}_{W,G}^{(0)} \cdot \bar{F}_g^{(0)} \end{array}\right\} \tag{4.22}$$

Where $G$ is the middle point of the gasket. Equation (4.22) can be directly inserted into equation (4.21). To illustrate, gasket is modeled only with three spring constants that represents the stiffness in all the basis vectors of the inertial frame. Two case studies are performed with different gasket parameters and they are compared with the original system in Figures (4.23 & 4.24) to prove the effectiveness of the gasket of the system.

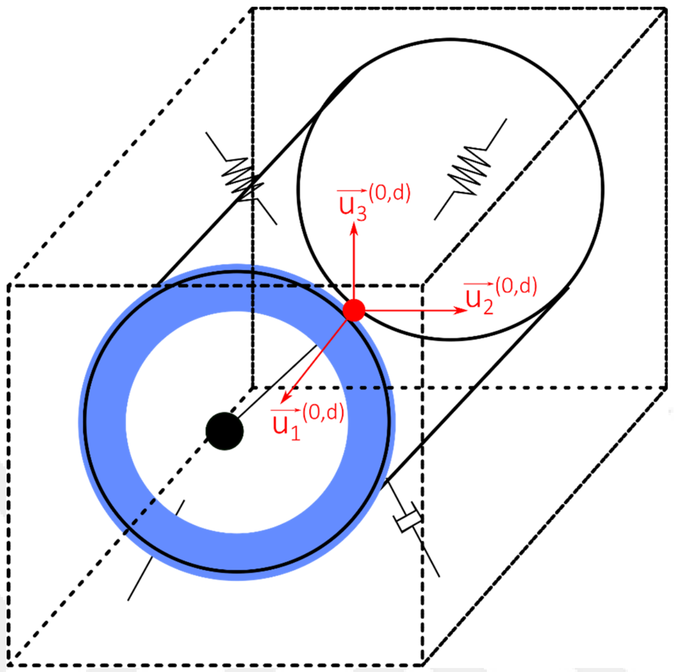


Figure 4.22. Isometric view of the horizontal drum type washing machine with gasket.

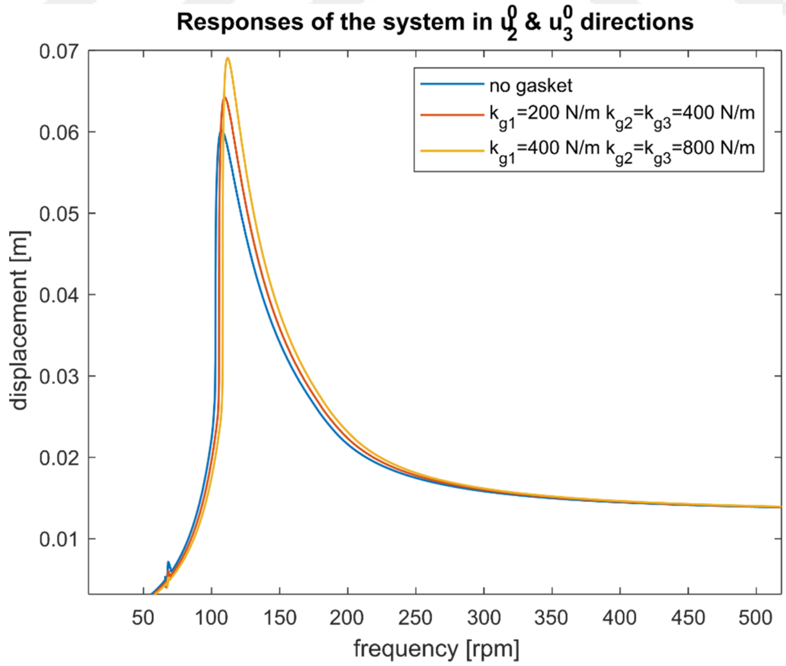


Figure 4.23. Effect of the gasket in the response.

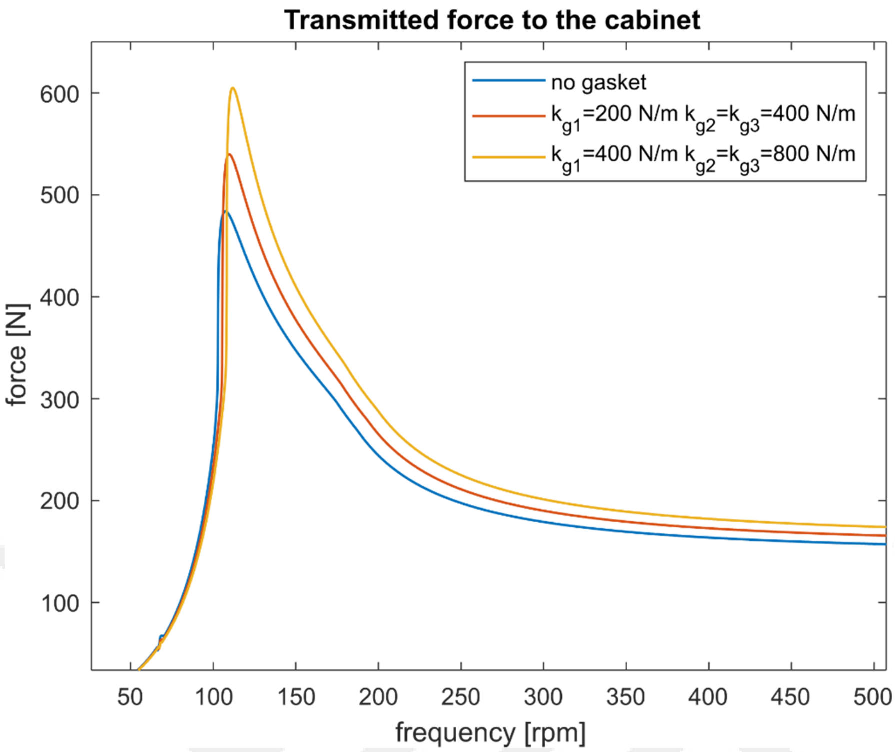


Figure 4.24. Effect of the gasket in the total transmitted force.

After all these analyses, it is obvious that there is no linear correlation between the parameters of the resilient elements and the total transmitted force to the cabinet. To find the minimum value of it an optimization process is necessary and in this optimization process, the amplitude of the displacement of the drum is essentially taken into consideration as a physical constraint.

# CHAPTER 5

# OPTIMIZATION

It is proved that for two and three dimensional systems, there is no linear correlation between the system response, in terms of force or displacement, and parameters of the resilient elements. Moreover, there are some constraints that come from the physical limitations of the system. To obtain the minimum value of the result an optimization process is necessary and as an optimization method genetic algorithm is selected in this thesis and as a cost function, the maximum transmitted force to the cabinet is selected.

## 5.1. Optimization in 2D Dynamical Model

For the two-dimensional system, constraints are listed below:

- The washing machine drum should not touch or get closer to the sides of the cabinet. To limit the motion of the drum, maximum displacement in horizontal and vertical directions are limited as six centimeters.
- At the static equilibrium, only the springs will carry the whole weight of the drum. Therefore, the minimum spring constant should be $6000\,N/m$.

For viscously damped systems results are obtained as follows:

$$k = 6000\ \frac{N}{m},\ c = 145.2\ \frac{Ns}{m} \tag{5.1}$$

Simulation is performed with these numerical values and in Figures (5.1 & 5.2), results are depicted. The maximum total force is calculated as $419.2\,N$ at $111.3\,rpm$ and $1433\,rpm$. For dry frictionally damped systems, results are obtained as follows:

$$k = 6000\ \frac{N}{m},\ \mu N = 116.4\ N,\ k_d = 194569\ \frac{N}{m} \tag{5.2}$$

Simulation is performed with these numerical values and in Figures (5.3 & 5.4), results are depicted. The maximum total force is calculated as $262.1\,N$ at $175\,rpm$.

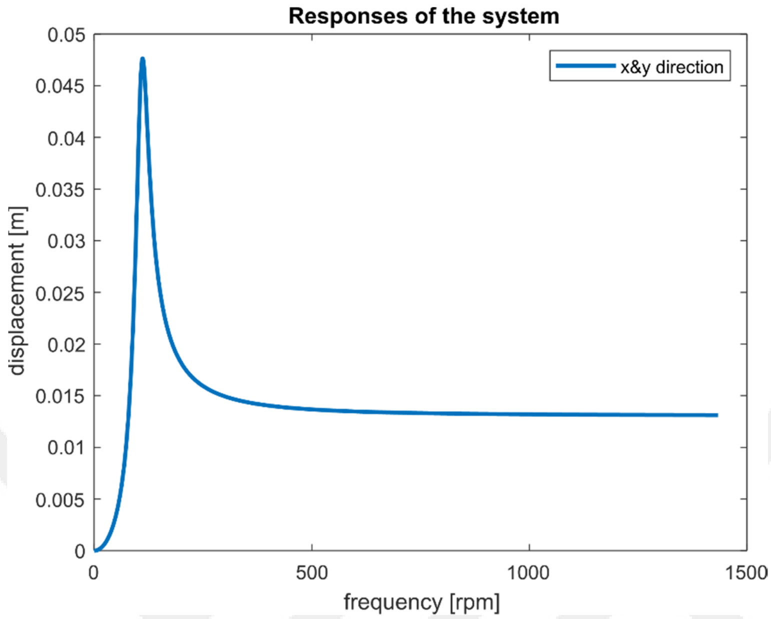


Figure 5.1. Displacements with optimized system parameters for the two-dimensional system with viscous dampers.

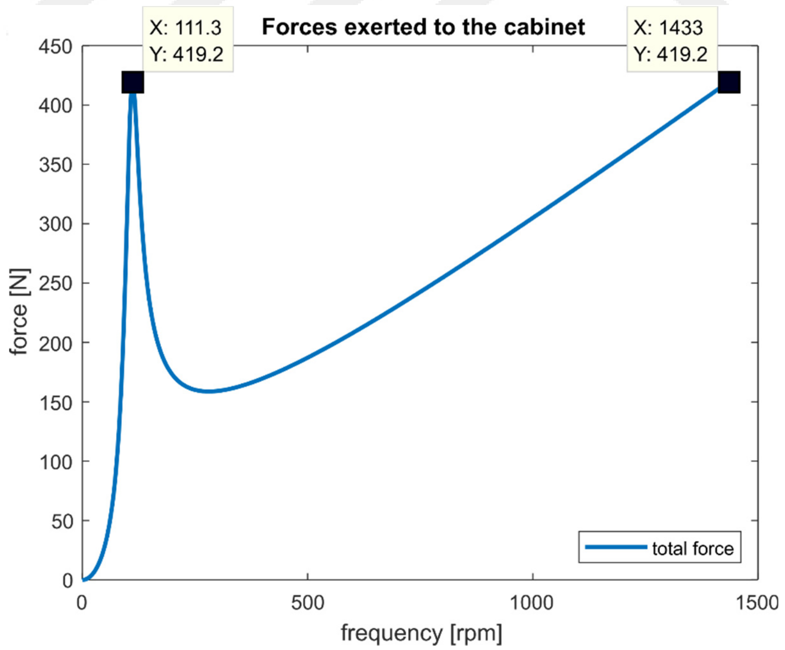


Figure 5.2. Total transmitted force to the cabinet with optimized system parameters for the two-dimensional system with viscous dampers.

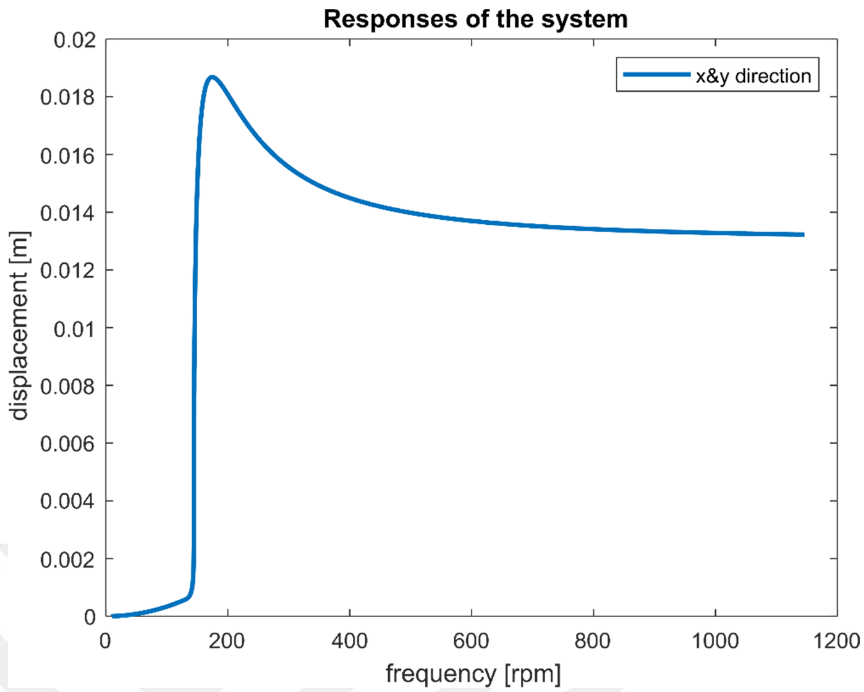


Figure 5.3. Displacements with optimized system parameters for the two-dimensional system with dry friction dampers.

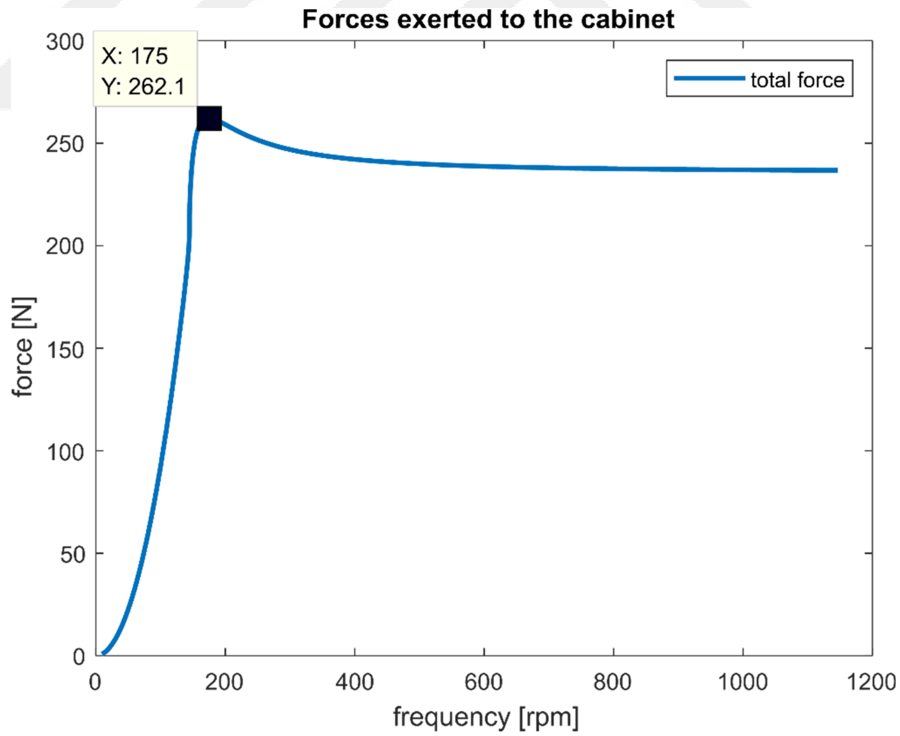


Figure 5.4. Total transmitted force to the cabinet with optimized system parameters for the two-dimensional system with dry friction dampers.

## 5.2. Optimization in 3D Dynamical Model

For the three-dimensional system, constraints are listed below:

- The washing machine drum should not touch or get closer to the sides of the cabinet. To limit the motion of the drum, maximum displacement in pitch and yaw axes are limited as six centimeters.
- The washing machine drum should not move much in the roll axis to prevent any damage on the backside of the cabinet or on the gasket placed between the drum and the front side of the cabinet. Therefore, maximum displacement in the roll axis is limited as two centimeters.
- At the static equilibrium, only the springs will carry the whole weight of the drum. Therefore, the minimum spring constant should be $3000\,N/m$.

Results are obtained as follows:

$$k = 3000\ \frac{N}{m},\ \mu N = 58.2\ N,\ k_d = 97284.5\ \frac{N}{m} \tag{5.3}$$

As may be noticed, these values are one-half of the results in the two-dimensional model. Simulation is performed with these numerical values and in Figures (5.5 & 5.6), results are depicted. The maximum total force is calculated as $261.7\,N$ at $174.2\,rpm$ which means there is almost no change in these calculations between the results of two dimensional and three-dimensional models.

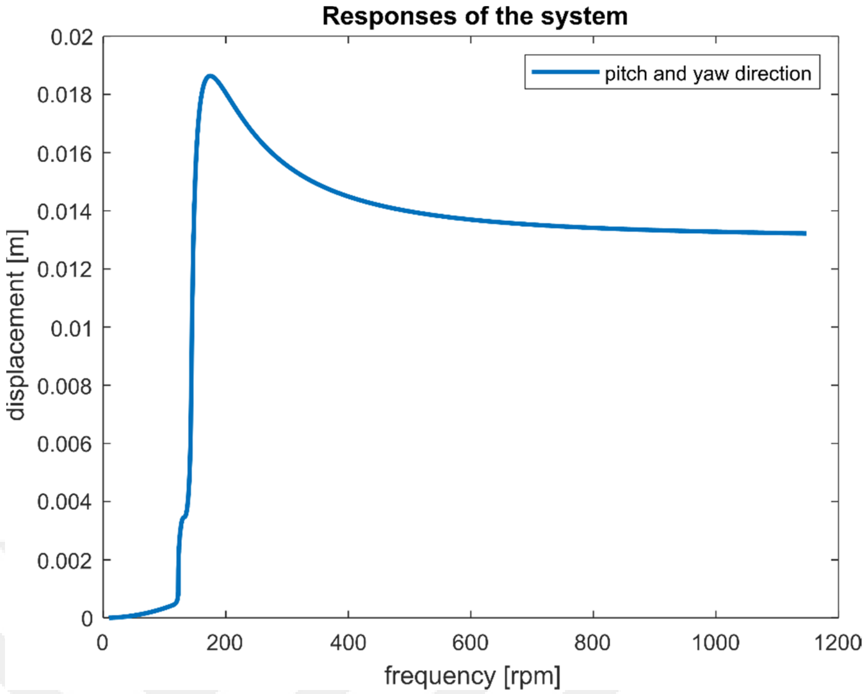


Figure 5.5. Displacements with optimized system parameters for the three-dimensional system with dry friction dampers.

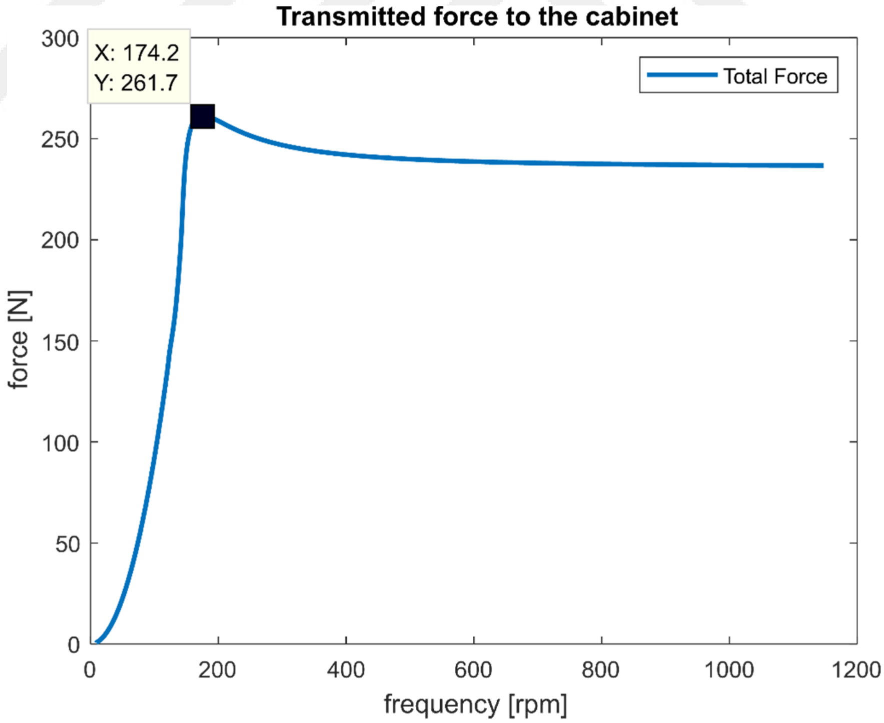


Figure 5.6. Total transmitted force to the cabinet with optimized system parameters for the three-dimensional system with dry friction dampers.

# CHAPTER 6

# CONCLUSION

## 6.1. Brief Overview of the Results

In this thesis, a two-dimensional and a three-dimensional nonlinear dynamic model for horizontal drum type washing machines are developed. Viscous and dry friction dampers are considered separately in the models developed. Harmonic Balance Method is used to transfer the nonlinear differential equations of motion to frequency domain resulting in a set of nonlinear algebraic equations and Newton's method with arc-length continuation is used to calculate the steady-state response. Multiple harmonics are analyzed in order to accurately capture the steady-state vibration response of the system. Several case studies performed to observe the effects of system parameters or geometrical orientations of resilient elements on the system frequency response function. In conclusion, the main findings of this thesis can be listed as follows:

- There is an approximately %30 difference between the results of the linear model and the suggested two-dimensional model. Therefore, it is wise to use the suggested two-dimensional model instead of the linear one.
- The best orientation angles of the resilient elements are selected as $45^o$ . This orientation leads both minimum amount of transmitted total force and uniform distribution of the force which prolongs the cabinet's life.
- Proper use of dry friction dampers can significantly limit the maximum transmitted force to the cabinet. When the total transmitted force is selected as the cost function in the optimization process, dry friction dampers significantly outperform viscous dampers throughout the whole operation range. However, highly damped systems have smaller peaks around natural frequency; therefore, combination of viscous and dry friction dampers may lead better performances.

- There is no linear relation between the system parameters and/or geometric orientations of the resilient elements to the response of the system.
- The three-dimensional system is developed to observe the effects of the eccentricity of the laundry in the roll axis of the drum. However, when Figures (3.11 & 4.11) are compared, the result of the eccentricity in the roll axis is totally negligible. The only difference between these two figures is tiny peaks around 70 rpm. Therefore, if the maximum value of the transmitted force is going to be analyzed, it is wise to choose the two-dimensional system since its computation time is much shorter. However, if the displacement in the roll axis becomes important, or gasket dynamics are going to be analyzed three-dimensional system becomes inevitable to use.
- If there is no direct contact force between the rigid bodies in a three-dimensional system, an inertial base frame is more suitable than the other reference frames to resolve all the equations. Because all the derivations should be taken in an inertial frame in the equation of motion and the Coriolis Transport Theorem is necessary unless an inertial frame is taken as the mainframe. Moreover, all resilient elements are floating in the three-dimensional space and it is simpler to define the forces on the elastic elements in the inertial frame to save computational effort.

### 6.2. Suggestions for the Future Work

Suggested procedure in this thesis is analyzing the two and three-dimensional washing machine dynamics in the frequency domain. In future studies, asymmetric orientations of resilient elements can be investigated.

In this study, optimization with viscously damped systems and dry frictionally damped systems are examined. Parameters of the gasket and other elastic elements can be optimized at the same time in future studies.

# REFERENCES


[1] Conrad, D. C., & Soedel, W. (1995). on the Problem of Oscillatory Walk of Automatic Washing Machines. *Journal of Sound and Vibration*, *188*(3), 301–314. https://doi.org/10.1006/jsvi.1995.0595

[2] Aldrin, J. C., Conrad, D. C., & Soedel, W. (1996). Investigation of passive and adaptive passive dynamic absorbers applied to an automatic washer suspension design (May 1996), 50–61. https://doi.org/10.1117/12.239111

[3] Kuo, J. L., & Wang, T. Y. (2008). Investigation of flexible multi-mode harmonic vibration for the automatic washing process. *Proceedings of the Institution of Mechanical Engineers, Part C: Journal of Mechanical Engineering Science*, *222*(12), 2373–2384. https://doi.org/10.1243/09544062JMES1056

[4] Lyu, J. C., Nho, G. H., Chung, B. S., Lee, J. H., Jung, S. W., & Yoo, W. S. (2008). Suggestion of MSTV (Modified-Stick-Transition-Velocity) model for hysteretic damping mechanism. *Journal of Mechanical Science and Technology*, *22*(7), 1305–1312. https://doi.org/10.1007/s12206-008-0406-9

[5] Bascetta, L., Rocco, P., Zanchettin, A. M., & Magnani, G. (2012). Velocity control of a washing machine: A mechatronic approach. *Mechatronics*, *22*(6), 778–787. https://doi.org/10.1016/j.mechatronics.2012.04.005

[6] Boyraz, P., & Gündüz, M. (2013). Dynamic modeling of a horizontal washing machine and optimization of vibration characteristics using Genetic Algorithms. *Mechatronics*, *23*(6), 581–593. https://doi.org/10.1016/j.mechatronics.2013.05.006

[7] Nguyen, Q. H., Choi, S. B., & Woo, J. K. (2014). Optimal design of magnetorheological fluid-based dampers for front-loaded washing machines. *Proceedings of the Institution of Mechanical Engineers, Part C: Journal of Mechanical Engineering Science*, *228*(2), 294–306. https://doi.org/10.1177/0954406213485908

[8] Clerc, C., Carbonelli, A., & Augez, R. (2015). An auto-balancer device for high spin-drying frequencies (LoWash Project). *MATEC Web of Conferences*, *20*, 03001. https://doi.org/10.1051/matecconf/20152003001

[9] Yalçin, B. C., & Erol, H. (2015). Semiactive vibration control for horizontal axis washing machine. *Shock and Vibration*, *2015*. https://doi.org/10.1155/2015/692570

[10] Türkay, O. S., Sümer, I. T., Tuğcu, A. K., & Kiray, B. (1998). Modeling and Experimental Assessment of Suspension Dynamics of a Horizontal-Axis Washing Machine. *Journal of Vibration and Acoustics*, *120*(2), 534. https://doi.org/10.1115/1.2893862

[11] Türkay, O. S., Kiray, B., Tugcu, A. K., & Sümer, T. (1995). Formulation and implementation of parametric optimisation of a washing machine suspension system. *Mechanical Systems and Signal Processing*, *9*(4), 359–377. https://doi.org/10.1006/mssp.1995.0029

[12] Papadopoulos, E., & Papadimitriou, I. (2001). Modeling, design and control of a portable washing machine during\nthe spinning cycle. *2001 IEEE/ASME International Conference on Advanced Intelligent Mechatronics. Proceedings (Cat. No.01TH8556)*, *2*(July), 899–904.

[13] Argentini, T., Belloli, M., Gaudiano, N., Fraternale, G., Panetta, F., Sabato, D., & Vanali, M. (2007). On a numerical model of a complete washing machine. *WIT Transactions on Modelling and Simulation*, *46*, 723–733. https://doi.org/10.2495/CMEM070711

[14] Argentini, T., Belloli, M., Fraternale, G., Gaudiano, N., Sabato, D., & Vanali, M. (2007). Experimental characterization of the vibro-acoustic behaviour of a washing machine. In *Conference Proceedings of the Society for Experimental Mechanics Series*.

[15] Argentini, T., Belloli, M., Robustelli, F. C., Martegani, L., & Fraternale, G. (2013). Innovative Designs for the Suspension System of Horizontal-Axis Washing Machines: Secondary Suspensions and Tuned Mass Dampers. *Volume 4B: Dynamics, Vibration and Control*, *4 B*, V04BT04A058. https://doi.org/10.1115/IMECE2013-64425

[16] Lim, H. T., Jeong, W. B., & Kim, K. J. (2010). Dynamic modeling and analysis of drum-type washing machine. *International Journal of Precision Engineering and Manufacturing*, *11*(3), 407–417. https://doi.org/10.1007/s12541-010-0047-7

[17] Roizman, V. P., Tkachuk, V. P., Bubulis, A., & Pauliukas, A. (2011). Principles for design of washing-machines with low vibro-activity. *Journal of Vibroengineering*, *13*(2), 376–384.

[18] Nygårds, T., & Berbyuk, V. (2012). Multibody modeling and vibration dynamics analysis of washing machines. *Multibody System Dynamics*, *27*(2), 197–238. https://doi.org/10.1007/s11044-011-9292-5

[19] Nygårds, T., & Berbyuk, V. (2014). Optimization of washing machine kinematics, dynamics, and stability during spinning using a multistep approach. *Optimization and Engineering*, *15*(2), 401–442. https://doi.org/10.1007/s11081-012-9206-2

[20] Buśkiewicz, J., Pittner, G., & Barczewski, R. (2012). Numerical and experimental vibration analysis of domestic washing machine drum. *Int. J. of Applied Mechanics and Engineering*, (May). Retrieved from https://www.researchgate.net/publication/244995265

[21] Buškiewicz, J., & Pittner, G. (2016). Reduction in vibration of a washing machine by means of a disengaging damper. *Mechatronics*, *33*, 121–135. https://doi.org/10.1016/j.mechatronics.2015.11.002

[22] Minorowicz, B., Stefa, F., Pittner, G., & Regulski, R. (2015). Share Mode Magnetorheological Dampers for Vibration Attenuation in Domestic Washing Machines. *Progress in Automation, Robotics and Measuring Techniques, 351.* https://doi.org/10.1007/978-3-319-15847-1

[23] Chen, H. W., Zhang, Q. J., & Wu, X. Q. (2015). Stability and dynamic analyses of a horizontal axis washing machine with a ball balancer. *Mechanism and Machine Theory*, *87*, 131–149. https://doi.org/10.1016/j.mechmachtheory.2015.01.001

[24] Chen, H. W., & Zhang, Q. (2017). Design of horizontal axis washing machine with ball balancer and MR dampers. *International Journal of Precision Engineering and Manufacturing*, *18*(12), 1783–1793. https://doi.org/10.1007/s12541-017-0207-0

[25] Vass, J., Randall, R., & Kara, S. (2008). Vibration-based approach to lifetime prediction of washing machines. *Proceedings of the 15th*, (January 2008), 1–6. Retrieved from http://amber.feld.cvut.cz/user/vass/papers/LCE08_reuse.pdf

[26] Spelta, C., Savaresi, S., Fraternale, G., & Gaudiano, N. (2008). Vibration reduction in a washing machine via damping control. In *IFAC Proceedings Volumes (IFAC-PapersOnline)* (Vol. 17). https://doi.org/10.3182/20080706-5-KR-1001.0320

[27] Spelta, C., Previdi, F., Savaresi, S. M., Fraternale, G., & Gaudiano, N. (2009). Control of magnetorheological dampers for vibration reduction in a washing machine. *Mechatronics*, *19*(3), 410–421. https://doi.org/10.1016/j.mechatronics.2008.09.006

[28] Michael J. Chrzan, J. David Carlson, "MR fluid sponge devices and their use in vibration control of washing machines," Proc. SPIE 4331, Smart Structures and Materials 2001: Damping and Isolation, (2 July 2001).

[29] Ulasyar, A., & Lazoglu, I. (2018). Design and analysis of a new magneto rheological damper for washing machine. *Journal of Mechanical Science and Technology*, *32*(4), 1549–1561. https://doi.org/10.1007/s12206-018-0308-4

[30] De Carlo, F., Borgia, O., & Tucci, M. (2014). Accelerated degradation tests for reliability estimation of a new product: A case study for washing machines. *Proceedings of the Institution of Mechanical Engineers, Part O: Journal of Risk and Reliability*, *228*(2), 127–138. https://doi.org/10.1177/1748006X13500650

[31] Yuan, Y. (2008). Sensor fusion based testing station for unbalanced load estimation in horizontal washing machines. *Conference Record - IEEE Instrumentation and Measurement Technology Conference*, 1424–1428. https://doi.org/10.1109/IMTC.2008.4547266

[32] Yörükoğlu, A., & Altuğ, E. (2013). Estimation of unbalanced loads in washing machines using fuzzy neural networks. *IEEE/ASME Transactions on Mechatronics*, *18*(3), 1182–1190. https://doi.org/10.1109/TMECH.2012.2199510

[33] Starc, B., Čepon, G., & Boltežar, M. (2017). The influence of washing machine-leg hardness on its dynamics response within component-mode synthesis techniques. *International Journal of Mechanical Sciences*, *127*(August 2016), 23–30. https://doi.org/10.1016/j.ijmecsci.2016.10.005

[34] Zhang, Y., Wang, Z., & Zhou, Y. (2003). An active control strategy of vibration attenuation system based on nonlinear decoupling. *IEEE International Symposium on Industrial Electronics*, *I*, 448–453. https://doi.org/10.1109/ISIE.2003.1267291

[35] Tomigashi, Y., Okonogi, A., & Kishimoto, K. (2005). Simple Non-regenerative Deceleration Control of Permanent Magnetic Synchronous Motor for Vibration Control in Drum-type Washer/Dryer. *IEEJ Transactions on Industry Applications*, *125*(7), 673–680. https://doi.org/10.1541/ieejias.125.673

[36] Dev Barpanda and Jay M. Tudor, The Dow Chemical Company, Midland, M. (2009). Solutions-Based Approach for Reducing Noise in Washing Machines. *Sound & Vibration*, *43*(November), 6–10.

[37] Lladó Paris, J., & Sanchez Tabuenca, B. (2015). Acoustic analysis of the drainage cycle in a washing machine. *Dyna*, *82*(190), 121–127. https://doi.org/10.15446/dyna.v82n190.43635

[38] Jung, B. K., & Jeong, W. B. (2015). Mode selection of modal expansion method estimating vibration field of washing machine. *Journal of Sound and Vibration*, *340*, 343–353. https://doi.org/10.1016/j.jsv.2014.12.016

[39] Jeong, U. C., Kim, J. S., Jeong, J. E., Yang, I. H., & Oh, J. E. (2015). Development of a sound quality index for the wash cycle process of front-loading washing machines considering the impacts of individual noise sources. *Applied Acoustics*, *87*, 183–189. https://doi.org/10.1016/j.apacoust.2014.06.001

[40] Moravec, M., Ižaríková, G., Liptai, P., Badida, M., & Badidová, A. (2018). Development of psychoacoustic model based on the correlation of the subjective and objective sound quality assessment of automatic washing machines. *Applied Acoustics*, *140*(June), 178–182. https://doi.org/10.1016/j.apacoust.2018.05.025

[41] Krack, M., & Gross, J. (2019). Harmonic balance for nonlinear vibration problems. Cham, Switzerland: Springer.

[42] Chapra, S. C., & Canale, R. P. (2015). Numerical methods for engineers. New York: McGraw-Hill.

[43] Ozgoren, M. K. (2016). Robot Manipülatörlerin Dinamiği ve Kontrolü (Ser. 2). Ankara: Makina Teorisi Derneği Yayınları.

# APPENDICES

## A. Gauss-Quadrature Integration Points

Some of the Gauss-Quadrature points are tabulated here. In general, the integral is calculated as follows:

$$\int_{-1}^{1} f(x)dx = I \cong \sum_{i=1}^{n} w_i \cdot f(x_i) \tag{A.1}$$

To be accurate enough, 64 points Gauss-Quadrature integration is used throughout the thesis to take integrals numerically.

Table A.1. Two points Gauss-Quadrature integration points

| $i$ | $x_i$ | $w_i$ |
|---|---|---|
| 1 | -0.5773502691896257645092 | 1 |
| 2 | 0.5773502691896257645092 | 1 |

Table A.2. Eight points Gauss-Quadrature integration points

| $i$ | $x_i$ | $w_i$ |
|---|---|---|
| 1 | -0.9602898564975362316836 | 0.1012285362903762591525 |
| 2 | -0.7966664774136267395916 | 0.2223810344533744705444 |
| 3 | -0.5255324099163289858177 | 0.3137066458778872873380 |
| 4 | -0.1834346424956498049395 | 0.3626837833783619829652 |
| 5 | 0.1834346424956498049395 | 0.3626837833783619829652 |
| 6 | 0.5255324099163289858177 | 0.3137066458778872873380 |
| 7 | 0.7966664774136267395916 | 0.2223810344533744705444 |
| 8 | 0.9602898564975362316836 | 0.1012285362903762591525 |

Table A.3. 16 points Gauss-Quadrature integration points

| $i$ | $x_i$ | $w_i$ |
|---|---|---|
| 1 | -0.9894009349916499325962 | 0.02715245941175409485178 |
| 2 | -0.944575023073232576078 | 0.0622535239386478928628 |
| 3 | -0.8656312023878317438805 | 0.0951585116824927848099 |
| 4 | -0.7554044083550030338951 | 0.1246289712555338720525 |
| 5 | -0.6178762444026437484467 | 0.1495959888165767320815 |
| 6 | -0.4580167776572273863424 | 0.169156519395002538189 |
| 7 | -0.2816035507792589132305 | 0.1826034150449235888668 |
| 8 | -0.0950125098376374401853 | 0.1894506104550684962854 |
| 9 | 0.0950125098376374401853 | 0.189450610455068496285 |
| 10 | 0.281603550779258913230 | 0.182603415044923588867 |
| 11 | 0.458016777657227386342 | 0.1691565193950025381893 |
| 12 | 0.617876244402643748447 | 0.149595988816576732082 |
| 13 | 0.7554044083550030338951 | 0.124628971255533872052 |
| 14 | 0.8656312023878317438805 | 0.0951585116824927848099 |
| 15 | 0.944575023073232576078 | 0.0622535239386478928628 |
| 16 | 0.9894009349916499325962 | 0.0271524594117540948518 |

Table A.4. 64 points Gauss-Quadrature integration points

| $i$ | $x_i$ | $w_i$ |
|---|---|---|
| 1 | -0.9993050417357721394569 | 0.0017832807216964329473 |
| 2 | -0.9963401167719552793469 | 0.0041470332605624676353 |
| 3 | -0.9910133714767443207394 | 0.006504457968978362856 |
| 4 | -0.9833362538846259569313 | 0.008846759826363947723 |
| 5 | -0.9733268277899109637419 | 0.0111681394601311288186 |
| 6 | -0.9610087996520537189186 | 0.0134630478967186425981 |
| 7 | -0.9464113748584028160625 | 0.015726030476024719322 |
| 8 | -0.9295691721319395758215 | 0.0179517157756973430850 |
| 9 | -0.9105221370785028057564 | 0.020134823153530209372 |
| 10 | -0.8893154459951141058534 | 0.0222701738083832541593 |
| 11 | -0.8659993981540928197608 | 0.0243527025687108733382 |
| 12 | -0.840629296252580362752 | 0.026377469715054658672 |

| | | |
|---|---|---|
| 13 | -0.81326531512279755974 2 | 0.02833967261425948322 75 |
| 14 | -0.7839723589433414076102 | 0.0302346570724024788679 7 |
| 15 | -0.75281990726053189661 2 | 0.03205792835485155358 55 |
| 16 | -0.7198818501716108268489 | 0.0338051618371416093915 7 |
| 17 | -0.68523631305423324256 36 | 0.03547221325688238381 07 |
| 18 | -0.64896547125465733985 8 | 0.03705512854024004604 04 |
| 19 | -0.6111553551723932502489 | 0.03855015317861562912 9 |
| 20 | -0.57189564620263403428 39 | 0.03995374113272034138 67 |
| 21 | -0.53127946401989454565 8 | 0.04126256324262352861 |
| 22 | -0.4894031457070529574785 | 0.0424735151236535890073 4 |
| 23 | -0.44636601725346408798 5 | 0.04358372452932345337 7 |
| 24 | -0.40227015796399160369 58 | 0.04459055816375656306 |
| 25 | -0.35722015833766811595 04 | 0.04549162792741814447 98 |
| 26 | -0.31132287199021095615 75 | 0.04628479658131441729 6 |
| 27 | -0.26468716220876741637 4 | 0.0469681828162100173253 3 |
| 28 | -0.21742364374000708414 97 | 0.04754016571483030866 23 |
| 29 | -0.16964442042399281803 73 | 0.04799938859645830772 8 |
| 30 | -0.12146281929612055447 04 | 0.04834476223480295716 98 |
| 31 | -0.07299312178779903944 95 | 0.04857546744150342693 48 |
| 32 | -0.0243502926634244325089 6 | 0.04869095700913972038 34 |
| 33 | 0.02435029266342443250 9 | 0.04869095700913972038 34 |
| 34 | 0.07299312178779903944 95 | 0.04857546744150342693 5 |
| 35 | 0.12146281929612055447 04 | 0.04834476223480295717 |
| 36 | 0.16964442042399281803 73 | 0.04799938859645830772 81 |
| 37 | 0.21742364374000708414 97 | 0.04754016571483030866 23 |
| 38 | 0.26468716220876741637 4 | 0.04696818281621001732 5 |
| 39 | 0.31132287199021095615 8 | 0.04628479658131441729 6 |
| 40 | 0.35722015833766811595 04 | 0.04549162792741814448 |
| 41 | 0.40227015796399160369 58 | 0.04459055816375656306 01 |
| 42 | 0.44636601725346408798 5 | 0.04358372452932345337 7 |
| 43 | 0.48940314570705295747 9 | 0.04247351512365358900 7 |
| 44 | 0.53127946401989454565 8 | 0.04126256324262352861 02 |
| 45 | 0.57189564620263403428 39 | 0.03995374113272034138 67 |
| 46 | 0.61115535517239325024 9 | 0.03855015317861562912 9 |

| | | |
|---|---|---|
| 47 | 0.6489654712546573398578 | 0.0370551285402400460404 |
| 48 | 0.6852363130542332425636 | 0.03547221325688238381069 |
| 49 | 0.7198818501716108268489 | 0.0338051618371416093392 |
| 50 | 0.7528199072605318966119 | 0.0320579283548515535585 |
| 51 | 0.7839723589433414076102 | 0.0302346570724024788868 |
| 52 | 0.8132653151227975597419 | 0.0283396726142594832275 |
| 53 | 0.8406292962525803627517 | 0.0263774697150546586672 |
| 54 | 0.8659993981540928197608 | 0.0243527025687108733338 |
| 55 | 0.8893154459951141058534 | 0.0222701738083832541593 |
| 56 | 0.9105221370785028057564 | 0.0201348231535302093723 |
| 57 | 0.9295691721319395758215 | 0.0179517157756973430850 |
| 58 | 0.9464113748584028160625 | 0.0157260304760247193220 |
| 59 | 0.9610087996520537189186 | 0.0134630478967186425981 |
| 60 | 0.9733268277899109637419 | 0.0111681394601311288186 |
| 61 | 0.9833362538846259569313 | 0.0088467598263639477230 |
| 62 | 0.9910133714767443207394 | 0.0065044579689783628560 |
| 63 | 0.9963401167719552793469 | 0.0041470332605624676353 |
| 64 | 0.9993050417357721394569 | 0.0017832807216964329473 |